2007-04-18

Investigation of Novel Microseparation Techniques

Yansheng Liu
Brigham Young University - Provo

INVESTIGATION OF NOVEL MICROSEPARATION TECHNIQUES

by

Yansheng Liu

A dissertation submitted to the faculty of

Brigham Young University

in partial fulfillment of the requirements for the degree of

Doctor of Philosophy

Department of Chemistry and Biochemistry

Brigham Young University

August 2007

BRIGHAM YOUNG UNIVERSITY

GRADUATE COMMITTEE APPROVAL

of a dissertation submitted by

Yansheng Liu

This dissertation has been read by each member of the following graduate committee and by majority vote has been found to be satisfactory.

Date	Milton L. Lee, Chair
Date	David V. Dearden
Date	Paul B. Farnsworth
Date	Steven R. Goates
Date	Steven W. Graves

BRIGHAM YOUNG UNIVERSITY

As chair of the candidate's graduate committee, I have read the dissertation of Yansheng Liu in its final form and have found that (1) its format, citation, and bibliographical style are consistent and acceptable and fulfill university and department style requirements; (2) its illustrated materials including figures, tables, and charts are in place; and (3) the final manuscript is satisfactory to the graduate committee and is ready for submission to the university library.

Date

Milton L. Lee
Chair, Graduate Committee

Accepted for the Department

David V. Dearden
Graduate Coordinator

Accepted for the College

Thomas W. Sederberg
Associate Dean, College of Physical and Mathematical Science

ABSTRACT

INVESTIGATION OF NOVEL MICROSEPARATION TECHNIQUES

Yansheng Liu

Department of Chemistry and Biochemistry

Doctor of Philosophy

Ultrahigh pressure liquid chromatography (UHPLC) makes it possible to use very small particles (< 2 μm) as packing materials to provide high column efficiencies. Results from a careful comparison of small porous and nonporous particles show that when the particle size is small enough (< 2 μm), both porous and nonporous particles give excellent performance, and the differences in column efficiencies between porous and nonporous particles become insignificant.

Columns packed with bare diamond particles could separate small molecules, especially polar molecules, however, severe tailing occurred for less polar compounds. The polybutadiene coated diamond particles gave greater retention and better separation of small molecules compared to bare particles, although no improvement in column efficiency was observed. Changes in surface bonding of thermally hydrogenated diamond

particles was achieved by chemical modification using various organic peroxides with or without reagents containing long carbon chain functional groups. It appears that the alkyl groups were attached onto the diamond surface with limited coverage. LC experiments did not demonstrate good separation; however, changes in LC behavior were observed.

A repetitive solvent programming approach was successfully applied to the analysis of a continuous sample stream in microbore LC. Each analysis cycle consisted of three steps: pseudo-injection, elution and rinse. In the pseudo-injection step, elution with a non- or poor-eluting solvent produced a concentrated sample plug due to on-column focusing. Factors influencing peak symmetry, resolution and analysis cycle length were investigated. Quantitative analysis of a continuous sample stream is possible under certain operating conditions.

Electric field gradient focusing (EFGF) devices with distributed resistor substrates could focus proteins in the separation channel, however, the focused bands were not stable, and the repeatability was poor due to the formation of bubbles and pH gradient in the separation channel. Both fiber-based and porous glass capillary-based planar EFGF devices with changing cross-sectional area (CCSA) channels were constructed and evaluated with the aid of a home-made scanning laser-induced fluorescence detection system. The fiber-based CCSA EFGF devices gave poorer performance compared with glass capillary based devices. Porous glass capillary-based EFGF devices could focus single proteins and separate mixtures of two to three proteins.

ACKNOWLEDGMENTS

This work could not have been possible without the assistance and support of many people. First and foremost, I give my thanks to my adviser, Dr. Milton L. Lee, for his consistent guidance, insight, patience, support and encouragement through my education at Brigham Young University. I feel fortunate to have had the opportunity to study and perform research in his group. What I have learned from him is invaluable for my future career and personal life.

I thank all of the professors in my current and former advisory committees, Dr. David V. Dearden, Dr. Paul B. Farnsworth, Dr. Steven R. Goates, Dr. Steven W. Graves, Dr. Matthew R. Linford, Dr. Adam T. Woolley, and Dr. Karl F. Warnick, for their guidance, discussions and suggestions. I also thank the professors who taught me during my doctoral studies. I express my thanks to Dr. Steven R. Goates for his teaching and his generosity in allowing me access to the argon ion laser. I appreciate Dr. Paul B. Farnsworth's teaching and help with the UV fluorescence detection system. I give thanks to Dr. Matthew R. Linford for providing some of the diamond powders and giving me suggestions.

I thank Mr. David A. Lefebre for his collaboration in the EFGF project, and his good ideas and suggestions. I thank Dr. Edgar D. Lee for his guidance and suggestions. I

have learned a lot from him. I also thank Dr. Dennis H. Tolley for his discussions, suggestions and concern.

Current and past members of the Lee group are gratefully acknowledged for their helpful discussions and friendship. In particular, I would like to thank Dr. Naijun Wu and Dr. Yanqiao Xiang for their collaboration and helpful suggestions. I have learned a lot from them about practical liquid chromatography techniques. I also thank Dr. Qinggang Wang for his collaboration, helpful ideas, deep discussions and friendship. I thank Jesse Contreras for his cooperation, discussions and friendship.

I express my gratitude to people in the department instrument shop, especially Robert B. Hallock, Bart F. Whitehead and Keith R. Kling. I give special thanks to Susan Tachka for her high quality service and kind help.

I am grateful to the Department of Chemistry and Biochemistry at Brigham Young University for providing me the opportunity to pursue my PhD degree in chemistry and for financial support. I also gratefully acknowledge financial support from a Charles E. and Margaret P. Maw Fellowship and an NIH grant.

Last but not least, I thank my wife, Zhifeng Ye, for her love, support and helpful discussions about my research. I express my thanks to my parents and brother for their continued love and encouragement. I owe many thanks to all my tutors and friends with names not mentioned here who paved the way for me during my life.

TABLE OF CONTENTS

Page

LIST OF TABLES

LIST OF FIGURES

PART I. ULTRAHIGH PRESSURE LIQUID CHROMATOGRAPHY

I.1. Development of Ultrahigh Pressure Liquid Chromatography

I.1.1. Introduction

One of the most significant developments in liquid chromatography (LC) during the past decade has been the extension of the operating pressure to levels described by terms such as "very high" and "ultrahigh." Ultrahigh pressures in LC (UHPLC) allow the use of stationary phases with particle sizes smaller than 2 μm.

The overall goal of LC is to resolve analytes of interest within the shortest time possible [1, 2]. Theoretically, the most effective way to achieve fast and highly efficient separations is to reduce the particle size of the stationary phase [2]. With regard to efficiency, the smaller the particle size, the smaller the theoretical plate height, and the higher the column efficiency. Additionally, the relationship between retention time of an analyte and diameter of the spherical stationary phase particles can be described by [1]

$$t_R = \frac{(1+k)Nhd_P^{\,2}}{D_m u} \qquad \text{(I.1.1)}$$

where t_R is the retention time for the analyte, k is the retention factor, N is the theoretical plate number, h is the reduced plate height, d_p is the particle diameter of the packings, u is the linear velocity of the mobile phase, and D_m is the diffusion coefficient of the analyte in the mobile phase. For the same column efficiency, smaller particles lead to shorter retention times. Furthermore, since smaller particles improve solute mass transfer in the mobile phase (i.e., smaller interparticle volume leads to shorter distance the solute must travel to the surface of the stationary phase), the dependence of separation efficiency on mobile phase velocity is lessened and a broad range of velocities higher than the optimum can be utilized to achieve fast analysis [3].

Unfortunately, small particles lead to high pressure drop over the length of the packed column, which can be described by [4]

$$\Delta P = \frac{\varphi \eta L u}{d_P^{\,2}} \qquad \text{(I.1.2)}$$

where φ is the flow resistance factor, η is the viscosity of the mobile phase, L is the length of the packed column, u is the linear velocity of the mobile phase, and d_P is the particle size of the packing materials. It can be easily seen that the pressure drop is inversely proportional to the square of the particle diameter. If a pressure of 6.89 MPa (1,000 psi) is needed for a column packed with 5 μm particles, a pressure greater than 75.8 MPa (11,000 psi) will be required to maintain the same linear velocity when the particle diameter is reduced to 1.5 μm. Most conventional HPLC systems have upper pressure limits of ~ 41.4 MPa (6,000 psi). Therefore, to take full advantage of columns packed with sub-2 μm particles, pumps that can deliver much higher pressures are required.

The first report UHPLC was published by Jorgenson's group in 1997 [5]. High efficiencies and fast separations were obtained as predicted. An inlet pressure of 137.9 MPa (20,000 psi) was applied to a 66 cm long capillary column packed with 1.5 μm nonporous particles to achieve the optimal flow rate and generate 300,000 theoretical plates. When the inlet pressure was increased to 406.8 MPa (59,000 psi) and the column length was shortened to 52 cm, the analysis time was reduced from 30 min to 10 min. The early work by Jorgenson's group stimulated entry of groups led by Lee [6, 7] and Colón [8] into research on UHPLC.

Recently, several instrument companies have engineered LC instrumentation to take advantage of elevated pressure operation. However, these systems are limited to between

103.4 and 137.9 MPa (15,000–20,000 psi). Pressures greater than 137.9 MPa (20,000 psi) are usually necessary to take full advantage of sub-2 μm particles. Even today, ultrahigh pressures are still only studied in a relatively few research laboratories.

The high linear velocities that can be realized in UHPLC can produce significant frictional heating, which could cause band broadening due to temperature gradients in the column. The low thermal mass and thin walls of fused silica packed capillary columns help to dissipate any heat generated during analysis and, therefore, are most suitable for UHPLC.

I.1.2. Instrumentation

The use of ultrahigh pressures imposes unique requirements on LC system hardware, such as pumps, valves, injectors, connecting tubing, and columns. These instrumental requirements and current solutions are described in the following sections.

Pumping system. According to the practice of conventional HPLC, an ideal solvent delivery system should be a dual pump system for which the pressures and flow rates can be automatically and accurately controlled. The system should be operational in both isocratic and gradient modes with good reproducibility. As mentioned previously, the maximum pressure limit for commercial syringe pumps with flow rate control is approximately 137.9 MPa (20,000 psi). For ultrahigh pressures, alternative pumps or pump modifications are required.

The earliest and still most commonly used pumps for UHPLC are air-driven liquid pumps, or pneumatic amplifier pumps [5-7, 9, 10]. For such pumps, the floating piston surface area in the air driven side is much larger than that in the liquid side, so that very high liquid pressures can be generated via relatively low air pressures. A major advantage

of this type of pump is that it can reach extremely high pressures, even greater than 689.5 MPa (100,000 psi). Other benefits are that they are commercially available, are of relatively low cost, and come in moderate sizes. The main drawback of pneumatic amplifier pumps is that they are controlled by pressure instead of volume, which makes it difficult to generate mobile phase composition gradients. However, a pneumatic amplifier dual pump system that can provide pressures up to 896.3 MPa (130,000 psi) as well as accurate flow rate control was reported by Jorgenson's group [11]. The flow rate was controlled electronically. An unattractive feature of this system is that the pumps were extremely large (42" high, 36" long and 24" wide).

Another approach to generate ultrahigh pressures is to use a conventional HPLC pump with a hydraulic amplifier [12]. Eschelbach et al. reported the use of a binary LC pump filled with vehicle brake fluid to drive a custom-built hydraulic amplifier piston with 30:1 amplification. Pressures of more than 344.7 MPa (50,000 psi) were achieved.

The highest reported pressure that can be generated from a commercially available gradient pumping system is 137.9 MPa (20,000 psi). With this dual syringe pump system, Shen et al. [13] was able to reproducibly generate various gradient profiles.

Injector. The operating pressure for a conventional injection valve typically cannot exceed 68.95 MPa (10,000 psi). Sample introduction is the most difficult operation to accomplish in UHPLC, and new approaches are needed. For capillary columns packed with sub-2 μm particles, the maximum allowable injection volumes were estimated [10] to be below 20 nL [14]. Therefore, the injector should be capable of quickly and reproducibly injecting extremely small volumes, on the order of 20 nL, at ultrahigh

pressures. Special connectors are needed to hold the column in place under ultrahigh pressures.

Three injection strategies have been reported in the literature; one must be conducted at low pressure while the other two can be effected at elevated pressures. The low-pressure approach involves a static split of the sample. Static-split injection has been used in most work with UHPLC [5-7, 10] and has been shown to deliver samples as small as 0.2 nL. Injection into the column is completed at low pressure (typically around 500 psi), followed by flushing the remaining sample out of the injection region around the column entrance before rapid pressurization up to operating pressure. A few minutes of depressurization is required after each run before the next injection. The injection procedure involves several steps and is time-consuming. Also, it requires a relatively large sample volume (i.e., approximately 100 μL of sample must be loaded in the injector) and it suffers from poor injection reproducibility [15]. Also, it is not suitable for gradient capillary LC because of the large (100 μL) sample chamber in the injector. For gradient elution, the column must be disconnected from the injector after sample introduction and coupled directly to the small diameter tubing from the pumping system. Another drawback of low-pressure injection is that a linear velocity surge occurs when high pressure is applied to the capillary column, which causes some band broadening [16]. Unfortunately, low-pressure injection is still the only injection method for UHPLC at pressures higher than 275.8 MPa (40,000 psi).

A second approach is pressure-balanced injection reported by Wu et al. [15], which provides better reproducibility, shorter injection time, ease of operation and reduced sample consumption. The pressure-balanced injection valve allows high pressure mobile

phase to pass by both the front and back of the valve needle, so that the force of the needle on the valve seat is not extraordinarily high. The main drawback of this injection valve is that it can withstand pressures only up to approximately 103.4 MPa (15,000 psi).

By far, the most desirable injection system for UHPLC is a recently developed high pressure valve injection assembly [14, 17]. This injection valve assembly is composed of six small needle valves, each of which is electrically controlled. Different combinations of the "open" or "closed" state of these valves allow loading of the sample loop, injection of the sample into the column, and flushing the remaining sample out of the injection loop and valve assembly. Injection is completed at the operating pressure, so depressurization and pressurization steps are not needed. This new injector is automatic and, hence, convenient, fast, and precise, and it can be used at pressures up to 275.8 MPa (40,000 psi). It is suitable for both isocratic and gradient operation modes, and shows excellent performance for fast separations.

Gradient generation. Methods used for generating mobile phase composition gradients usually depend on the type of pumps used. However, gradient generation using any single pump can be accomplished using a simple mixing volume. Mobile phase A is first loaded into the mixing volume, which is located between the pump filled with mobile phase B and the injector. As mobile phase B is introduced into the mixer before the column, an exponential gradient profile is created. MacNair et al. [11] reported gradient separations of tryptic digests of proteins using the exponential dilution method. Injection was accomplished at low pressure (2.76 MPa or 400 psi) and, after depressurization, the column was connected to the mixer through a high pressure tee. Xiang et al. [14] reported gradient UHPLC of protein digests using a pneumatic amplifier

pump with mixer and injection valve assembly. The major shortcoming of gradient generation using a single pump and a simple mixer is that the variety of gradient profiles that can be generated is extremely limited and a linear profile is not obtainable.

A gradient profile for UHPLC can also be generated using a preloaded gradient. Eschelbach et al. [12] used a conventional capillary LC system to generate a desired gradient profile at low pressure, followed by storing or preloading the gradient profile in a gradient storage tube of a hydraulic amplifier. Ultrahigh pressures were then used to push the gradient profile into the column during the chromatographic run. The main advantage of this strategy is that various gradient profiles, including linear gradients, can be generated. However, generating and preloading the gradient profile are time-consuming, which offsets the speed advantage of UHPLC.

While the previously described approaches for gradient generation are useful for demonstrating gradient UHPLC, they are not ideal for practical use. Clearly, more effort is required to develop a simple, reproducible, easy to use solution.

Detection. Theoretically all detection methods utilized in conventional and microcolumn LC systems can be used in UHPLC. One specific characteristic is that when using UHPLC for fast separations the data acquisition rate should be fast enough so as not to miss any narrow peaks. That is why all commercial very high pressure LC manufacturers have developed various detectors with data acquisition rates no less than 40 Hz for their new systems.

UV absorbance detection is the most widely used detection method in both conventional and capillary LC because it has the best combination of convenience, sensitivity, linearity, versatility and reliability of all the LC detectors so far developed. It

also gives good performance in UHPLC [6-8, 10]. For packed capillary columns, usually on-column detection is used to prevent extracolumn band broadening. A detection window is made just adjacent to the outlet frit of the capillary column by removing the polymeric coating on the silica capillary [6]. The main disadvantage of on-column detection is that the short path length limits the concentration sensitivity of the UV detector.

Laser-induced fluorescence detection is very attractive for capillary LC due to its increased sensitivity and selectivity. MacNair et al. [11] used on-column laser-induced fluorescence detection in separation of TRITC-labeled peptides from protein digests. However, the application of fluorescence detection is usually limited by shortcomings such as narrow linear response range, lack of fluorescence active analytes and difficulties in synthesizing fluorescent derivatives. On-column fluorescence detection also suffers from poor sensitivity caused by short optical path length and small excitation volumes.

Amperometric detection was utilized to detect electroactive compounds in UHPLC research [5, 9-11]. A long carbon fiber microelectrode was inserted into the outlet end of the packed capillary, and detection was accomplished by amplifying the current from a carbon microelectrode that was held +1.00 V versus Ag/AgCl reference electrode. Amperometric response requires that the species of interest are easily oxidized and reduced at the set potential.

Obviously, the significance of mass spectrometry (MS) detection in modern LC extends to UHPLC. In the first report of coupling UHPLC to MS, Lippert et al. [6] interfaced an UHPLC system that could operate at inlet pressures up to 275.8 MPa (40,000 psi) to a time-of-flight mass spectrometer (TOFMS), and found that the retention

times were in excellent agreement with those obtained by on-column UV-absorption detection. Wu et al. [7] reported an UHPLC-TOFMS system with a liquid-sheath electrospray interface. At the maximum inlet pressure of 275.8 MPa (40,000 psi), combinatorial chemistry samples, pharmaceutical compounds and herbicides were analyzed in less than 100 s with high separation efficiency. For fast separations, TOFMS is preferred over scanning mass spectrometers due to its fast data acquisition rates. It was found during optimization that the column outlet position in the liquid-sheath interface was very important to maintain high separation efficiency.

Tolley et al. [18] reported the analysis of protein digests using a very high pressure (VHP) gradient LC-MS/MS system. The VHPLC system was connected to a hybrid quadrupole time-of-flight mass spectrometer via a nanospray interface. By employing the data-dependent scanning capability of the mass spectrometer, 26 different eluting peptides from a protein digest were interrogated for identification of the original protein. Shen and co-workers [13] investigated separations of peptides from protein digests by coupling long capillary LC columns to different mass spectrometers via electrospray interfaces at pressures up to 137.9 MPa (20,000 psi). For a 200 cm × 50 μm i.d. capillary packed with 3 μm porous C18-bonded silica particles, a chromatographic peak capacity of 1,500 was obtained in just under 34 h. The separation time could be reduced greatly by reducing the particle size to 1.4 μm and shortening the column length from 200 cm to 40 cm, however, smaller particles did not provide higher peak capacity within the pressure limit of 137.9 MPa (20,000 psi), but they improved the peak capacity generation rate.

I.1.3. Safety

The pressures required for UHPLC naturally stimulate a concern for safety. In reality, UHPLC has been shown to be very safe if simple precautionary steps are followed [19]. This is because the compressibilities of liquid solvents used as mobile phases are rather low, even under ultrahigh pressures (e.g., water can be compressed approximately 10% at 275.8 MPa or 40,000 psi), and the volume of solvent in the weakest component of the system, i.e., the column, is relatively small. The two major safety concerns, liquid jets and capillary projectiles produced by column rupture, can be easily eliminated by placing a plastic shroud around the initial 2-cm of the installed capillary column.

I.1.4. Elevated Temperature

The use of elevated temperature in LC has been advocated primarily as a means of decreasing the back pressure, shortening the separation time and increasing the column efficiency [20, 21]. UHPLC also can be further improved by running at elevated temperatures to achieve high-speed, highly efficient separations. Xiang et al. [22] investigated the effects of elevated temperatures in UHPLC using columns packed with small zirconia particles as well as silica particles. Polybutadiene encapsulated 1 μm nonporous zirconia particles, which possess high chemical stability at elevated temperatures, were packed into 50 μm i.d. capillaries. The pressure drop decreased as expected when the temperature increased. The analysis time for 4 standard parabens was reduced from 6 min at 25^{o}C to approximately 2 min at 80^{o}C, primarily due to an increase in linear velocity caused by a decrease in mobile phase viscosity and a decrease in

analyte retention caused by an increase in the speed of adsorption/desorption. Separation of five herbicides was completed in 60 s at 179.3 MPa (26 000 psi) and 90^{o}C.

Similar results were obtained when using nonporous 1.0 μm isohexylsilane-modified C6 silica particles [23]. Elevating the temperature while the pressure was held constant led to a reduction in retention factor of the standard parabens. At a pressure of 227.5 MPa (33,000 psi) and temperature of 80^{o}C, only 33 s were required to separate a mixture of 7 barbitals, showing the advantage of combining high pressure with elevated temperature.

I.1.5. Stationary Phases

Although the use of ultrahigh pressures in LC is not by itself desirable, it makes possible the realization of the full benefits of small particles, including fast separation speed, high efficiency and high peak capacity. Therefore, stationary phases prepared from small diameter particles that are optimized for use at high pressures are very important. Stationary phases for UHPLC systems should first be able to withstand the high operating pressures to which they will be subjected. This includes resistance to collapse and stripping of the stationary phase coating. Particle uniformity becomes more difficult as the particle size decreases. Currently, sources of good quality sub-2 μm particles are still limited.

Initially, the stationary phases used in UHPLC were primarily nonporous silica particles with average diameters of 1.0 and 1.5 μm [5-7]. With these particles, fast and highly efficient separations were demonstrated. Recently, 1.7 μm ethylene-bridged hybrid (BEH) particles have been introduced, which can withstand pressures up to 448.1 MPa (65,000 psi) in a packed bed without measurable breakdown [9]. The

chromatographic performance of the BEH porous particles was found to be similar to nonporous particles for small, retained molecules [9]. Normally, nonporous particles give better efficiencies at high mobile phase linear velocities than porous particles because they do not have a stagnant mobile phase inside the particles that becomes the major contribution to resistance to mass transfer at high velocities. However, this difference between porous and nonporous particles becomes insignificant when the particle size is reduced to less than 2 μm [24]. Small BEH porous particles can provide higher sample loading capacities than nonporous particles as predicted by comparing the phase ratios of the two materials [9]. Shen et al. [13] used 1.4 μm C18-bonded porous particles to achieve a peak capacity of 1,000 at 137.9 MPa (20,000 psi) pressure for the separation of protein digests using gradient elution.

Xiang et al. evaluated 1 μm nonporous polybutadiene-coated zirconia particles at temperatures up to 100^{o}C [22, 25]. These nonporous zirconia particles showed efficiencies comparable to, and selectivities better than, C18 bonded silica particles for the separation of barbitals. Also, the small zirconia particles demonstrated good thermal stability at elevated temperature. Uniform spherical organosilica nano-particles (nano-SiC_{18}, 670 nm diameter) containing octadecyl moieties were synthesized by Clintron et al. [26]. Using columns packed with these nano-SiC_{18} particles, an approximate efficiency of 500,000 plates per meter were observed at a pressure of 344.7 MPa (50,000 psi), and the analysis time was reduced significantly compared with conventional HPLC. These particles appeared to be stable under acidic (pH < 1) and basic (pH > 11) conditions.

I.1.6. Applications

Fast separation speeds and high efficiencies provided by small (< 2 μm) particles and ultrahigh pressures promise broad applications of UHPLC. High resolution separations of peptides and proteins were mentioned already. UHPLC can also improve separations of chiral compounds because long columns can be used to generate high plate numbers. Xiang et al. [27] reported separations of enantiomers using columns packed with nonporous C6 silica particles at ultrahigh pressures. β-Cyclodextrin (β-CD) and 2-hydroxypropyl- β-cyclodextrin (HP-β-CD) were added to the mobile phase as modifiers to produce transient diastereomeric complexes with the analytes. The effects of pressure, additive concentration, and injection amount were studied. Chlorthalidone enantiomers were separated on a 13.5 cm x 29 μm i.d. fused silica capillary packed with 1.0 μm Kovasil MS-H nonporous particles with an inlet pressure of 275.8 MPa (40,000 psi), and efficiencies of more than 200,000 plates per meter within 2 min were obtained. Using chiral additives in the mobile phase to separate chiral compounds is typically an expensive but convenient method. The high speed and low volumetric flow characteristic of UHPLC greatly reduces the cost of the additive and makes the method more practical.

References

1. Chen, H.; Horvath, C. *J. Chromatogr. A* **1995**, *705*, 3-20.

2. Halasz, I.; Endele, R.; Asshauer, J. *J. Chromatogr.* **1975**, *112*, 37-60.

3. Mazzeo, J.R.; Neud, U.D.; Kele, M.; Plumb, R.S. *Anal. Chem.* **2005**, *77*, 460A-467A.

4. Snyder, L.R.; Kirkland, J.J. *Introduction to Modern Liquid Chromatography*, *2nd ed.*; John Wiley & Sons: New York, 1979.

5. MacNair, J.E.; Lewis, K.C.; Jorgenson, J.W. *Anal. Chem.* **1997**, *69*, 983-989.

6. Lippert, J.A.; Xin, B.; Wu, N.; Lee, M.L. *J. Microcol. Sep.* **1999**, *11*, 631-643.

7. Wu, N.; Collins, D.C.; Lippert, J.A.; Xiang, Y.; Lee, M.L. *J. Microcol. Sep.* **2000**, *12*, 462-469.

8. Colón, L.A.; Cintrón, J.M. *Analyst* **2004**, *129*, 503-504.

9. Mellors, J.S.; Jorgenson, J.W. *Anal. Chem.* **2004**, *76*, 5441-5450.

10. Patel, K.D.; Jerkovich, A.D.; Link, J.C.; Jorgenson, J.W. *Anal. Chem.* **2004**, *76*, 5777-5786.

11. MacNair, J.E.; Patel, K.D.; Jorgenson, J.W. *Anal. Chem.* **1999**, *71*, 700-708.

12. Eschelbach, J.W.; Jorgenson, J.W. *Anal. Chem.* **2006**, *78*, 1697-1706.

13. Shen, Y.; Zhang, R.; Moore, R.J.; Kim, J.; Metz, T.O.; Hixson, K.K.; Zhao, R.; Livesay, E.A.; Udseth, H.R.; Smith, R.D. *Anal. Chem.* **2005**, *77*, 3090-3100.

14. Xiang, Y.; Liu, Y.; Stearns, S.D.; Plistil, A.; Brisbin, M.P.; Lee, M.L. *Anal. Chem.* **2006**, *78*, 858-864.

15. Wu, N.; Lippert, J.A.; Lee, M.L. *J. Chromatogr. A* **2001**, *911*, 1-12.

16. Jerkovich, A.D.; Mellors, J.S.; hompson, J.W.; Jorgenson, J.W. *Anal. Chem.* **2005**, *77*, 6292-6299.

17. Anspach, J.A.; Maloney, T.D.; Brice, R.W.; Colon, L.A. *Anal. Chem.* **2005**, *77*, 7489-7494.

18. Tolley, L.; Jorgenson, J.W.; Moseley, M.A. *Anal. Chem.* **2001**, *73*, 2985-2991.

19. Xiang, Y.; Maynes, D.R.; Lee, M.L. *J. Chromatogr. A* **2003**, *991*, 189-196.

20. Dolan, J.W. *LC-GC* **2002**, *20*, 524-530.

21. Antia, F.D.; Horváth, C. *J. Chromatogr. A* **1988**, *435*, 1-15.

22. Xiang, Y.; Yan, B.; Yue, B.; McNeff, C.V.; Carr, P.W.; Lee, M.L. *J. Chromatogr. A* **2003**, *983*, 83-89.

23. Xiang, Y.; Liu, Y.; Lee, M.L. *J. Chromatogr. A* **2006**, *1104*, 198-202.

24. Wu, N.; Liu, Y.; Lee, M.L. *J. Chromatogr. A* **2006**, *1131*, 142-150.

25. Xiang, Y.; Yan, B.; McNeff, C.V.; Carr, P.W.; Lee, M.L. *J. Chromatogr. A* **2003**, *1002*, 71-78.

26. Cintron, J.M.; Colon, L.A. *Analyst* **2002**, *127*, 701-704.

27. Xiang, Y.; Wu, N.; Lippert, J.A.; Lee, M.L. *Chromatographia* **2002**, *55*, 399-403.

I.2. Stationary Phases for Liquid Chromatography

I.2.1. Substrate Materials

The stationary phase is the most important element of LC. It provides interactions with analyte molecules to effect retention of analytes. The types and extents of these interactions vary from analyte to analyte, which allows them to be separated from each other.

The most widely used materials for packed columns are silica based particles [1-3], including unmodified silica and chemically modified silica. The popularity of silica-based stationary phases is due to several reasons. Silica has special physical and chemical properties [2, 4] that make it suitable for stationary phases in LC. Silica has strong mechanical strength so that it can withstand the high pressures used in LC, and it does not swell or shrink when in contact with organic-water mobile phases. Silica can be synthesized in pure form and in uniform shapes and sizes with high reproducibility. The chemistry of silica surfaces is well understood, and modifications can be readily conducted. Silica is chemically composed of silicon atoms (with sp^3 hybrid orbitals) connected through oxygen atoms, forming siloxane bonds (Si-O-Si). This structure is terminated by silanol (Si-O-H) groups on the surface, and can be chemically modified at these groups [5]. Different functional groups can be attached on silica surfaces to provide different interactions with solutes for different modes of chromatography. For example, pure silica particles are good for normal phase LC, while silica particles attached with C_{18} or C_8 chains are good stationary phases for reversed phase LC. If anion or cation exchangers are attached to the surface, silica particles can be used to separate ions bearing positive or negative charges [2, 6, 7].

The main drawback of silica stationary phases is their instability in basic and extremely acidic pH ranges and at elevated temperatures. Silica based stationary phases are usually stable within the pH of 3 to 9. For chemically modified silica stationary phases, the siloxane bonds hydrolyze when pH values are less than 3, causing loss of bonded phase and change in chromatographic retention [2, 8-10]. When pH values are greater than 7, the dissolution of the silica backbone becomes serious and leads to rapid loss in column efficiency [2, 10, 11]. Elevated temperatures can accelerate the dissolution of the silica structure [10, 12]. Various means have been tried to prevent silica columns from deterioration [13], however, harsh chemical environments and elevated temperatures still lead to instability of silica columns.

Other materials that are far less popular than silica, can provide some advantages over silica based stationary phases in LC [14]. These include other metal oxides like alumina, titania and zirconia, and polymers such as cross-linked poly(divinylbenzyl)-styrene.

Polymer stationary phases are usually stable in wide pH ranges and give more freedom in selecting mobile phase compositions to optimize their chromatographic performance [6, 15]. Separations of bases can be conducted with mobile phases at high pH. This is an advantage over silica based particles. However, they cannot withstand high pressures, and also swell/shrink depending on the mobile phase composition. These weaknesses prevent them being widely used as stationary phases in LC. Their use is limited to reversed phase LC in extreme pH ranges and to size exclusion and ion exchange chromatographies.

Surfaces of alumina, titania and zirconia are very different from that of silica, although they all have hydroxyl groups [14]. Due to difficulties in functionalizing the surfaces of these metal oxides, polymer coating procedures have typically been used to modify their surfaces. Polybutadiene coated zirconia is the most successful among the alternative metal oxides. Zirconia based stationary phases have shown excellent stabilities over the whole pH range as well as at high temperatures [16]. Carr and co-workers [17] reported that polybutadiene coated zirconia particles showed comparable efficiencies to silica based stationary phases in reversed phase LC. Very high chemical and thermal stabilities were observed in these studies.

Porous graphitic carbon (PGC) is another material that has been investigated extensively as a stationary phase for LC [18, 19]. PGC materials are highly hydrophobic and usually show different selectivities than silica based columns. They do not swell or shrink, have sufficient hardness and well defined porous structures, and are stable throughout the whole pH range. However, they have found only limited applications up to now.

Efforts have continued to explore new materials for LC stationary phases. The motivation is to find new materials that are stable under extreme chemical environments to replace silica columns in certain situations, that can withstand ultrahigh pressures for use in UHPLC, and that can provide new surface chemistries to achieve improved separations.

I.2.2. Mirco Structure

Conventional stationary phases are small particles, which can be spherical particles or irregular in shape. Irregular particles usually produce low efficiencies due to the low

quality of the column packing [20-22], although a recent study reported that comparable performance was achieved using irregular silica based stationary phases [23]. Commonly accepted concepts are that to obtain high efficiency in LC, the particles should be spherical in shape, very uniform in size and have a narrow size distribution [1]. As mentioned earlier, small particles allow fast separation with high efficiency, but give rise to high back pressure. The advent of UHPLC provided one way to overcome this high back pressure. A relatively new approach to eliminate the high back pressure altogether is to utilize monolithic columns instead of particulate columns [24]. A monolithic column, which is a continuous porous rod usually formed in-situ, often has a higher porosity than a conventional column packed with particles. Therefore, lower pressures are needed to achieve the same mobile phase linear velocity without loss in efficiency.

I.2.3. Comparison of Columns

The chromatographic performances of columns can be evaluated and compared in terms of efficiency, selectivity and separation speed. A simple plot of height equivalent of a theoretical plate, *H*, versus operating linear velocity, i.e., the famous van Deemter plot, can provide much information about a column, such as minimum plate height achievable and optimal operating linear velocity range. Fitting this plot to the van Deemter equation or other alternative equations for peak dispersion (such as the Knox equation) can reveal more about the causes of band broadening on the column. This is the most commonly used method for column evaluation and comparison.

Kinetic plots provide information about kinetic properties of columns, and also can be used to compare columns, even those having different morphologies. Giddings [25] compared the performance limits of GC and LC in terms of analysis time and plate

number. Poppe [26] suggested a plot of H/u_0, or t_0/N, the "plate time", versus N, the plate number, to obtain a clearer view of the C term in the van Deemter equation. A typical Poppe plot shows the minimum plate times achievable under certain maximum inlet pressures for obtaining required plate numbers. Conventionally, a Poppe plot is obtained through an iterative procedure which is complicated and time-consuming. Recently, Desmet et al. [27] promoted another straightforward method to compose various kinetic plots, including the Poppe plot. The procedure starts from a series of plate heights, H, and accordant linear velocities, u_0, with calculations conducted using the following equations

$$N = \left(\frac{\Delta P}{\eta}\right)\left[\frac{K_v}{u_0 H}\right]_{\exp} \qquad \text{(I.2.1)}$$

and

$$t_0 = \left(\frac{\Delta P}{\eta}\right)\left[\frac{K_v}{u_0^{\,2}}\right]_{\exp} \qquad \text{(I.2.2)}$$

where ΔP is the maximum inlet pressure of a chromatography system, H is the height equivalent of a theoretical plate at linear velocity of u_0, η is the viscosity of the mobile phase, K_v is the column permeability, and the subscript *exp* indicates that the parameters in the square bracket were obtained from experiments. From equation (I.2.1), we can obtain an expression for ΔP as a function of L

$$\Delta P = \frac{\eta u_0 L}{K_v} = \frac{\eta u_0 HN}{K_v} \qquad \text{(I.2.3)}$$

where L is the column length. N obtained from equation (I.2.1) is the plate number that can be obtained at the maximum inlet pressure, ΔP, assuming that the plate height is constant at a specific linear velocity, u_0, and this linear velocity is kept constant by using a column with suitable length. The t_0 obtained from equation (I.2.2) is just the respective

hold up time. From a series of N and t_0 pairs, kinetic plots in various forms, including the Poppe plot, can be constructed.

I.2.4. Scope of This Section of the Dissertation

This section of my dissertation mainly deals with two subjects relating to stationary phases for LC. One is a comparison of the chromatographic performances of small porous and nonporous particles using UHPLC. Kinetic plots and van Deemter curves were used to represent the column efficiencies and kinetic properties. The other subject is an investigation of the possibility of using diamond particles as a stationary phase for LC. Preliminary evaluations of bare and modified synthetic diamond particles were conducted using a capillary UHPLC system.

References

1. Snyder, L.R.; Kirkland, J.J. *Introduction to Modern Liquid Chromatography*, *2nd ed.*; John Wiley & Sons: New York, 1979.

2. Nawrocki, J. *J. Chromatogr. A* **1997**, *779*, 29-71.

3. Berthod, A. *J. Chromatogr.* **1991**, *549*, 1-28.

4. Unger, K.K. *Porous Silica: Its Properties and Use as Support in Column Liquid Chromatography*; Elsevier: Amsterdam, 1979.

5. Scott, R.P.W. *Silica Gel and Bonded Phases: Their Production, Properties, and Use in LC* John Wiley & Sons Ltd: Chichester, 1993.

6. Neud, U.D. *HPLC Columns: Theory, Technology and Practice*; Wiley-VCH: New York, 1997.

7. Lough, W.J.; Wainer, I.W. *High Performance Liquid Chromatography: Fundamental Principles and Practice* Blaclue Academic and Professional: London, 1995.

8. Kirkland, J.J.; Glajch, J.L.; Kohler, J. *J. Chromatogr.* **1987**, *384*, 81-90.

9. Kirkland, J.J.; Glajch, J.L.; Farlee, R.D. *Anal. Chem.* **1989**, *61*, 2-11.

10. Snyder, L.R.; Kirkland, J.J.; Glajch, J.L. *Practical HPLC Method Development*, *2nd ed.*; Willey-Interscience: New York, 1997.

11. Claessens, H.A.; Straten, M.A.v.; Kirkland, J.J. *J. Chromatogr. A* **1996**, *728*, 259-270.

12. McCalley, D.V. *J. Chromatogr. A* **2000**, *902*, 311-321.

13. Claessens, H.A.; Straten, M.A.v. *J. Chromatogr. A* **2004**, *1060*, 23-41.

14. Nawrocki, J.; Dunlap, C.; McCormick, A.; Carr, P.W. *J. Chromatogr. A* **2004**, *1028*, 1-30.

15. Hosoya, K.; Teramachi, M.; Tanaka, N.; Kobayashi, A.; Kanda, T.; Ohtsu, Y. *Anal. Chem.* **2001**, *73*, 5852-5857.

16. Nawrocki, J.; Dunlap, C.; Li, J.; Zhao, J.; McNeff, C.V.; McCormick, A.; Carr, P.W. *J. Chromatogr. A* **2004**, *1028*, 31-62.

17. Li, J.; Carr, P.W. *Anal. Chem.* **1997**, *69*, 2193-2201.

18. Unger, K.K. *Anal. Chem.* **1983**, *55*, 361A-373A.

19. Ross, P.; Knox, J.H. *Adv. Chromatogr.* **1997**, *37*, 73-162.

20. Perry, J.A.; Szczerba, T.J. *J. Liq. Chromatogr.* **1993**, *16*, 1371-1383.

21. Verzele, M.; Dijck, J.v.; Mussche, P.; Dewaele, C. *J. Liq. Chromatogr.* **1982**, *5*, 1431-1448.

22. Unger, K.K.; Messer, W.; Krebs, K.F. *J. Chromatogr.* **1978**, *149*, 1-12.

23. Vissers, J.P.C.; Hoef, E.C.J.V.D.; Claessens, H.A.; Laven, J.; Cramers, C.A. *J. Microcol. Sep.* **1995**, *7*, 239-245.

24. Svec, F. *J. Sep. Sci.* **2004**, *27*, 1419-1430.

25. Giddings, J.C. *Anal. Chem.* **1965**, *37*, 60-63.

26. Poppe, H. *J. Chromatogr. A* **1997**, *778*, 3-21.

27. Desmet, G.; Clicq, D.; Gzil, P. *Anal. Chem.* **2005**, *77*, 4058-4070.

I.3. Comparison of Small Porous and Nonporous Particles *

I.3.1. Introduction

As described above, using small particle stationary phases in LC will help to obtain fast and highly efficient separations [1]. Inherent in the evolution of high performance LC has been the reduction in particle size of column packings [2]. The size of the packing material has been reduced to as small as 1 μm today from greater than 100 μm in the 1960s. At the same time, the separation time has been decreased from minutes to seconds for comparable separations. The advent of UHPLC allows the possibility to take advantage of stationary phases with particle sizes smaller than 2 μm.

Nonporous and porous particles are the two major types of spherical packing materials that have been used for HPLC [3-8]. Perfusion particles are a special type of porous packing materials that contain large intraparticle pores [9] through which the mobile phase can flow. Superficially porous particles are hybrid packings that consist of a nonporous core covered by a layer of porous material [10]. Sub-2 μm nonporous silica particles such as 1.5-μm Micra C_{18} have been used as stationary-phase support material in both ultra-high pressure LC and somewhat lower pressure LC systems [4-7]. Nonporous particles are easily prepared in the sub-2-μm size range and they are mechanically strong enough to withstand very high pressures. Furthermore, nonporous particles can provide lower mass transfer resistance and higher efficiency than porous particles, since porous particles have a mass-transfer resistance contribution originating from the stagnant mobile phase in the pores [11]. Stegeman *et al.* observed that reduced plate heights for a column packed with 1.5-μm nonporous particles did not change with

* This chapter (except Figure I.3.1, Figure I.3.3, and discussion about Poppe plots) is reproduced with permission from *J. Chromatogr. A* **2006**, *1131*, 142-150 (Copyright 2006 Elsevier).

increasing linear velocity when polystyrenes (average molecular weights as high as 775,000) were used as analytes [12]. Barder *et al.* demonstrated that the column efficiency for nonporous silica particles was considerably higher than that for porous particles at high flow rates [4]. Issaeva *et al.* showed super-high-speed separations of proteins and peptides using 1.5-µm nonporous Micra particles [13].

It was not until recently that uniform sub-2-µm porous particles with various bonding chemistries have become commercially available. These particles include Waters 1.7 µm ACQUITY and Agilent 1.8 µm ZORBAX particles, which were developed for fast separation or ultra-performance LC [14]. Compared to nonporous particles, porous particles have greater surface areas and can provide much higher sample loading capacity. Seifar *et al.* estimated a 50-fold higher sample capacity for porous particles than nonporous particles of the same size. They also showed that a column packed with 1.8 µm octadecylsilane (ODS) modified porous silica particles provided higher column efficiency in capillary electrochromatography (CEC) than one with nonporous particles of approximately the same size [15]. More recently, Mellors *et al.* compared the efficiencies of 1.5 µm porous and 1.0 µm nonporous C_{18} particles and found that the reduced plate heights for the two types of particles were essentially the same [6].

The above column efficiency results were somewhat contradictory; it seemed unclear whether or not sub-2 µm nonporous particles had significant advantages over porous particles in terms of column efficiency and separation speed. Furthermore, the kinetic properties also needed to be evaluated to compare the speeds needed to obtain the required column efficiencies. In this part of my dissertation, column efficiencies were investigated for small porous and nonporous particles. The contribution of stagnant

mobile phase to mass transfer resistance for porous particles is discussed in terms of particle size. Pressure drop and kinetic properties were also compared.

I.3.2. Experimental

Chemicals and materials. Acetonitrile (ACN) and water used in this study were HPLC grade (Fisher, Springfield, NJ, USA). Uracil, nitromethane, isopropanol, and parabens were purchased from Sigma-Aldrich (Milwaukee, WI, USA). The 0.2% TFA aqueous and ACN solutions were prepared by dissolving 2 mL TFA into 1 L deionized water and 1 L ACN, respectively. The 20 mM HAc/NaAc aqueous buffer solution (pH 3.5) was prepared by dissolving solid NaAc into 500 mL deionized water, and then adjusting the pH to the assigned value by adding HCl solution.

UHPLC instrumentation, columns, and conditions. A home-made UHPLC system with a Valco high pressure injector, shown in Figure I.3.1, was utilized to conduct chromatography of small molecules using columns packed with porous and nonporous particles. Extra column effects, which may be significant for an unretained analyte, can be minimized by using such a system with long columns and static split injection. Nitromethane was used as both analyte and unretained marker when neat ACN was used as mobile phase. For retained solute conditions, parabens were used as analytes and uracil as unretained marker.

The UHPLC system was based on a pneumatic amplifier pump (Model DSHF-302, Haskel, Burbank, CA, USA), as described elsewhere [7, 16], except for an injection valve assembly (VICI Valco, Houston, TX, USA) was utilized as a high pressure injector [17]. Briefly, a high pressure three-way valve (Model 60-13HF2, HiP) was used to connect the pump outlet, a high pressure tee (Model 60-23HF2, HiP) and a high pressure

two-way valve (Model 60-11HF2, HiP), which was used for pump depressurization. The other two ports of the high pressure tee were connected to a high precision pressure transducer (Model THE/4834-06TJG) and a high pressure injector. This high pressure injector was electronically controlled to operate at pressures as high as 30,000 psi. A Model UV3000 scanning detector (Thermo Separations, Sunol, CA, USA) was used to monitor UV absorbance on-column, and data were acquired with ChromQuest 2.5.1 (ThermoQuest, Sunol, CA, USA).

A home-made high-pressure packing system was used to prepare columns for this study [7]. Fused-silica capillaries with 75 μm i.d. and 365 μm o.d. were used. For non-porous particles, slurries were made by mixing particles in isopropanol, which was then transferred to the packing reservoir. Liquid carbon dioxide from a compressed cylinder was used to drive the particle slurry into the capillary column. Both the column and the reservoir were placed in an ultrasonic bath (Branson Ultrasonic, Danbury, CT, USA) that was maintained at room temperature until ~40 cm of the column was filled. The initial pressure was generally 900 psi. The pressure was increased gradually to maintain a constant packing rate until the column was filled to the required length. The final packing pressure generally ranged from 1,030 to 1,170 bar (15,000 to 17,000 psi). The column was sonicated for an additional 30 min to allow the particles to settle in a dense and uniform packed bed. The column was then left to depressurize overnight. Before burning frits at the ends of the silica bed, the packed capillary was wetted with acetonitrile for 1 h at 20,000 psi and then flushed with water at the same pressure. Inlet and outlet frits were prepared by sintering the packing materials at the ends of the capillary column with a resistive heating device (InnovaTech, Hertfordshire, UK) while

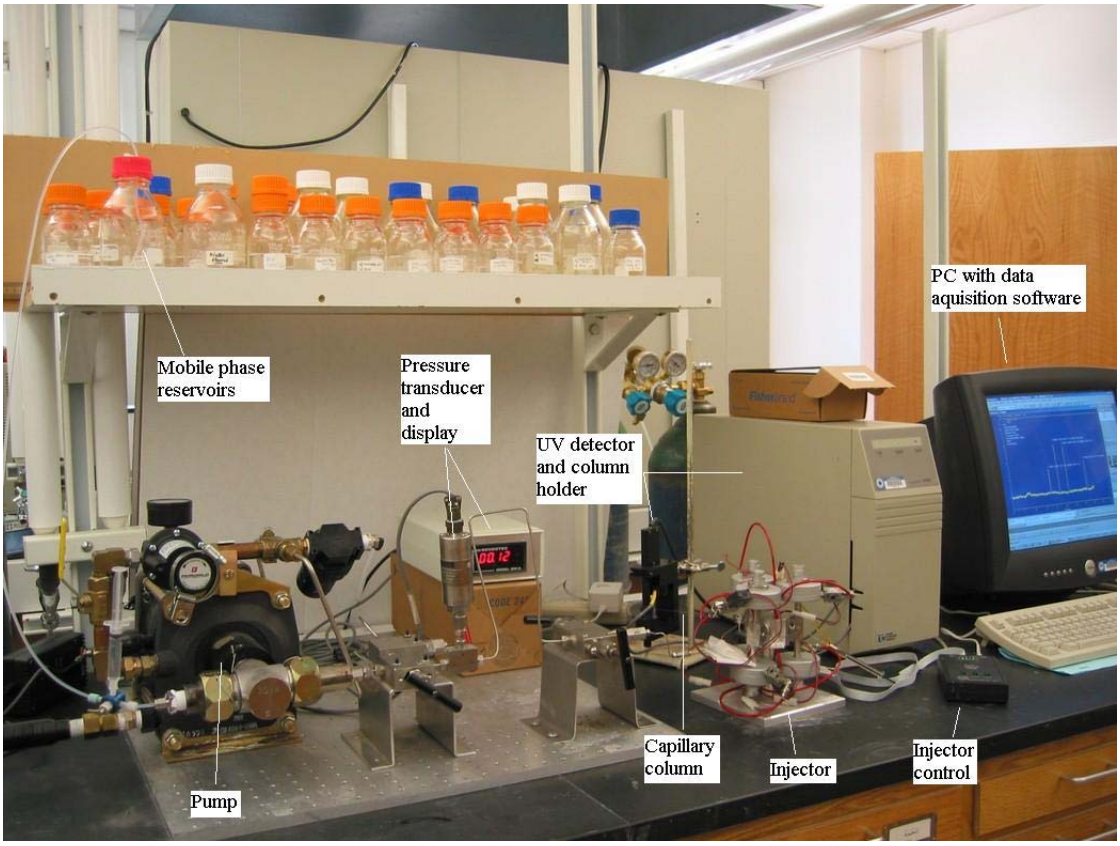

Figure I.3.1. Photograph of the capillary UHPLC system used in these studies.

water was pumped through the column at 12,000 psi. The excess non-sintered packing material following the outlet frit was removed from the capillary by pumping with water. A window for on-column detection was created as close as possible to the outlet frit by burning off the polyimide coating using the same heating device.

Column preparation using porous particles was slightly more complicated than that for nonporous particles because it was difficult to prepare frits by heating the porous particles used in this study. Typically, a capillary column with 75 μm i.d. was first packed with 1.5 μm bare silica particles to a few centimeters long. A frit, which would become the outlet frit, was then sintered on the very top of this segment of bare silica particles while flushing the column with water at a pressure of 12,000 psi. Porous particles were then packed into the column to a length of approximately 30 cm. The final pressure was generally 15,000 to 17,000 psi. A mark was made on the very top of the porous particle segment. Then additional bare silica particles were packed on the top of the porous particles, and fused to form an inlet frit. Particles located after the outlet frit were removed, and a detection window was burned as close as possible to the outlet frit.

I.3.3. Results and Discussion

Column efficiency. For LC separations, the mass transfer resistance term in the van Deemter equation becomes more significant when high linear velocities are used. The major difference between porous and nonporous particles is that porous particles have a resistance to mass transfer contribution from the stagnant mobile phase in the pores. The Horváth-Lin equation describes such a contribution for unretained solutes [11]

$$C_{stag} = \frac{\theta k_0 d_p^2}{30 D_m (1 + k_0)^2} \qquad \text{(I.3.1)}$$

where θ is the tortuosity factor for porous particles, k_o is the ratio of the intraparticle void space to the interstitial void space in the column, D_m is the diffusion coefficient of the solute in the mobile phase, and d_p is the particle diameter. It can be seen from equation (I.3.1) that the resistance to mass transfer from the stagnant mobile phase is proportional to the square of the particle diameter and inversely proportional to the diffusion coefficient of the solute in the mobile phase if other parameters are kept constant. Decreasing the particle size and increasing the diffusion coefficient can improve the mass transfer of solutes in the stagnant mobile phase. In other words, when small particles or mobile phases of low density are used, such as enhanced fluids or even gases, the contribution to mass transfer resistance from the stagnant mobile phase will become less significant. It was demonstrated that the stagnant mobile phase contribution to the mass transfer resistance decreased significantly from LC to supercritical fluid chromatography to gas chromatography [18].

In order to accurately estimate the contribution of mass transfer resistance from the stagnant mobile phase, any contribution to mass transfer resistance from the stationary phase must be eliminated; therefore, an unretained solute with low molecular weight was chosen. Figure I.3.2 shows the experimental results of plate height as a function of mobile phase linear velocity for 1.5 and 3.0 μm nonporous and porous particles when nitromethane was used as an unretained solute [19]. It can be seen that at high linear velocities, columns packed with nonporous particles produced smaller plate heights for both 1.5 and 3.0 μm particles. The difference in plate height between porous and nonporous particles, however, was reduced significantly from 3.0 to 1.5 μm. The

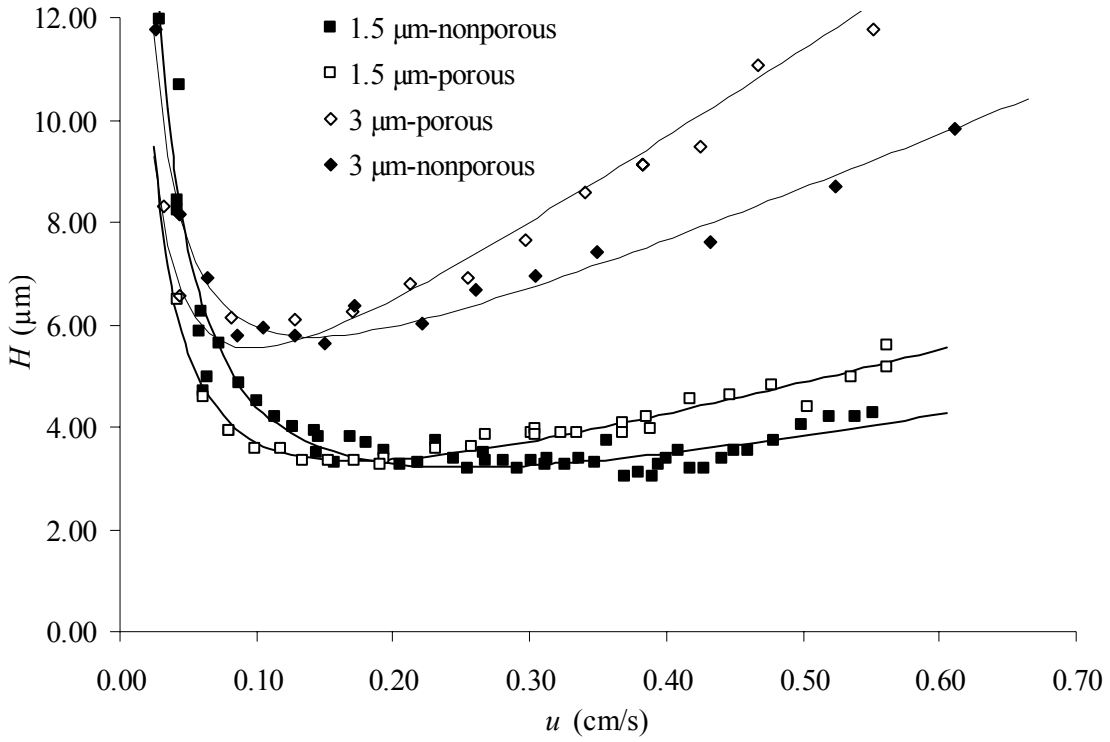

Figure I.3.2. van Deemter curves for 1.5 and 3.0 µm porous and nonporous particles. Conditions: 30 cm × 75 µm i.d. and 60 cm × 75 µm i.d fused silica capillary columns for 1.5 µm particles and 3.0 µm particles, respectively; 100% acetonitrile mobile phase; nitromethane analyte; 214 nm UV detection. Key: ■ 1.5 µm Micra nonporous C_{18} particles; □ 1.7 µm porous ACQUITY C_{18} particles; ♦ 3 µm nonporous Micra C_{18} particles; ◊ 3 µm porous YMC C_{18} particles. The plate heights for 1.7 µm particles were corrected to those for 1.5 µm particles by multiplying by 1.5/1.7 for comparison.

Table I.3.1. van Deemter coefficients for porous and nonporous particles.

	1.5 μm		3.0 μm	
	Porous ($r^2 = 0.94$)	Nonporous ($r^2 = 0.93$)	Porous ($r^2 = 0.98$)	Nonporous ($r^2 = 0.98$)
A ($\times 10^{-4}$)	0.88 ± 0.15	0.60 ± 0.29	2.04 ± 0.31	2.62 ± 0.22
B ($\times 10^{-4}$ cm^2 s^{-1})	0.21 ±0 .01	0.33 ± 0.02	0.17 ± 0.01	0.22 ± 0.01
C ($\times 10^{-4}$s)	7.13 ± 0.34	5.15 ± 0.71	18.01 ± 0.76	11.50 ± 0.57

Conditions: same as in Figure I.3.2.

experimental data shown in Figure I.3.2 were analyzed using least-squares analysis according to the van Deemter equation

$$H = A + \frac{B}{u} + C\,u \qquad \text{(I.3.2)}$$

where H is the plate height, u is the linear velocity of the mobile phase, and A, B, and C are constants which account for contributions to band broadening from eddy diffusion, longitudinal diffusion, and resistance to mass transfer of analytes, respectively. The van Deemter A, B, and C terms calculated from Figure I.3.2 are listed in Table I.3.1. The R^2 values for all columns were around 0.95. This indicates that the LC data fit the van Deemter equation quite well. The results show that the A term for 3.0 μm particles is higher than that obtained for 1.5 μm particles. This can be explained by the direct relationship of the A term to the particle size. In addition, no obvious relationship was observed between the B term and the particle size. However, the B terms for nonporous particles are slightly higher than those for porous particles. The possible reason for this is that the constriction and tortuosity factors for columns packed with nonporous particles are favorable for free longitudinal molecular diffusion because nonporous particles have a solid sphere structure and smooth surface [20].

Table I.3.1 also shows that the C terms for nonporous particles are lower than those for porous particles. If the mass transfer resistance for the stagnant mobile phase is considered to be the only difference in C terms between nonporous and porous particles, the difference can be used as an estimate of the contribution of the mass transfer resistance from the stagnant mobile phase to the plate height [19]. Comparing the differences in C terms in Table I.3.1, it can be seen that the C term difference decreased from 7.5 to 2.0 when the particle size was reduced from 3.0 to 1.5 μm. This result is in

agreement with the prediction by equation (I.3.1) that $C_{stagnant}$ is inversely proportional to the square of the particle size. This can readily be explained by the fact that the distance a solute must diffuse in pores decreases as the particle size decreases. These results suggest that sub-2 μm nonporous particles provide no significant efficiency advantage over porous particles for fast separations of small molecules.

Applications of LC are usually accomplished using retained solute conditions. Comparisons of efficiencies between porous and nonporous particles were also made using retained solute conditions for which the retention factors of a specific compound on both porous and nonporous particles were similar. Figure I.3.3 shows a plot of plate height versus linear velocity for a retained compound, ethyl 4-hydroxybenzoate. Conditions were chosen so that similar retention factors were obtained for both porous and nonporous columns. It can be seen that the plate heights for porous and nonporous columns were closer to each other in the high linear velocity part of the van Deemter plot, compared to results for an unretained compound. In order to obtain similar retention factors, highly aqueous mobile phases are needed for nonporous particles. Such mobile phases often lead to low diffusion coefficients and, as a result, low efficiencies. Consequently, the improvement in efficiency due to the use of nonporous particles can be offset by the low solute diffusion coefficients of solutes in the highly aqueous mobile phase. This makes the difference in efficiencies between porous and nonporous particles less significant at high linear velocities.

Kinetic properties. Figure I.3.4 shows the relationship between pressure and linear velocity for porous and nonporous particles under the same conditions as for Figure I.3.3.

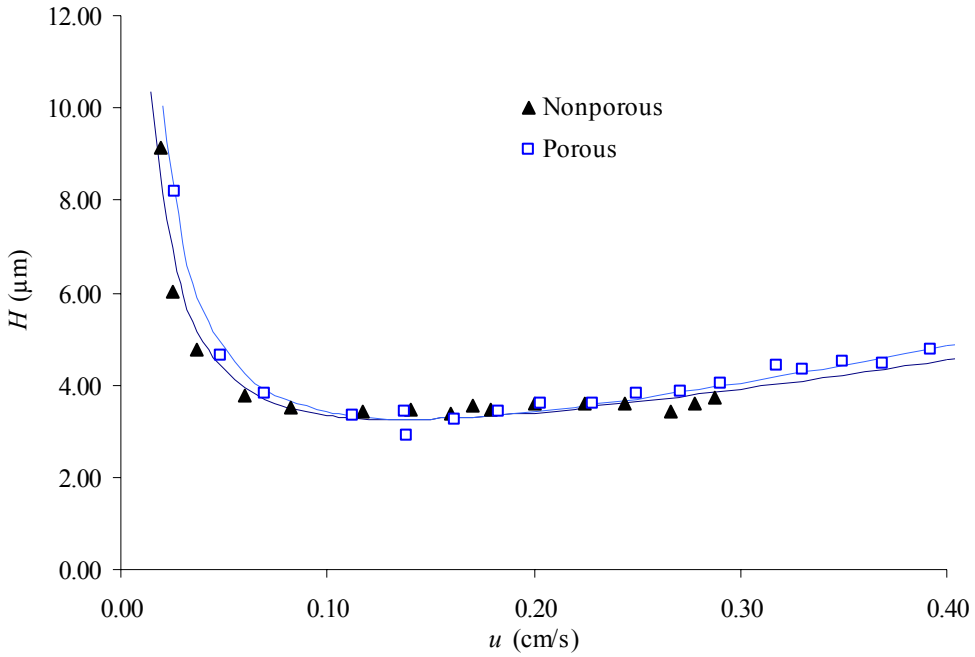

Figure I.3.3. Plate height versus linear velocity for an retained compound. Conditions: 30 cm × 75 µm i.d. fused silica capillary; 70% acetonitrile/30% 20 mM HAc/NaAc buffer, pH 3.5, for 1.7 µm porous BEH C_{18} particles; 30% acetonitrile/70% 20 mM HAc/NaAc buffer, pH 3.5, for 1.5 µm Micra nonporous C_{18} Micra particles; ethyl 4-hydroxybenzoate analyte; 254 nm UV detection. The plate heights for 1.7 µm particles were corrected to those for 1.5 µm particles by multiplying by 1.5/1.7 for comparison.

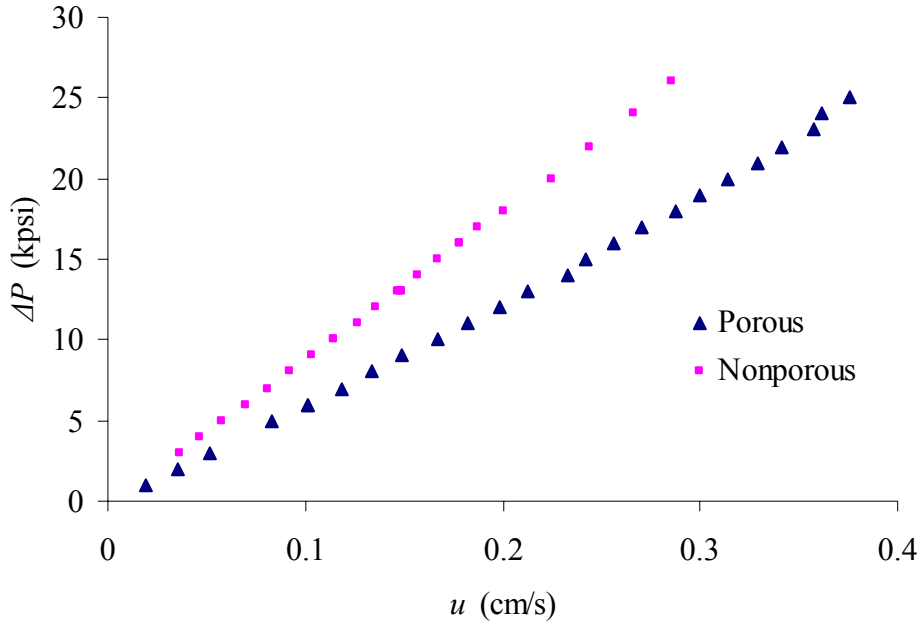

Figure I.3.4. Pressure drop vs linear velocity. Conditions: 75 µm i.d. fused silica capillary; uracil unretained marker. The data for the column containing 1.7 µm porous particles were adjusted for comparison to those for the column containing 1.5 µm nonporous particles according to equation (I.1.2) to eliminate the effects caused by differences in column length and particle size. Other conditions are the same as in Figure I.3.3.

The slopes of the plots in Figure I.3.4 represent the rate of change in pressure drop of each column as a function of the linear velocity. The experimental conditions were the same as in Figure I.3.3. A more aqueous mobile phase is required for nonporous particles in order to obtain similar retention factors. A 70:30 acetonitrile/20 mM HAc/NaAc (pH 3.5) mobile phase for a column packed with 1.7 μm BEH C_{18} porous particles provided a similar retention factor as 30:70 acetonitrile/20 mM HAc/NaAc (pH 3.5) mobile phase for 1.5 μm Micra nonporous C_{18} particles when ethyl 4-hydroxybenzoate was used as solute. Consequently, a nonporous packed column with acetonitrile/20 mM HAc/NaAc (pH 3.5) mobile phase provided about 1.38 times higher pressure drop than a porous packed column with acetonitrile/20 mM HAc/NaAc (pH 3.5) mobile phase. Therefore, a column packed with nonporous particles produces higher pressure drops than a column packed with porous particles in many situations in practice because the former requires a mobile phase with higher aqueous composition, which has higher viscosity.

Figure I.3.5 shows a kinetic Poppe plot obtained by using equations (I.2.1) and (I.2.2) and the (H, t_0) pairs from experiments conducted under unretained solute conditions. A kinetic plot is actually an extrapolation of results obtained from a real column assuming that the plate height remains the same at the same linear velocity no matter what the column length is, or that the packing quality remains the same as the column in the original experiment. The curve in the Poppe plot indicates the shortest plate time to achieve a desired plate number [21]. Therefore, every point in a Poppe plot actually represents a virtual column that can achieve the required plate number in the shortest plate time. The lengths of these virtual columns are usually different from each other.

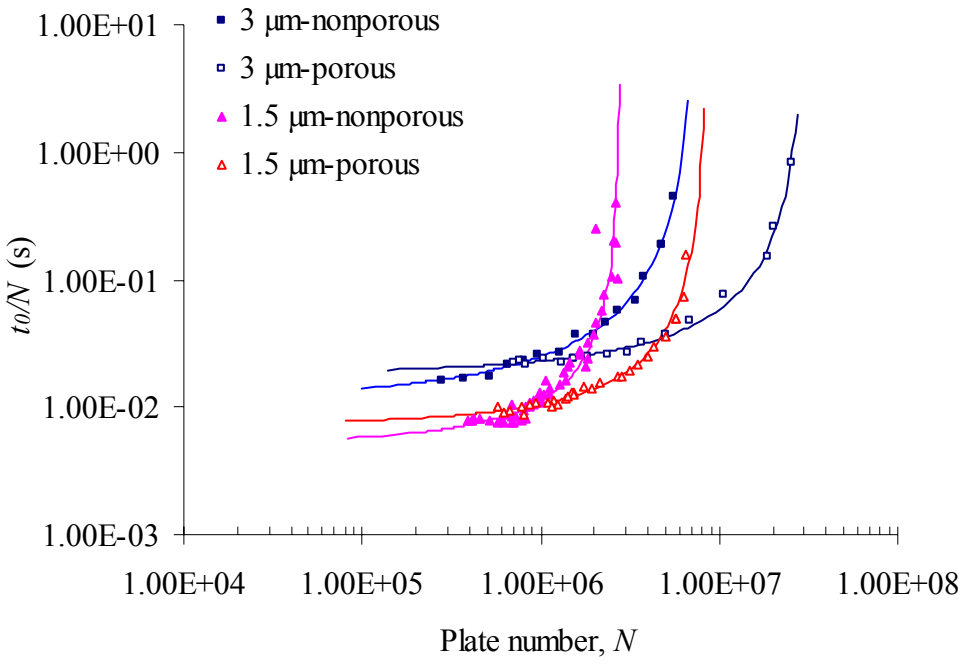

Figure I.3.5. Poppe plot for sub-2 µm porous and nonporous particles. Conditions: original (H,t_0) data obtained in experiments for Figure I.3.2; maximum inlet pressure was set at 25 kpsi.

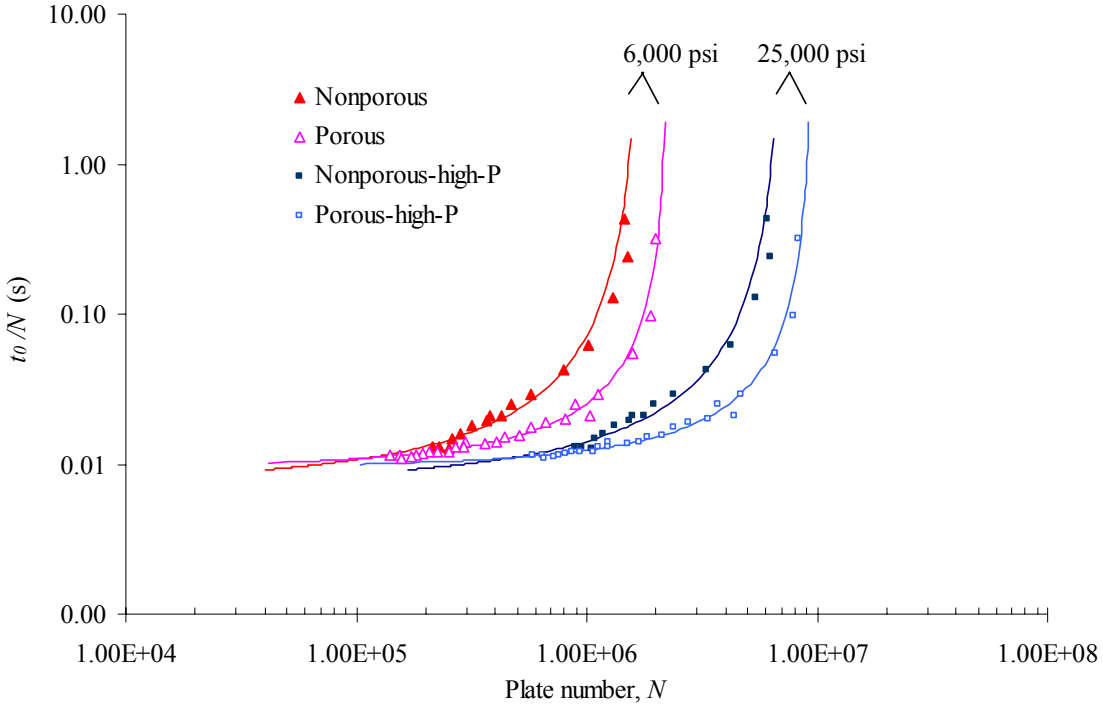

Figure I.3.6. Poppe plots for different maximum inlet pressures. Original data from retained solute conditions in Figure I.3.3.

The plate time increases rapidly after certain values of the required plate number. The curve appears to approach some vertical asymptote with a plate number, N_{max}, as predicted by Poppe [22]. A plate time that is too long represents a separation that cannot be accomplished in practice. This sets limitations of the stationary phase for maximum inlet pressure and mobile phase. Comparing porous and nonporous particles of the same sizes in Figure I.3.5, it can be seen that the maximum plate numbers, N_{max}, achievable for porous particles were greater than those for nonporous particles, probably due to the higher column permeability of columns packed with porous particles, which allows longer columns to be used under the specific maximum inlet pressure. As for the maximum speed achievable, porous particles gave shorter plate times at higher plate numbers than nonporous particles, while nonporous particles gave shorter plate times at lower plate numbers.

It can be seen by comparing particles of different sizes in Figure I.3.5 that larger particles have vertical asymptotes at greater plate numbers. Keep in mind that large plate number does not necessarily mean higher column efficiency, which can be expressed by plate number per unit length. The plate times and, hence, the analysis times for small particles are usually shorter in the lower plate number range than for large particles. This means that smaller particles can provide faster separations. These results are similar to those reported recently [21].

It can be seen from Figure I.3.6 that an increase in the maximum inlet pressure achievable could increase N_{max} and also shorten the plate times for larger required plate number, but the minimum plate times, which usually are achieved for lower plate numbers, did not show much difference. Similar phenomena were also observed by other

researchers [21, 23]. This means that higher inlet pressures, as occurs when moving from HPLC to UHPLC, will increase the highest plate numbers achievable for the packed bed.

I.3.4. Conclusions

The efficiency difference between porous and nonporous particles under unretained solute conditions, which results mainly from the contribution of mass transfer resistance from the stagnant mobile phase in the pores, decreased significantly for small molecules when the particle size was reduced from 3 to 1.5 μm. Under retained solute conditions, the efficiencies of sub-2 μm porous and nonporous particles were quite similar in the high linear velocity range. When comparing results for similar retention factors, we can see that pressure drops for nonporous particles were higher than those for porous particles in practice because highly aqueous mobile phases are required for nonporous particles to obtain similar retention factors. Kinetic plots derived from data obtained in this research showed that with a specific maximum inlet pressure, porous particles can generate higher N_{max}, the highest possible plate number, than nonporous particles; as for maximum speed, the porous particles gave shorter plate times for higher required plate numbers, but longer plate times for lower required plate numbers when compared with nonporous particles of the same particle size.

References

1. Martin, A.J.P.; Synge, R.L.M. *Biochem. J.* **1941**, *35*, 1358-1368.

2. Snyder, L.R. *Anal. Chem.* **2000**, *72*, 412A-420A.

3. Kirkland, J.J. *J. Chromatogr. Sci.* **2000**, *38*, 535-544.

4. Barder, T.J.; Wohlman, P.J.; Thrall, C.; DuBois, P.D. *LC-GC* **1997**, *15*, 918-926.

5. MacNair, J.E.; Lewis, K.C.; Jorgenson, J.W. *Anal. Chem.* **1997**, *69*, 983-989.

6. Mellors, J.S.; Jorgenson, J.W. *Anal. Chem.* **2004**, *76*, 5441-5450.

7. Wu, N.; Collins, D.C.; Lippert, J.A.; Xiang, Y.; Lee, M.L. *J. Microcol. Sep.* **2000**, *12*, 462-469.

8. Wu, N.; Lippert, J.A.; Lee, M.L. *J. Chromatogr. A* **2001**, *911*, 1-12.

9. Afeyan, N.B.; Gordon, N.F.; Mazsaroff, I.; Varady, L.; Fulton, S.P.; Yang, Y.B.; Regnier, F.E. *J. Chromatogr.* **1990**, *519*, 1-29.

10. Kirkland, J.J.; Truszkowski, F.A.; Jr., C.H.D.; Engel, G.S. *J. Chromatogr.* **2000**, *890*, 3-13.

11. Horvath, C.; Lin, H.-J. *J. Chromatogr.* **1978**, *149*, 43-70.

12. Stegeman, G.; Kraak, J.C.; Poppe, H. *J. Chromatogr. A* **1993**, *634*, 149-159.

13. Issaeva, T.; Kourganov, A.; Unger, K. *J. Chromatogr. A* **1999**, *846*, 13-23.

14. Swartz, M.E. *J. Liq. Chromatogr.* **2005**, *28*, 1253-1263.

15. Seifar, R.M.; Kraak, J.C.; Kok, W.T.; Poppe, H. *J. Chromatogr. A* **1998**, *808*, 71-77.

16. Lippert, J.A.; Xin, B.; Wu, N.; Lee, M.L. *J. Microcol. Sep.* **1999**, *11*, 631-643.

17. Xiang, Y.; Liu, Y.; Stearns, S.D.; Plistil, A.; Brisbin, M.P.; Lee, M.L. *Anal. Chem.* **2006**, *78*, 858-864.

18. Wu, N.; Tang, Q.; Shen, Y.; Lee, M.L. *Anal. Chem.* **1999**, *71*, 5084-5092.

19. Wu, N.; Liu, Y.; Lee, M.L. *J. Chromatogr. A* **2006**, *1131*, 142-150.

20. Giddings, J.C. *Dynamics of Chromatography, Part I. Principles and Theory*; Marcel Dekker: New York, 1965.

21. Villiers, A.d.; Lestremau, F.; Szucs, R.; Gelebart, S.; David, F.; Sandra, P. *J. Chromatogr. A* **2006**, *1127*, 60-69.

22. Poppe, H. *J. Chromatogr. A* **1997**, *778*, 3-21.

23. Desmet, G.; Clicq, D.; Gzil, P. *Anal. Chem.* **2005**, *77*, 4058-4070.

I.4. Diamond Particles

I.4.1. Introduction

Rationale. As mentioned earlier in this dissertation, the exploration of stationary phases in LC has been a continuous process. Researchers are always searching for new stationary phases that perform better and have better characteristics. Several reasons make diamond particles worth evaluating as a stationary phase support for LC. First, diamonds exhibit a combination of extreme hardness, chemical inertness, high thermal conductivity and other unique properties [1, 2]. Their strong mechanical strength allows them to withstand the high pressures in UHPLC systems. Due to their chemical stability, they can be used under harsh chemical environments such as in solutions with extreme pH values. Good thermal conductivity helps dissipate any heat generated in the column. Second, diamonds are composed of carbon atoms with sp^3 hybrid orbitals, just as are carbon atoms in organic compounds. This means that the chemistry involved is similar to that of typical organic chemistry, and many well studied reactions can be utilized for modifying the surface of the diamond particles. The versatility in derivatization of the surface leads to different types of stationary phases. Third, diamonds are known to be biocompatible materials [3]. This point is important today because of the increasing requests for separations of biomolecules which greatly rely on LC techniques. Stationary phases used in bioanalysis must be compatible with the analytes of interest. Fortunately, a breakthrough in the production of diamond particles occurred in the mid-1950s [1], which greatly reduced the cost of using diamonds in a variety of applications including chromatography. As expected, stationary phases made from small particle sizes give high

efficiencies and short analysis time. Coincidentally, the production costs of diamond particles decrease as the particle size decreases.

One of the possible drawbacks of diamonds as stationary phases is their irregular shape. High column efficiencies usually come from stationary phases that have spherical shapes, small diameters, and narrow size distribution [4]. However, a recent study [5] reports no distinction in performance between spherically and irregularly shaped packing materials. Actually, it is not the shape of the particles but the porous structure of the packed bed, or the mobile phase zone, that mainly determines the column performance [6]. A monolithic column is a porous rod consisting of irregular porous and solid structures. When proper structures have been manufactured, monolithic columns can give column efficiencies comparable to those of particulate packed columns. Also, spherical porous diamond particles can be constructed from nanoscale diamond powders [7]. Therefore, the real issue is to determine the usefulness of the diamond surface for LC separations.

Previous research. Reports of applications of diamonds in chromatography are rare. The most relevant research was reported by Patel and co-workers [7]. They packed 4.6 mm i.d. columns with 3.8 μm average diameter porous disperse diamond (PDD) powders and conducted chromatographic experiments using small organic compounds as analytes. They found that the PDD columns showed opposite trends in retention patterns compared to a conventional octadecylsilane (ODS) column. Polar analytes were retained on the PDD column. They also obtained a partial separation of p- and o-xylene isomers, which are usually hard to separate on silica columns. Björkman et al. [8] reported fast chromatography of proteins on microchips made of diamond. The stationary phase was

an in-situ generated polymeric monolithic bed. Xu and Bowden [9] claimed in a patent that diamond powders chemically modified with various types of functional groups could be used as stationary phases for LC. However, they did not show any chromatographic experimental results.

Surface modifications of diamond particles. Diamond surfaces are partially oxidized during the manufacturing process so that they are terminated not only with hydrogen atoms but also with oxygen atoms. Chemical modification of diamond surfaces has been intensely studied during the last decade [10-19]. Although the surfaces of diamonds are hard to modify due to their chemical inertness, surface modification of diamond materials still can be conducted through various reactions, including fluorination [12, 14], chlorination [9], cycloaddition [13], radical addition with the aid of initiators [17, 20] or UV light [15, 19], hydrogenation [10, 21] and electrochemical reduction [22]. Usually, harsh reagents and conditions, such as fluorine gas and plasma or high temperature, were utilized to initiate reaction on the diamond surfaces [12, 14, 18, 21], and fluorination was regarded as an efficient way to modify and control the surface properties [12, 14]. Attaching long carbon chains on the diamond surface is especially attractive for applications of diamond particles as stationary phases in chromatography. Although most related papers focused on thin diamond films on surfaces, surface modification of diamond powders was also studied by several groups [16-18, 20, 23].

Diamond powders were usually hydrogenated first to generate hydrogen-terminated surfaces by heating the diamond powders in vacuum or in a hydrogen environment [16]. Matsumoto and co-workers [16, 17, 20, 23] reported modification of hydrogen-terminated surfaces of diamond powders through radical additions under mild reaction

conditions with benzoyl peroxide as radical initiators. The reactions were conducted with diamond particles suspended in a liquid phase, which facilitated reaction evenly on the surfaces of all particles. The presumed reaction scheme for this type of treatment is

$$\text{(diamond)–H} + C_6H_5COO\bullet \rightarrow \text{(diamond)} \bullet + C_6H_5COOH \qquad \text{(I.4.1)}$$

$$C_6H_5COO\bullet + \text{(diamond)}\bullet \rightarrow C_6H_5COO\text{–(diamond)} \qquad \text{(I.4.2)}$$

which involves the attachment of an organic peroxide to the diamond surface. Changes in the diamond surface were usually tracked by means of diffuse infrared spectroscopy. The researchers noticed [20, 23] that radicals from other reagents induced by the peroxide could also attach to the diamond surface. Actually, this type of reaction is a rather good route for preliminary trials to produce surface functionalized diamond particles for use as stationary phases in LC.

Another possible choice for modification of the surface of diamond particles for use in LC is to coat the surface with suitable polymers. Polymer coating has been extensively used in production of stationary phases. One of the most successful examples is the polybutadiene (PBD) coated zirconia particles [24], which exhibit chromatographic performance approaching that of silica-based stationary phases, but with additional high stability when using mobile phases at high and low pH and at high temperatures [25]. A typical coating procedure [26] involved first treating the particles with a solution containing low molecular weight PBD and radical initiator, and then removing the solvent to allow the deposition of PBD and initiator on the particle surface. Finally the particles were heated at a temperature of 120^{o}C to effect polymerization of PBD. There is no reason that this procedure could not be applied to materials other than zirconia. Actually, diamond surfaces could react with radicals generated during polymerization

and establish covalent connections with the PBD coating. This would produce more stable PBD coatings than on zirconia surfaces.

In this part of my dissertation, attempts to modify and coat diamond particles with a polymeric coating are described. Both bare and surface-modified diamond particles were packed into capillary columns, and chromatographic experiments were conducted using these columns using a UHPLC system.

I.4.2. Experimental

Chemicals and materials. Polybutadiene of molecular weight 5000 (20% vinyl, 80% *cis*- and *trans*-1,4-polybutadiene), dicumyl peroxide and acetone (analytical grade), and reagent grade (ACS grade) 1-octene, 1-chlorooctane and dodecane, were purchased from Aldrich (Milwaukee, WI, USA). HPLC grade acetonitrile, chloroform, and water were obtained from Fisher (Fair Lawn, NJ, USA). HPLC grade isopropanol was purchased from Mallinckrodt (Phillipsburg, NJ, USA) and HPLC grade hexane was purchased from EM Sciences (Gibbstown, NJ, USA). All buffers and solvents for chromatographic use were filtered through 0.22 μm pore size Durapore® membrane filters (Millipore, Bedford, MA). Similarly, samples were filtered through 0.2 μm pore size polytetrafluoroethylene syringe filters (Chromacol, Trumbull, CT). Scanning electron microscopy (JEOL 8401, JEOL, Peabody, MA, USA) was used to observe the size, shape, and state of aggregation of diamond particles.

UHPLC conditions. The UHPLC system used for evaluation of diamond particles in LC was the same as described in the previous chapter. The same packing system and procedure described previously were also used to pack columns with diamond particles. One difference was that the fused silica capillary was packed with a segment of bare

silica beads both before and after being packed with diamond particles, and frits were sintered in the silica segments close to the packed diamond particles.

Procedure for coating diamond particles with polybutadiene. Two procedures were tested for coating diamond particles with PBD: dry and wet. The dry method basically followed a typical procedure for PBD coating of zirconia particles. A 50 mL volume of polybutadiene (5000 average molecular weight) solution in hexane was added to the diamond particles. The slurry was sonicated for 5 min to suspend the particles in the solution. Dicumyl peroxide crosslinking agent was then added to the slurry. The mixture was sonicated for 5 min and then swirled for at least 2 h, after which the solvent was evaporated by applying low vacuum at 55 ^{o}C. Then the coated particles were dried at this temperature for an additional 15 min. The polymer was thermally crosslinked in a vacuum oven at 120 ^{o}C for 5 h.

For the wet method, dodecane was used as solvent for the low molecular weight polybutadiene solution; 50 mL of this solution was added to a flask containing diamond particles and the diamond particles were suspended by sonicating for 5 min. After the initiator, dicumyl peroxide, was added to the flask, the slurry was sonicated for another 5 min and then heated to 120^{o}C for 2 h under a nitrogen environment. After allowing the slurry to cool to room temperature, the diamond particles were filtered and washed with chloroform, and then dried and stored under vacuum.

Chemical modification of diamond particle surfaces. The diamond particles were first hydrogenated by heating at high temperature. Typically, approximately 1 g of diamond particles was placed in an alumina boat and heated under a hydrogen

atmosphere to high temperature for 2 h. After cooling down to room temperature still in hydrogen, the diamond particles were stored under vacuum.

Preliminary experiments to chemically modify the hydrogen-terminated diamond particles were conducted following a procedure described in the literature [16, 20]. The diamond particles were first suspended in organic solvent by sonicating for 5 min, radical initiator was added to the slurry, and the flask was sonicated again for 5 min. A reagent that provided additional radical species with alkyl groups was added for some experiments. Then the slurry was heated to a temperature suitable for the initiator to release radical species, and held at that temperature for 2 h. Then the diamond particles were filtered, washed with chloroform, dried, and stored under vacuum.

I.4.3. Results and Discussion

Chromatographic behavior of bare diamond particles. Figures I.4.1A and B show images of diamond particles obtained by means of a scanning electron microscope (SEM). The diamond particles were irregularly-shaped. From Figure I.4.1C it can be seen that the diamond particles were packed tightly inside the fused silica capillary.

Figure I.4.2 shows chromatograms of a mixture of three small molecules using mobile phases with different acetonitrile concentrations. The three test compounds were phenol, 3,5-dimethylphenol and 2-napthol. The chromatograms illustrate two features: (1) compounds eluted in order of polarity from highest to lowest, and (2) symmetrical peaks were obtained for polar compounds such as phenol, but not for less polar compounds such as 2-naphthol. Decreasing the concentration of the organic component in the mobile phase produced greater retention and baseline separation of the three compounds. These

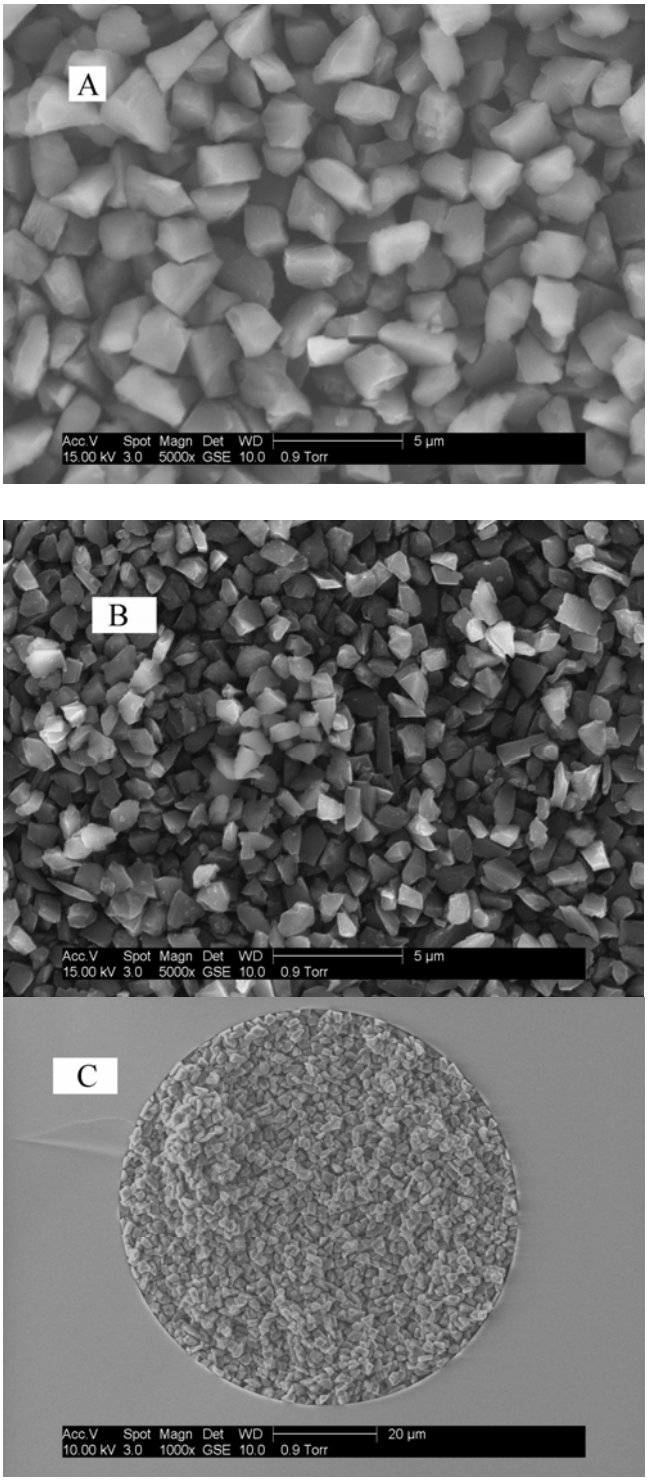

Figure I.4.1. SEM images of diamond particles. (A) 2 µm diamond particles, (B) 1 µm diamond particles, (C) 2 µm diamond particles packed inside a capillary column.

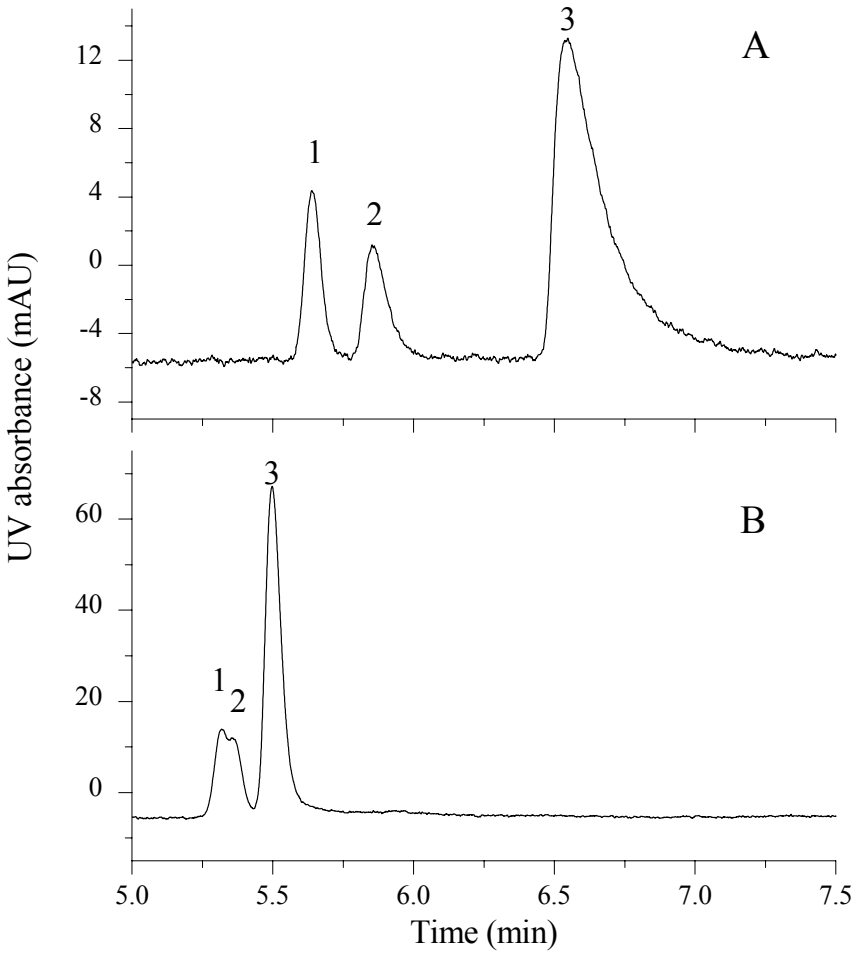

Figure I.4.2. Chromatograms of a mixture of three small molecules. Conditions: 37 cm × 75 μm i.d. fused silica capillary column, ~ 2 μm diamond particles; (A) 85% water (40 mM $NaHPO_4$, pH = 7) 15% acetonitrile; (B) 75% water (40 mM $NaHPO_4$, pH = 7) 25% acetonitrile; 15 kpsi. Peak identifications: (1) phenol, (2) 3,5-dimethylphenol, (3) 2-napthol.

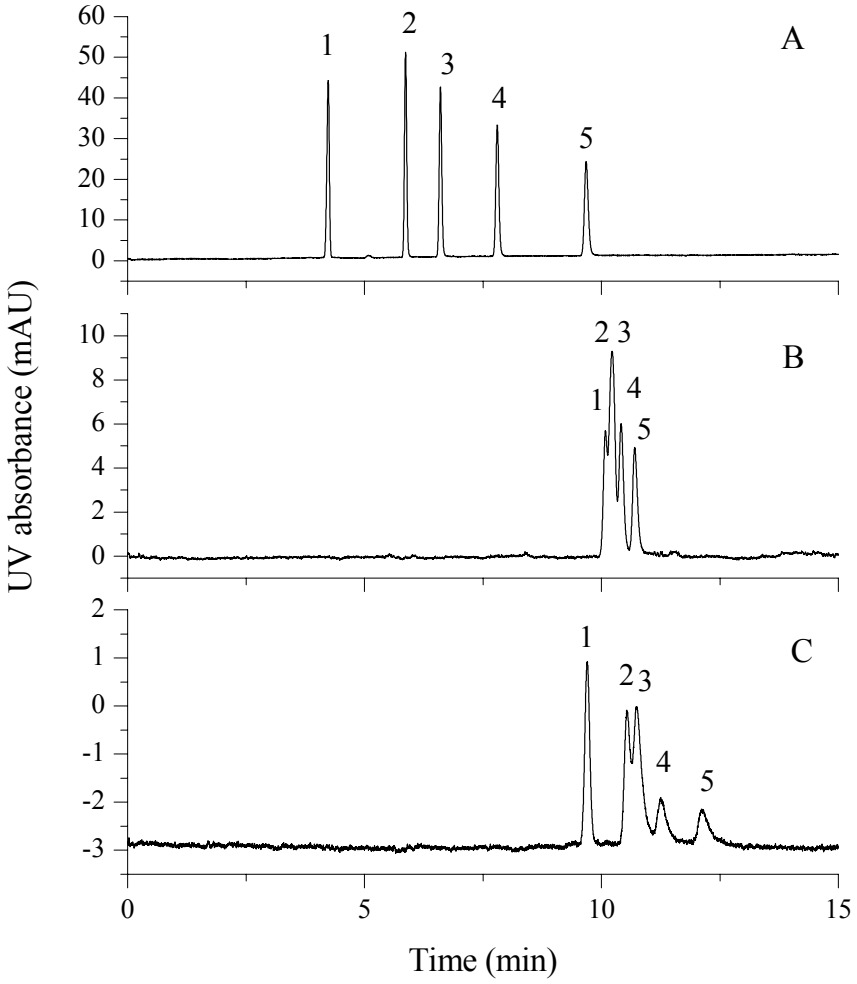

Figure I.4.3. Chromatograms of parabens. Conditions: (A) 28.4 cm × 75 μm i.d. fused silica capillary, 1.5 μm ODS-II nonporous particles; (B) 29.0 cm × 75 μm i.d. fused silica capillary, 2 μm bare diamond particles; (C) 21.5 cm × 75 μm i.d. fused silica capillary, 1 μm bare diamond particles; water (20 mM NH_4Ac, pH = 3.5)/acetonitrile (70:30, *v*/*v*); 254 nm UV detection. Peak identifications: (1) uracil, (2) methyl paraben, (3) ethyl paraben, (4) propyl paraben, (5) butyl paraben.

results indicated that the surfaces of the diamond particles were hydrophobic, and less polar compounds had stronger interactions with the diamond surfaces, were retained longer, and produced more tailing peaks. The bare diamond column behaved as a reversed phase column, allowing more polar compounds to elute early, and more aqueous mobile phases to retain organic compounds longer.

Figure I.4.3 shows chromatograms obtained for the separation of several alkyl 4-hydroxybenzoates. Figure I.4.3A shows baseline separation of a mixture of uracil and four parabens using a silica-based ODS column. When using a column containing 2 μm bare diamond particles, the same mixture could not be completely separated, as shown in Figure I.4.3B. When the sizes of the diamond particles were reduced to 1 μm (Figure I.4.3C), a better separation was obtained, but the mixture was still not separated completely. Obviously, the resolution must be improved for practical application. Again, tailing was observed for peaks representing less polar compounds.

Figure I.4.4 shows plots of the height equivalent of a theoretical plate, *H*, versus linear velocity for columns packed with 2 μm and 5 μm diamond particles. It can be seen that smaller particles gave smaller plate heights. The minimum plate height for the 2 μm column was approximately 4.7 μm, and that for the 5 μm column was approximately 9.5 μm. The minimum plate height was approximately proportional to the particle sizes and the reduced plate heights were approximately 2.4 μm and 1.9 μm, respectively, which are comparable to those of conventional silica columns. This indicates that efficiencies for small polar compounds were rather good. However, the problem of tailing, or adsorption,

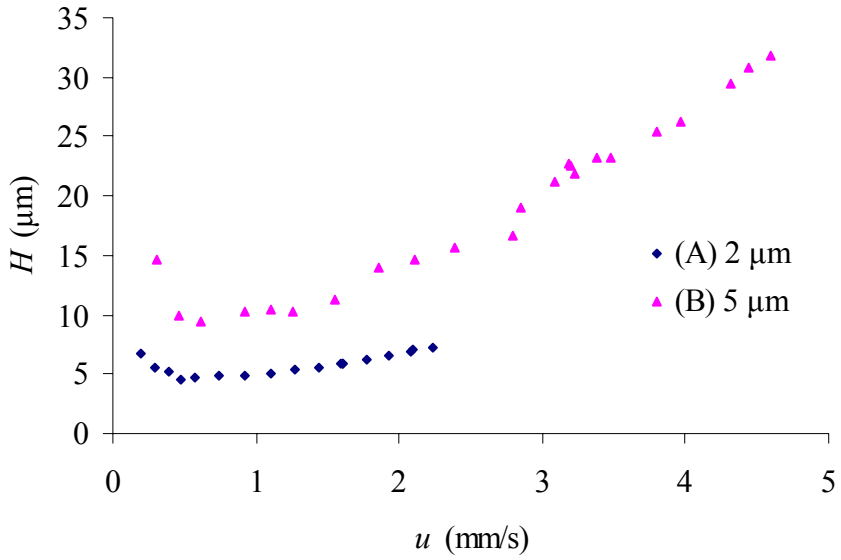

Figure I.4.4. Plate height versus linear velocity for columns containing particles of different sizes. (A) 29.4 cm × 75 µm i.d. fused silica capillary, 2 µm diamond particles, water (20 mM NH_4Ac, pH = 3.5)/acetonitrile (70:30, *v*/*v*), methyl 4-hydroxybenzoate; (B) 40 cm × 75 µm fused silica capillary, 5 µm diamond particles, water (0.1% TFA)/ acetonitrile (95:5, *v*/*v*), phenol. 254 nm UV detection.

of less polar compounds must be solved in order to improve the resolving power of the bare diamond particle column.

PBD-coated columns. Obviously, surface treatments are required to further improve the selectivity of the diamond particles for LC. One approach for this is coating the particles with polymers. Polybutadiene (PBD) coated zirconia particles have shown good chromatographic behavior [24, 25]. Therefore, preliminary experiments were conducted to explore the feasibility of applying the PBD coating process to diamond particles.

The dry PBD coating procedure [26] was first tried. In general, the procedure involved treating the diamond particles with a solution containing low molecular weight PBD and a radical initiator, evaporating the solvent to allow deposition of PBD and initiator molecules on the diamond surface, and heating in vacuum to induce polymerization. It was found that the resulting particles stuck together and were difficult to disperse. It is possible that the PBD reagent molecules connected diamond particles together through polymerization. The PBD-coated diamond particles had to be ground with an alumina mortar and pestle to separate the connected particles before packing. The wet method was also tried for PBD-coating. A reaction slurry was obtained by suspending the diamond particles in dodecane with PBD polymer and initiator. Then the slurry was heated to 120^{o}C for polymerization while nitrogen was bubbled through the slurry. The resulting PBD-coated diamond particles did not appear to aggregate.

Figure I.4.5 shows chromatograms obtained for the same mixture of uracil and four parabens as shown in Figure I.4.3. By comparing Figures I.4.5A and B with Figure

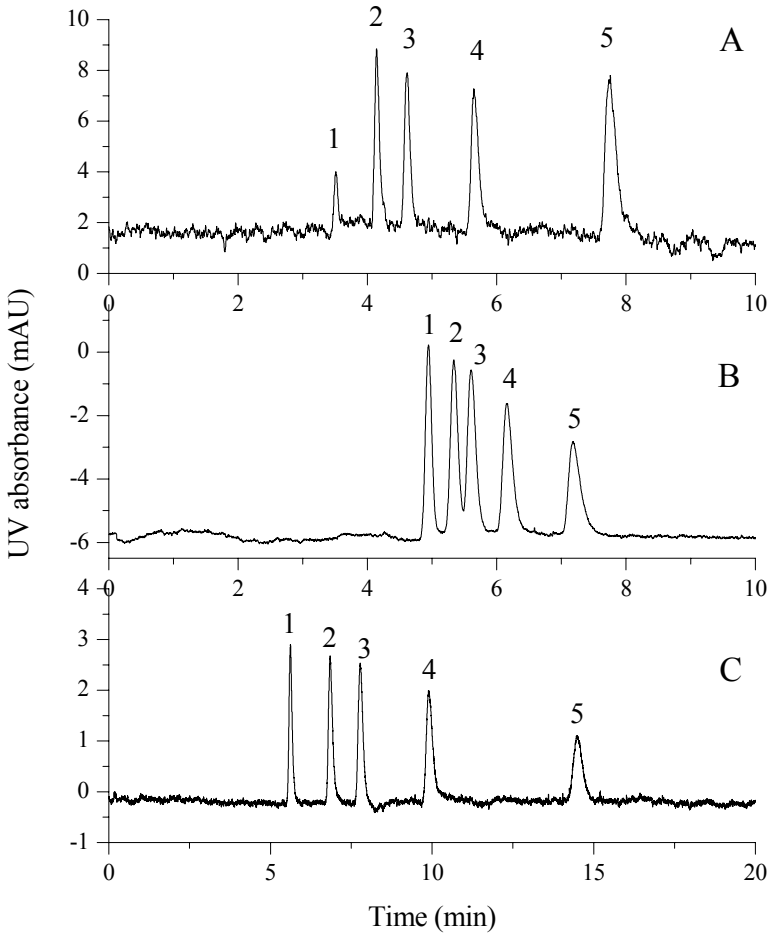

Figure I.4.5. Separation of parabens using a column packed with PBD-coated diamond particles. Conditions: (A) 18.8 cm × 75 μm i.d. fused silica capillary, 2 μm polybutadiene-coated (dry method) diamond particles; (B) 24.5 cm × 75 μm i.d. fused silica capillary, 2 μm polybutadiene-coated (wet method) diamond particles; (C) 16 cm × 75 μm i.d. fused silica capillary, 1 μm polybutadiene-coated (wet method) diamond particles; water/acetonitrile (70:30, *v*/*v*); 10 kpsi inlet pressure; 254 nm UV detection. Peak identifications: (1) uracil, (2) methyl 4-hydroxybenzoate, (3) ethyl 4-hydroxybenzoate, (4) propyl 4-hydroxybenzoate, (5) butyl 4-hydroxybenzoate.

I.4.3B for 2 μm particles, and comparing Figure I.4.5C with Figure I.4.3C for 1 μm particles, it can be readily seen that the PBD coating provided great improvement in resolution. The tailing phenomenon also became insignificant, even for the least polar compound.

The resolution of two adjacent peaks can be expressed by the widely used equation

$$R_s = \frac{1}{4}(\alpha - 1)\sqrt{N}[\frac{k'}{k'+1}] \qquad \text{(I.4.3)}$$

where R_s is the resolution, k' is the average of k_1 *and* k_2 (the retention factors of the early and later eluting peaks), $\alpha = k_2/k_1$ is the separation factor representing separation selectivity, and N is the plate number. According to this equation, the resolution can be improved by either increasing the column efficiency as measured by plate number, or increasing the separation selectivity, α, or the retention factors. Figure I.4.6 shows that plate heights for the PBD-coated diamond column were much greater than those for the bare diamond column at the same linear velocities, which revealed that the PBD-coating did not offer any advantage with respect to column efficiency. Therefore, resolution improvement was accomplished by changing the retention behavior of the solutes on the column.

Comparisons of retention factors, k, and separation factors, α, between separations shown in Figure I.4.3C (1 μm bare diamond column) and Figure I.4.5C (1 μm PBD-coated diamond column) are summarized in Figure I.4.7. Clearly the retention factors as well as separation factors of solutes on the PBD-coated column were much greater than those for the same solutes on the bare diamond column. Figure I.4.7 is a representative example of a common observation in experiments relating columns packed with bare diamond particles and PBD-coated diamond particles. This

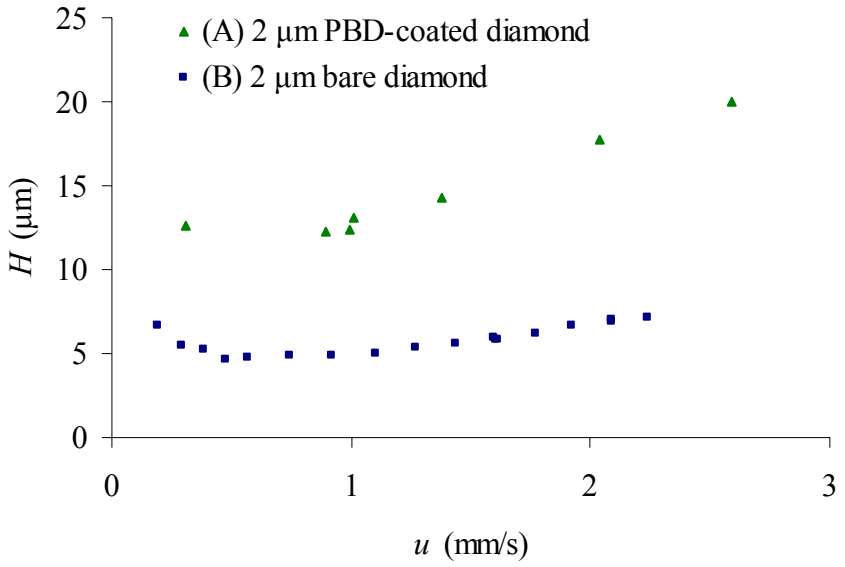

Figure I.4.6. Plot of height equivalent of a theoretical plate versus linear velocity. Conditions: (A) 11.2 cm × 75 µm i.d. fused silica capillary, 2 µm PBD-coated diamond particles; (B) 29 cm × 75 µm i.d. fused silica capillary, 2 µm bare diamond particle; water (20 mM NH_4Ac, pH = 3.5)/acetonitrile (70:30, *v*/*v*); 254 nm UV detection; methyl 4-hydroxybenzoate test solute.

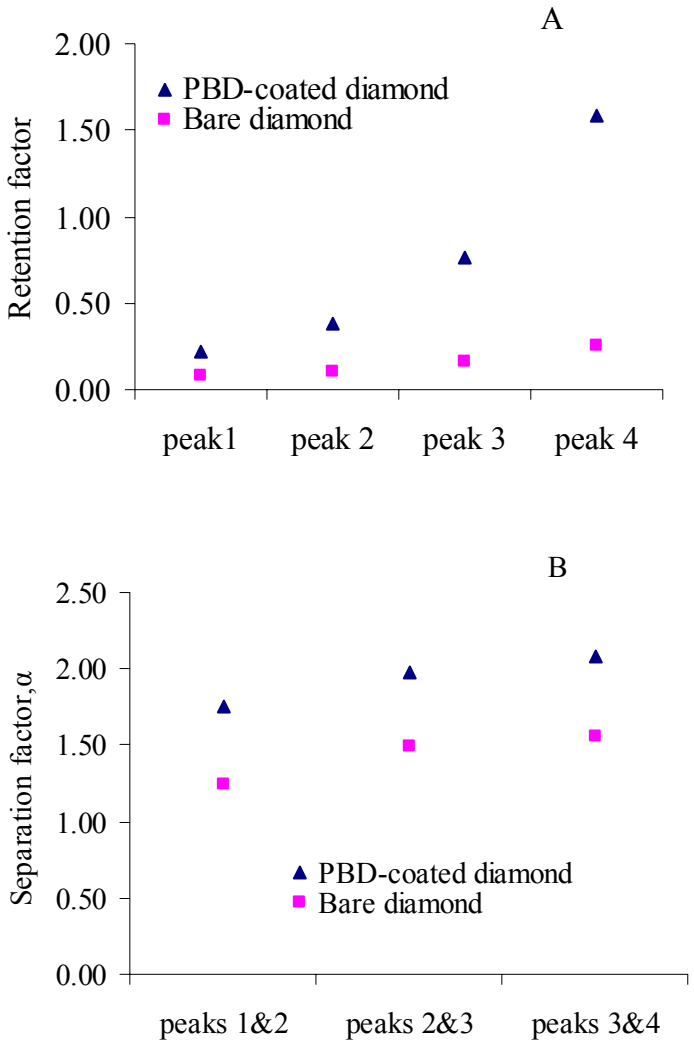

Figure I.4.7. Comparison between bare and PBD-coated diamond columns. (A) retention factors and (B) separation factors for adjacent peaks. Peak identifications: (1) methyl 4-hydroxybenzoate, (2) ethyl 4-hydroxybenzoate, (3) propyl 4-hydroxybenzoate, (4) butyl 4-hydroxybenzoate. Other conditions: see Figure I.4.3C for bare diamond column, see Figure I.4.5C for PBD-coated diamond column.

also can be seen by comparing the elution of uracil, an unretained marker, in Figures I.4.3C and I.4.5C, which eluted earlier on the PBD-coated column than on the bare diamond column.

The amount of PBD coating cannot be measured by the 'carbon content' method which is commonly used for polymer coated zirconia particles. However, the influence of polymer coating amount has been explored by varying the concentrations of polymer reagent and radical initiator. In the coating procedures, 27.3 mg of low molecular weight PBD reagent and 1.05 mg of dicumyl peroxide were used for batch I particles, whereas 55.5 mg of low molecular weight PBD reagent and 2.18 mg dicumyl peroxide were used for batch II particles; other conditions were the same for both batches of particles. Therefore, batch II, with more starting materials and higher initiator concentration, should have a thicker polybutadiene coating. Figure I.4.8 shows that the retention factors on columns packed with the more heavily coated batch II particles were greater than those of the same solutes on the less heavily coated particles. This is mainly due to greater solute interaction with the PBD coating (i.e., heavier coating means greater phase ratio and, hence, greater retention factors).

Figure I.4.9 shows the relationship between mobile phase linear velocity and inlet pressure for different columns. It can be seen that the larger the particle size, the greater the linear velocity at the same inlet pressure. The column packed with more heavily coated diamond particles gave greater linear velocity at the same inlet pressure compared to the column with less heavily coated particles, indicating that the PBD coating gave an effect similar to enlarging the particle size.

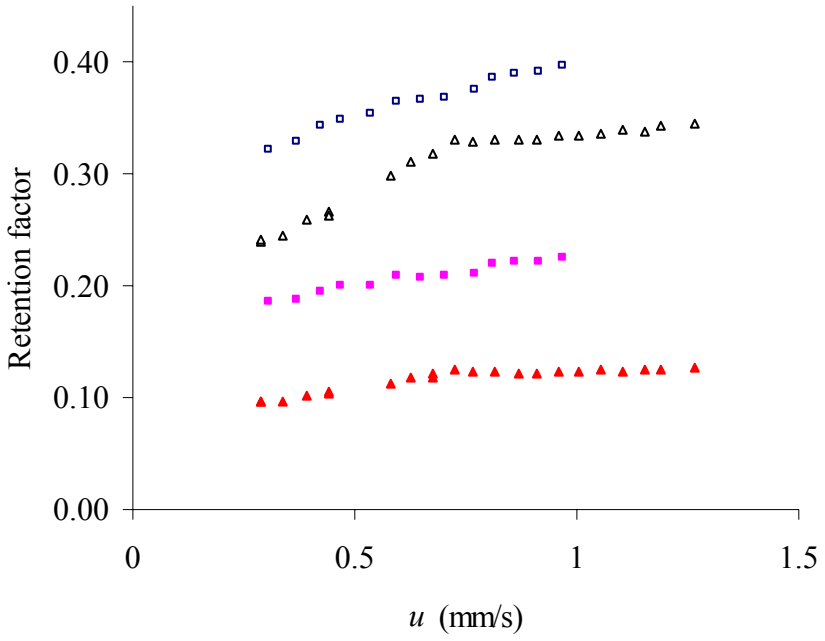

Figure I.4.8. Comparison of retention factors. Conditions: batch I, 20.1 cm × 75 μm i.d. fused silica capillary, 1 μm polybutadiene-coated (wet method) diamond particles; batch II, 20.0 cm × 75 μm i.d. fused silica capillary, 1 μm polybutadiene-coated (wet method) diamond particles; water/acetonitrile (70:30, *v*/*v*); 254 nm UV detection. Markers: hollow markers = propyl 4-hydroxybenzoate, solid markers = methyl 4-hydroxybenzoate; triangles—batch I particles, squares = batch II particles.

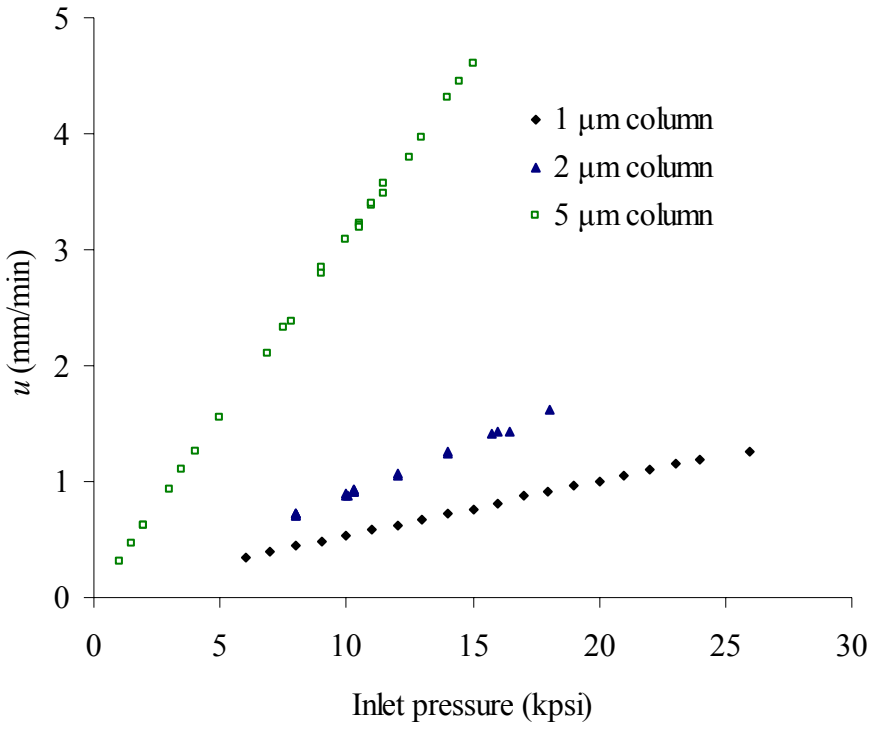

Figure I.4.9. Relationship of inlet pressure to linear velocity. Conditions: 1 µm diamond particles, 20.1 cm × 75 µm i.d. fused silica capillary, water (20 mM NH_4Ac, pH = 3.5)/acetonitrile (70:30, *v*/*v*); 2 µm diamond particles, 29.4 cm × 75 µm i.d. fused silica capillary, water/acetonitrile (90:10, *v*/*v*) + 0.1% TFA; 5 µm diamond particles, 40 cm × 75 µm i.d. fused silica capillary, water/acetonitrile (95:5, *v*/*v*) + 0.1% TFA.

Figure I.4.9 shows the relationship between linear velocity and inlet pressure for different columns. It can be seen that the larger the particle size, the greater the linear velocity at the same inlet pressure.

The column permeability can be estimated by the equation

$$K_v = \frac{\eta u_0 L}{\Delta P} \qquad \text{(I.4.4)}$$

where K_v is the column permeability, ΔP is the maximum inlet pressure of a chromatography system, L is the column length, u_0 represents the linear velocity, and η is the viscosity of the mobile phase. We calculated column permeabilities of 1.65×10^{-14}, 3.48×10^{-15}, and 1.68×10^{-15}, for 5 μm, 2 μm, and 1 μm particles, respectively. The column permeability of the 5 μm column is approximately 4.7 times that for the 2 μm column; the ratios of column permeabilities for the three columns were 9.83 : 2.06 : 1.

Columns packed with PBD-coated diamond particles can be utilized in fast separations with the aid of a UHPLC system. Figure I.4.10 shows that increasing the inlet pressure allowed fast separation of a mixture of parabens. The separation could be accomplished within 1.5 min when the inlet pressure was increased to 25 kpsi.

Chemical modification of diamond particles. Hydrogenation of the diamond particle surface is necessary for further chemical modification because it unifies the surface properties of the diamond particles. Hydrogenation was conducted by heating the diamond particles in an oven with hydrogen flow.

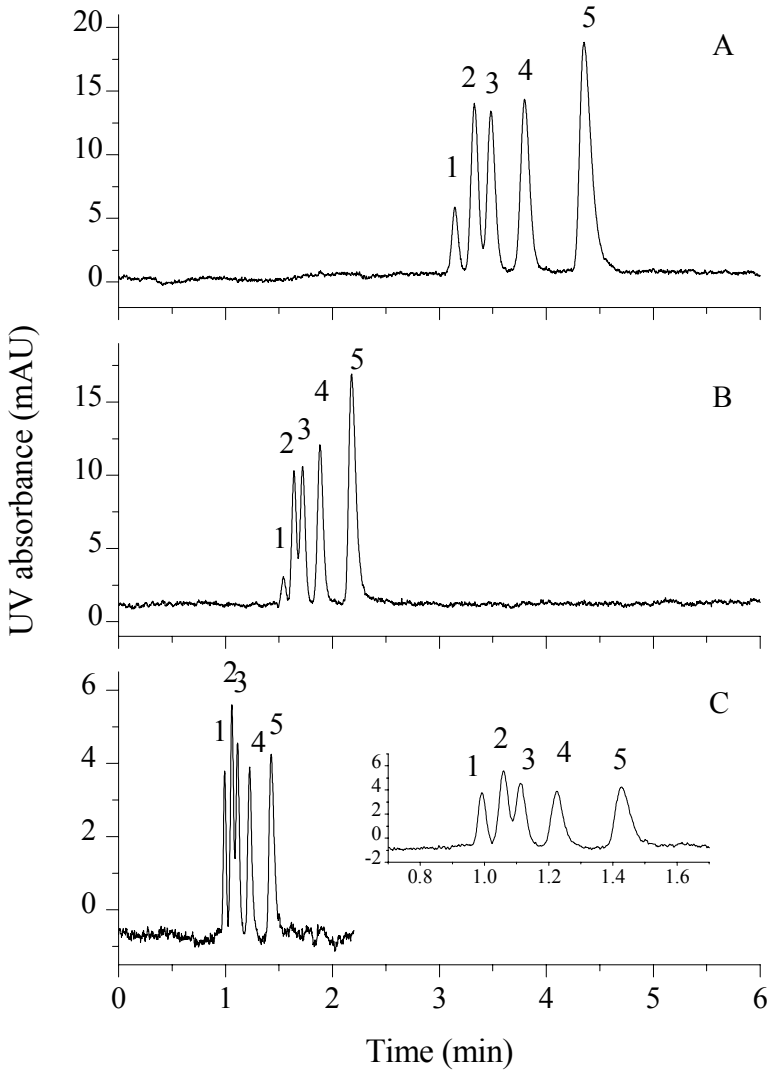

Figure I.4.10. Fast separation of small molecules. Conditions: 11.2 cm × 70 μm i.d. fused silica capillary, 2 μm PBD-coated diamond particles (dry method); water (40 mM NaH_2PO_4, pH = 7.0)/acetonitrile (60:40, *v*/*v*), 215 nm UV detection; (A) 7 kpsi, (B) 15 kpsi, (C) 25 kpsi inlet pressures. Peak identifications: (1) uracil, (2) methyl 4-hydroxybenzoate, (3) ethyl 4-hydroxybenzoate, (4) propyl 4-hydroxybenzoate, (5) butyl 4-hydroxybenzoate.

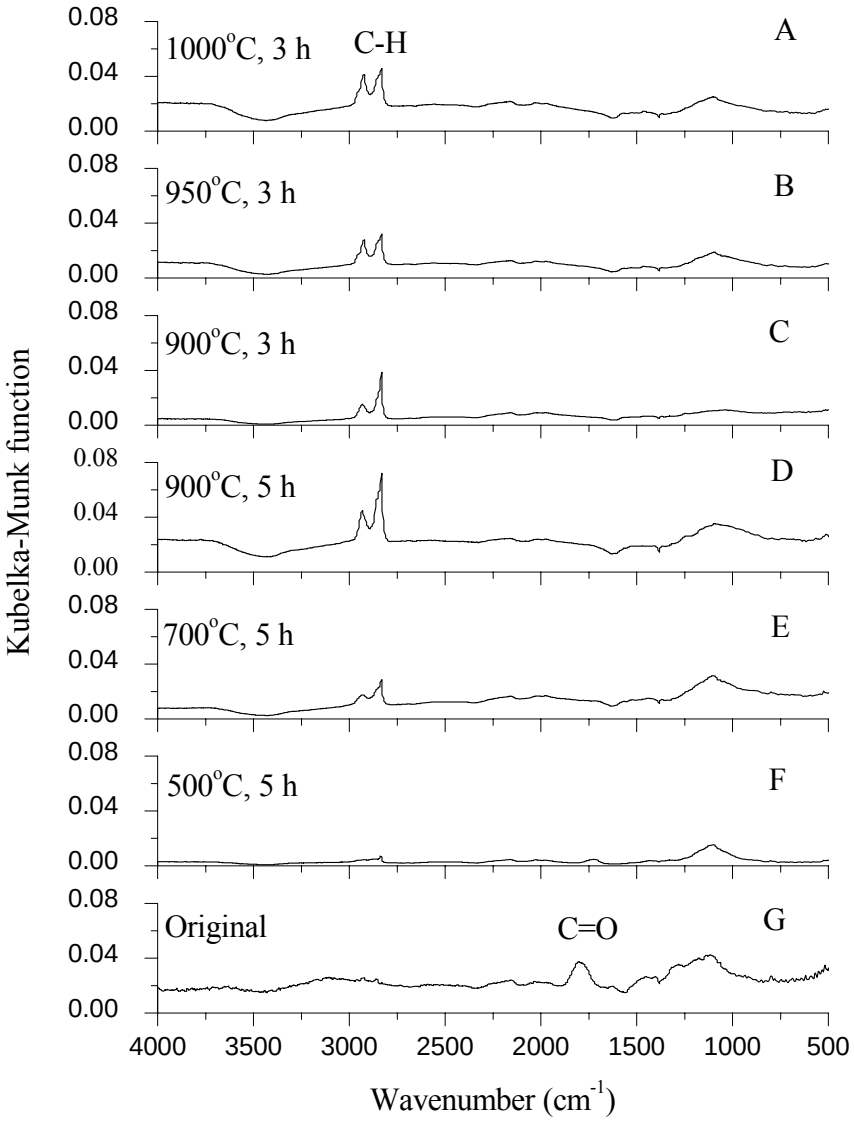

Figure I.4.11. Diffuse-reflectance FTIR spectra of diamond surfaces. Conditions: H_2 flow rate, 400 cm^3/min, temperatures and duration times given in figure.

Figure I.4.11 shows diffuse reflectance FTIR (DRIFT) spectra of diamond particles after heating at various temperatures for various periods of time. Peaks with a maximum around 2830 cm^{-1} were usually assigned to symmetrical stretching vibrations of the C–H bond, and peaks with a maximum about 2935 cm^{-1} were caused by asymmetrical stretching vibration of the C–H bond [21, 27]. Comparing A with C and D with G in Figure I.4.11, we can see that the intensity of the C–H stretch increased with an increase in treatment temperature, similar to that reported in the literature [10]. Spectra for the two 900^{o}C treatments (Figures I.4.11 C and D) showed that increasing the heating time also gave an increase in C–H peak intensity. Also, the C=O stretch peak disappeared with thermal treatment above 700^{o}C. It was reported that heating diamonds above 900^{o}C causes graphitization of the surface [28]. Therefore, a temperature of 900^{o}C was selected for hydrogenation of diamond surfaces in this work.

Figure I.4.12 shows x-ray photoelectron spectra (xps) of diamonds before and after hydrogenation. It can be seen that after heating in hydrogen, the surface oxygen was reduced to a trace level, indicating the formation of a hydrogen-terminated surface.

After comparing the various reported chemical modification approaches for diamond surfaces, I chose to use radical addition reactions with organic peroxides as radical initiators [16, 17, 20, 23] because these reactions can be conducted in liquid solutions, which is helpful for modifying the surfaces of particles evenly. Furthermore, mild reaction conditions could be conveniently controlled. The basic reactions are expressed by equations (I.4.1) and (I.4.2). It has also been reported that CN groups can be introduced onto diamond surfaces when this type of modification is conducted in the

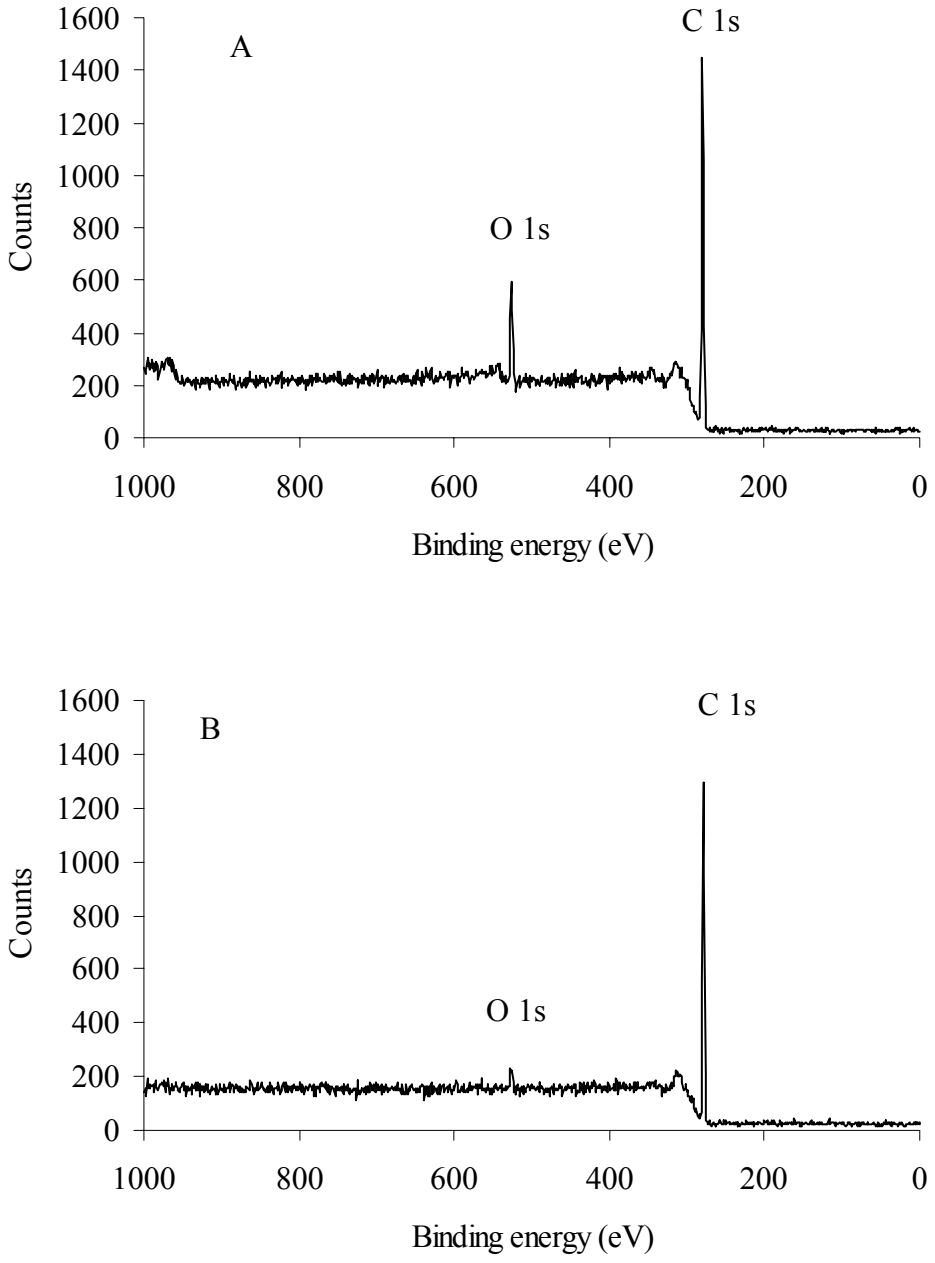

Figure I.4.12. xps spectra of diamond particles. Bare diamond particles (A) before thermal treatment and (B) after thermal treatment. Conditions: 900^{o}C, 5 h; H_2 flow rate, 400 cm^3/min.

presence of CN-group-containing compounds like acetonitrile. The possible mechanism is

$$C_6H_5COO\bullet + CH_3–CN \rightarrow C_6H_5COOH + \bullet CH_2–CN \qquad (I.4.5)$$

$$(diamond)\bullet + \bullet CH_2–CN \rightarrow (diamond)–CH_2–CN \qquad (I.4.6)$$

Most likely, radicals other than CN containing groups generated in the reaction may also be attached onto the surfaces of the diamond particles. Therefore, reagents capable of forming alkyl radicals were used in some experiment, in hopes of introducing long carbon chains on the surface.

Table I.4.1 lists the conditions for some of the experiments conducted in this work. Figure I.4.13 shows the diffuse reflectance FTIR spectra of the resulting powders from the experiments listed in Table I.4.1. Figure I.4.13 shows diffuse reflectance FTIR spectra of chemically modified diamond particles using various organic peroxides in dodecane. First, it can be seen by comparing diffuse reflectance FTIR spectra for both chemically modified and hydrogenated diamonds that radical species from peroxide become attached to the diamond surfaces by replacing hydrogen atoms. Diamond particles hydrogenated at 900 ^oC usually gave strong C–H stretch vibration bands in the DRIFT spectrum at 2800 – 3000 cm^{-1} with a sharp peak around 2830 cm^{-1} representing symmetrical stretch vibration. For diamond particles treated with benzoyl peroxide, as No. 1 shown in Figure I.4.13, the bands with a maximum at 1710 cm^{-1} can be assigned to the C=O band, and bands at 1000–1250 cm^{-1} may be assigned to the C–O–C stretch vibration [10, 17], both indicating attachment of the radical species from benzyl peroxide, i.e., $C_6H_5COO\bullet$. The dramatic decrease in the intensities of the C–H stretch bands was due to the elimination of hydrogen from the diamond surfaces by $C_6H_5COO\bullet$. For No. 3 and No.

Table I.4.1. Conditions for chemical modification of diamond particles.

No	Initiator	Mass of initiator (mg)	Solvent	Reagent	Solvent/ reagent (mL/mL)	T (^{o}C)	Time (min)
1	benzoyl peroxide	116.38	dodecane	—	50	80	120
2	PBD coated						
3	dicumyl peroxide	21.4	dodecane	—	50	120	120
4	dicumyl peroxide	21.6	dodecane	1-octene	35/15	120	120
5	benzoyl peroxide	22.3	dodecane	1-chlorooctane	35/15	75	122
6	benzoyl peroxide	22.8	dodecane	1-octene	35/15	75	125
7	benzoyl peroxide	2.0	dodecane	1-octene	35/15	75	61
8	benzoyl peroxide	2.0	dodecane	1-chlorooctane	35/15	75	61
9	di-tert-amyl peroxide	24.5	dodecane	—	50	112	127
10	di-tert-amyl peroxide	135	dodecane	1-octene	6.5/6.5	112	120

Benzoyl peroxide:

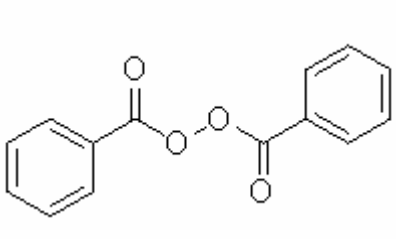

Dicumyl peroxide:

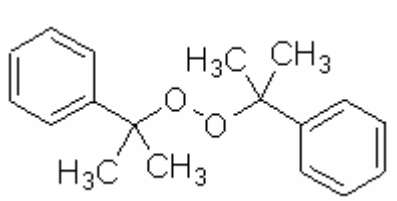

Di-*tert*-amyl peroxide:

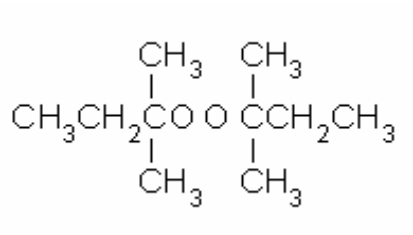

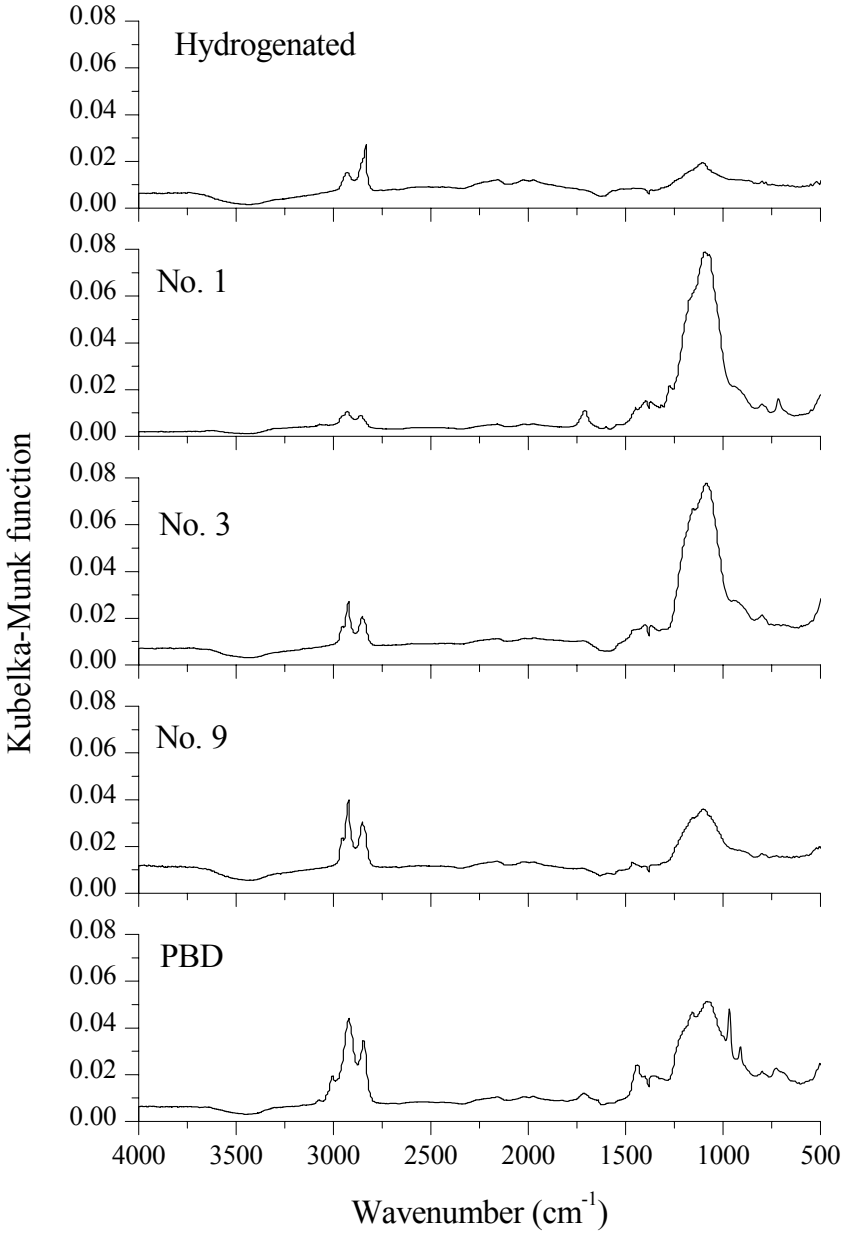

Figure I.4.13. Diffuse reflectance FTIR spectra of chemically modified diamond particles using peroxides. Hydrogenation conditions: 900 ^{o}C, 5 h; modification conditions: see Table I.4.1.

9 particles, broad bands in the area of 1200–950 cm^{-1}, which represent C–O–C stretch vibration, indicate the attachment of organic peroxide radicals. The strong C–H bands were generated by the CH_3 and CH_2 groups from the peroxides, which can be substantiated by the fact that the intensities of the C–H bands in No. 9 were greater than those in No. 3 because the radical from di-*tert*-amyl peroxide has a CH_2 and one more CH_3 than dicumyl peroxide. Also noteworthy is that the attached functional groups containing CH_3 moieties gave strong C–H bands with a sharp asymmetrical peak at 2930 cm^{-1}, which is different from the C–H bands from hydrogenated diamond particles. Therefore, it is not surprising that very strong C–H bands were found in the DRIFT spectra of PBD-coated diamond particles, which were coated with polymers bearing many CH_3 moieties. The xps spectrum illustrated in Figure I.4.14 showed an increase in oxygen composition after surface modification with peroxide.

Figure I.4.15 shows DRIFT spectra of chemically modified diamond particles using benzoyl peroxide with and without additional reagent for introducing long carbon chains. Comparing No. 1, No. 8 and No. 5, it can be seen that the addition of 1-chlorooctane produced higher C–H band intensities, indicating the attachment of long carbon chains. Similarly, compared with No. 1, the stronger C–H bands in No. 6 and No. 7 indicate the attachment of alkyl groups to diamond surfaces. The interesting phenomenon is that a larger amount of reagent with long carbon chain was used in No. 5 and No. 6, however, their C–H bands were lower than those of No. 8 and No. 7, for which less reagent was used. This indicates that there might be an optimum amount of reagent for attaching functional groups onto diamond surfaces. Too much reagent could reduce the number of attached groups due to self-termination of the free radicals.

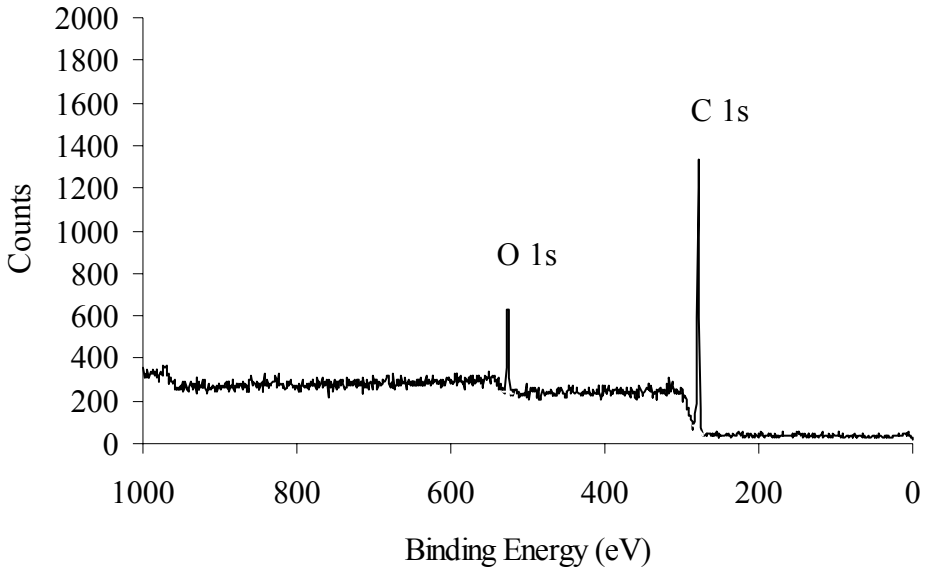

Figure I.4.14. xps spectrum of chemically modified diamonds. For modification conditions, see No. 3 in Table I.4.1.

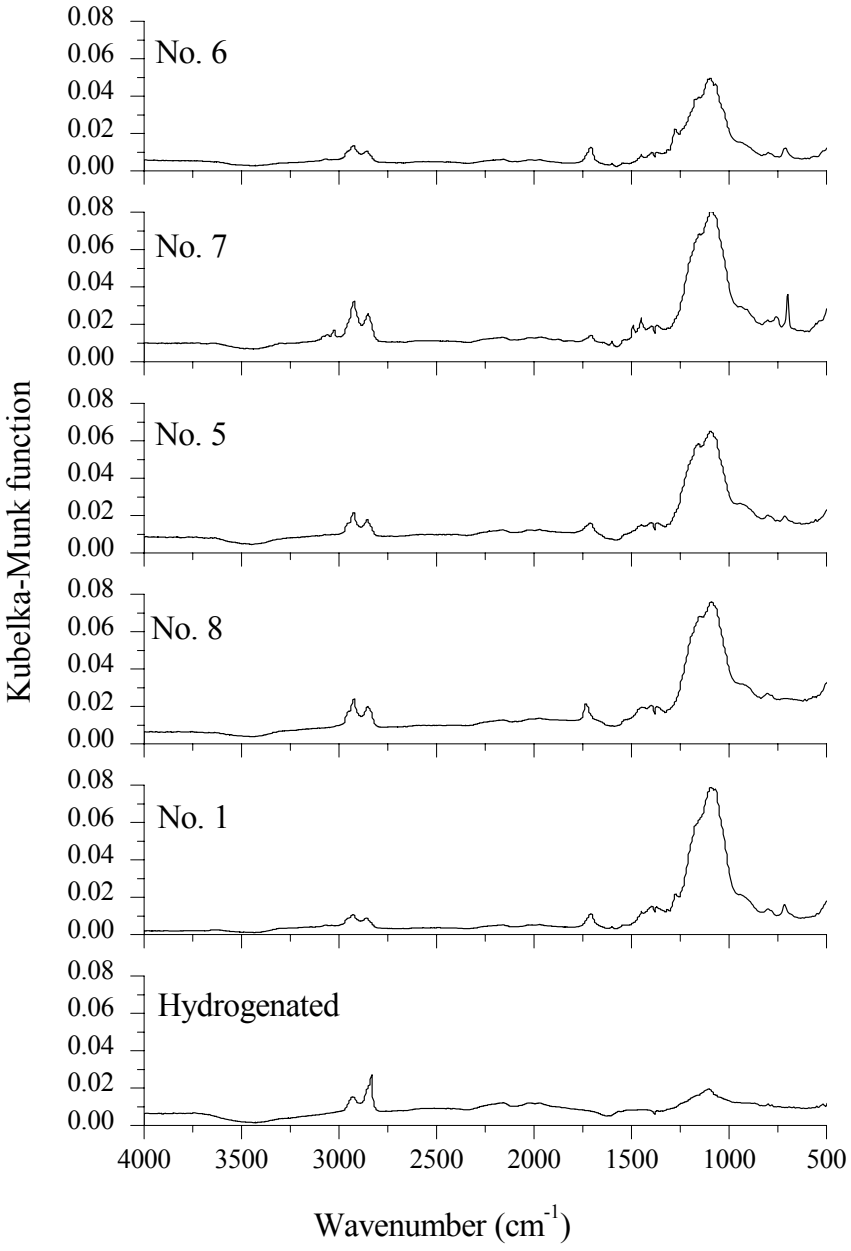

Figure I.4.15. Diffuse reflectance FTIR spectra of chemically modified diamond particles. Hydrogenation conditions: 900 ^{o}C, 5 h; modification conditions for other particles: see Table I.4.1.

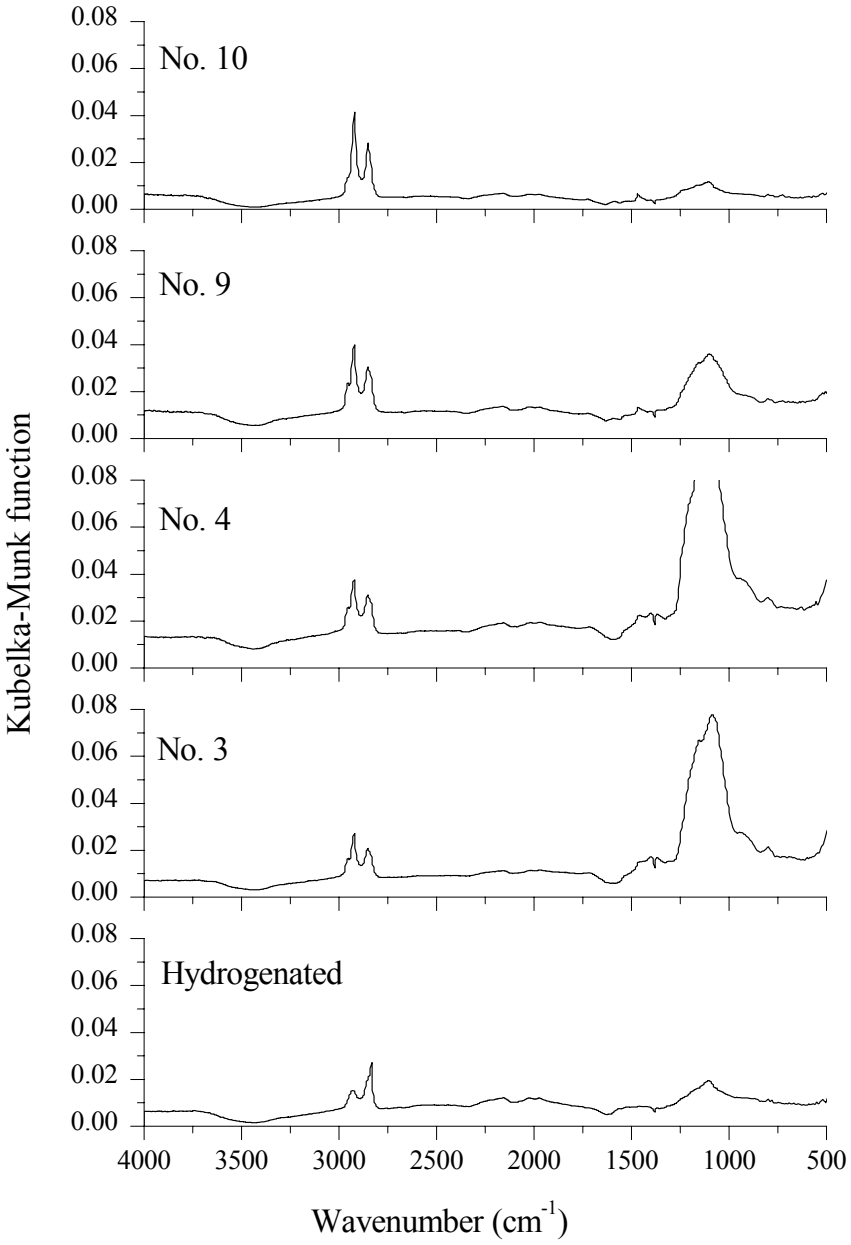

Figure I.4.16. Diffuse reflectance FTIR spectra of chemically modified diamond particles. Hydrogenation conditions: 900 ^{o}C, 5 h; modification conditions for other particles: see Table I.4.1.

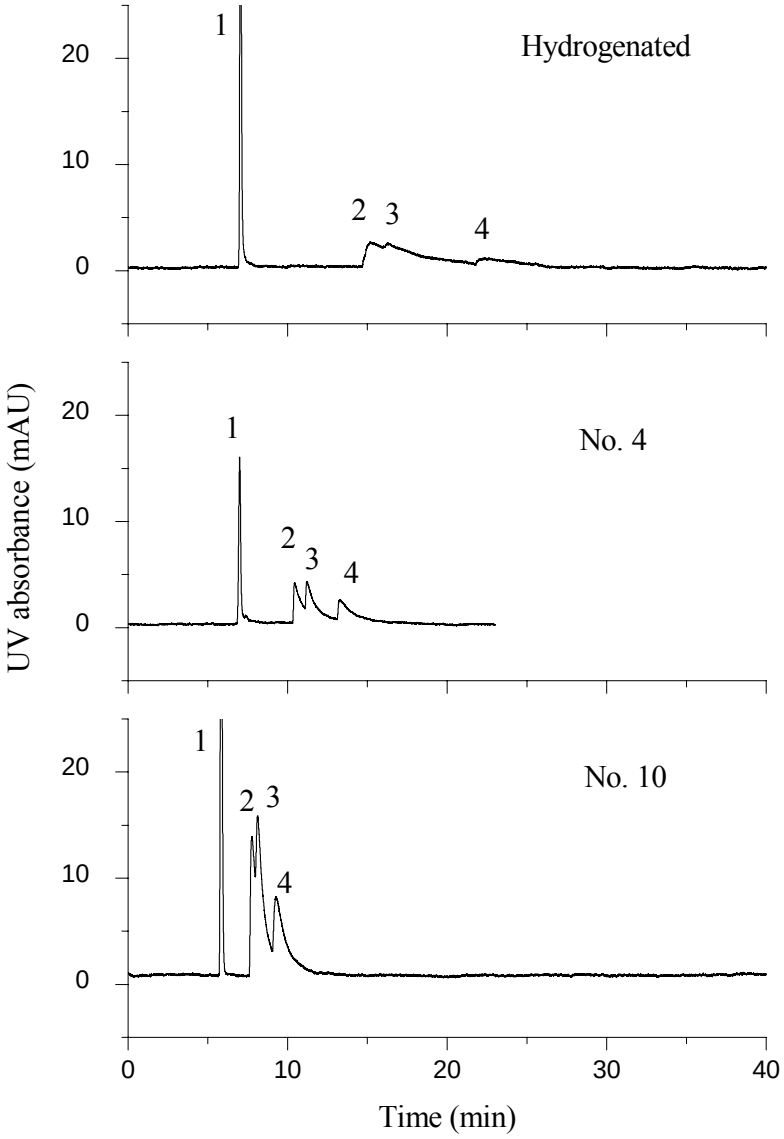

Figure I.4.17. Separation of parabens using columns containing chemically modified diamond particles. Chromatographic conditions: 20 cm × 75 μm i.d. fused silica capillary, water/acetonitrile (30:70, *v*/*v*), 254 nm UV detection, 10 kpsi inlet pressure. For modification conditions, see Table I.4.1. Peak identifications: (1) uracil, (2) methyl 4-hydroxybenzoate, (3) ethyl 4-hydroxybenzoate, (4) propyl 4-hydroxybenzoate.

Figure I.4.16 shows DRIFT spectra of chemically modified diamond particles using dicumyl peroxide and di-*tert*-amyl peroxide, with or without additional reagents to introduce radical species with long carbon chains. Comparing No. 3 with No. 4 and No. 9 with No. 10, obvious increases in the intensities of C–H bands were observed for cases with 1-octene added, indicating the attachment of alkyl groups to diamond surfaces. The lower C–O–C band at 950–1250 cm^{-1} for No. 10 particles means fewer radical species from peroxide were added to the surface.

LC results using columns packed with unmodified hydrogen-terminated diamond particles showed that the surfaces of hydrogenated diamond particles were extremely hydrophobic, just as expected, and produce strong retention of test compounds. LC experiments were conducted using columns packed with chemically modified particles. Changes in surface properties were observed, as shown in Figure I.4.17, however, the modified diamond particles were still quite hydrophobic and could not give acceptable separation of parabens. This is probably due to the fact that the modification conditions were not optimized and coverage by alkyl chains was incomplete. As is indicated by the broad tailing peaks, the surface modification method should be investigated further to improve the coverage of functional groups.

I.4.4. Summary and Future Work

The following conclusions can be made for this part of the dissertation:

1. Columns packed with bare diamond particles can separate some small molecules, especially polar molecules, however, severe tailing occurs for less polar compounds.

2. Coating with PBD can improve the performance of columns packed with diamond particles by changing the retention factors of solutes, although it does not

improve the column efficiency. Greater retention and better separations of small molecules were observed. In UHPLC, PBD-coated diamond particles can be utilized for fast separations of small molecules.

3. Bare diamond particles can be hydrogenated by heating the particles up to 900^{o}C in an oven with hydrogen flow. Several approaches for chemical modification of hydrogenated diamond particles were explored. Changes in surface bonding brought by the modifications were determined by means of diffuse-reflectance FTIR and x-ray photoelectron spectroscopy. It appears that long alkyl groups were attached onto the diamond surface, however, the coverage was limited. LC experiments using chemically modified diamond particles did not demonstrate good separation; however, changes in LC behavior could be observed.

Suggestions for future work:

1. The PBD coating procedure should be thoroughly explored and optimized. Development of methods to determine the amount of polymer coating on the diamond surface is necessary for further study of the coating process. The commonly used "carbon content" method cannot be applied to diamond particles because diamond itself consists of carbon.

2. Chemical modification of diamond particles must be systematically studied. Previous work on chemical modification of diamond surfaces using diamond powders, although promising, did not pay enough attention to surface coverage, which is very important when considering the use of diamonds as stationary phase. Organic peroxides that can produce radical species with long carbon chains should be used in surface

modification of diamond powders because only one type of radical species can be generated to react with the diamond particles.

3. Other diamond particle sources should be explored. Porous disperse diamond particles [7] can provide higher surface area, which is beneficial for improving sample loading capacity. Porous disperse diamond particles are produced by sintering nanoscale diamond particles together.

References

1. Pierson, H.O. *Handbook of Carbon, Graphite, Diamond and Fullerenes*; Noyes: Park Ridge, NJ, 1993.

2. WIlks, E.; Wilks, J. *Properties and Applications of Diamond*; Butterworth: Oxford, England, 1997.

3. Bakowicz, K.; Mitura, S. *J. Wide Bandgap Mater.* **2002**, *9*, 261-272.

4. Snyder, L.R.; Kirkland, J.J.; Glajch, J.L. *Practical HPLC Method Development*, *2nd ed.*; Willey-Interscience: New York, 1997.

5. Vissers, J.P.C.; Hoef, E.C.J.V.D.; Claessens, H.A.; Laven, J.; Cramers, C.A. *J. Microcol. Sep.* **1995**, *7*, 239-245.

6. Knox, J.H. *J. Chromatogr. A* **2002**, *960*, 7-18.

7. Patel, B.A.; Rutt, K.J.; Padalko, V.I.; Mikhalovsky, S.V. *J. SuperHard Mater. (Sverkhtverdye Materialy)* **2002**, 51-54.

8. Bjorkman, H.; Ericson, C.; Hjerten, S.; Hjort, K. *Sens. & Actuat. B* **2001**, *79*, 71-77.

9. Xu, J.; Bowden, E.: US, 2004; Vol. US2004/0118762 A1.

10. Ando, T.; ishii, M.; Kamo, M.; Sato, Y. *J. Chem. Soc., Faraday Trans.* **1993**, *89*, 1783-1789.

11. Miller, J.B.; Brown, D.W. *Langmuir* **1996**, *12*, 5809-5817.

12. Smentkowski, V.S.; Yates, J.T., Jr. *Science* **1996**, *271*, 193-195.

13. Hovis, J.S.; Coulter, S.K.; Hamers, R.J. *J. Am. Chem. Soc.* **2000**, *122*, 732-733.

14. Kealey, C.P.; Klapotke, T.M.; McComb, D.W.; Robertson, M.I.; Winfield, J.M. *J. Mater. Chem.* **2001**, *11*, 879-886.

15. Strother, T.; Knickerbocker, T.; John N. Russell, J.; Butler, J.E.; Smith, L.M.; Hamers, R.J. *Langmuir* **2002**, *18*, 968-971.

16. Tsubota, T.; Hirabayashi, O.; Ida, S.; Nagaoka, S.; Nagataa, M.; Matsumoto, Y. *Phys. Chem. Chem. Phys.* **2002**, *4*, 806-811.

17. Tsubota, T.; Tanii, S.; Ida, S.; Nagataa, M.; Matsumoto, Y. *Phys. Chem. Chem. Phys.* **2003**, *5*, 1474-1480.

18. Liu, Y.; Gu, Z.; Margrave, J.L.; Khabashesku, V.N. *Chem. Mater.* **2004**, *16*, 3924-3930.

19. Nichols, B.M.; Butler, J.E.; John N. Russell, J.; Hamers, R.J. *J. Phy. Chem. B* **2005**, *109*, 20938-20947.

20. Tsubota, T.; Ida, S.; Hirabayashi, O.; Nagaoka, S.; Nagataa, M.; Matsumotob, Y. *Phys. Chem. Chem. Phys.* **2002**, *4*, 3881-3886.

21. Ando, T.; Ishii, M.; Kamo, M.; Sato, Y. *J. Chem. Soc., Faraday Trans.* **1993**, *89*, 1383-1386.

22. Wang, J.; Firestone, M.A.; Auciello, O.; Carlisle, J.A. *Langmuir* **2004**, *20*, 11450-11456.

23. Ida, S.; Tsubota, T.; Tanii, S.; Nagata, M.; Matsumoto, Y. *Langmuir* **2003**, *19*, 9693-9698.

24. Li, J.; Carr, P.W. *Anal. Chem.* **1997**, *69*, 2193-2201.

25. Nawrocki, J.; Dunlap, C.; Li, J.; Zhao, J.; McNeff, C.V.; McCormick, A.; Carr, P.W. *J. Chromatogr. A* **2004**, *1028*, 31-62.

26. Xiang, Y.; Yan, B.; McNeff, C.V.; Carr, P.W.; Lee, M.L. *J. Chromatogr. A* **2003**, *1002*, 71-78.

27. Tsubota, T.; Hirabayashi, O.; Ida, S.; Nagaoka, S.; Nagata, M.; Matsumoto, Y. *Diamond Relat. Mater.* **2002**, *11*, 1360-1365.

28. Sun, C.Q.; Xie, H.; Zhang, W.; Ye, H.; Hing, P. *J. Phys. D: Appl. Phys.* **2000**, *33*, 2196-2199.

PART II. CONTINUOUS ON-LINE SAMPLE STREAM LIQUID CHROMATOGRAPHY ANALYSIS

II.1. Introduction

LC is a widely used separation and analysis technique. It is not uncommon to want to analyze a continuous sample stream using LC. For example, when controlling a production process in a chemical or pharmaceutical industry or monitoring a specific environment, samples are periodically withdrawn or extracted from the sample stream and analyzed using LC and other instruments for components which are often present in low concentrations [1-4]. The common practice is to use a multi-port valve to inject a sample plug into the LC column directly or after extraction and/or concentration [1, 3-6].

On the other hand, in most LC analyses, the sample is introduced into the column as a plug by injection of a specific volume of sample solution. There are no reports in the literature concerning continuous sample stream LC analysis. However, it should be possible to analyze a continuous sample stream containing analytes at low concentration in real time without any discreet injection steps. For this to be successful, an on-column focusing mechanism must be utilized to narrow the analyte peaks and concentrate them sufficiently for detection.

On-column focusing can be accomplished by accumulating or focusing the sample at the very front of the column by dissolving the sample in a non-eluting solvent and injecting it into the column [7, 8]. During injection, the displacement volume (V_d) at the front of the column covered by an unretained solute (i.e., $k = 0$) is usually assumed to be the same as the injection volume [9]. However, when a retained solute is injected, then the displacement volume can be expressed as

$$V_d = \frac{V_i}{k_s + 1} \qquad \text{(II.1)}$$

where V_i is the injection volume and k_s is the retention factor of the solute when eluting with the solvent used to dissolve the solute [10]. If the solute is dissolved in a non- or poor-eluting solvent, which leads to a very large k_s, the displacement volume is reduced to a much smaller value than the volume injected, and the solute concentration, when it is displaced, becomes much larger than its original concentration. Therefore, the solutes will be concentrated or focused in a small plug at the front of the column.

On-column focusing has been typically utilized in analyzing trace components by injecting large volumes of samples in non-eluting solvents [11-14]. With the aid of on-column focusing, Guetens and co workers [13] successfully quantified an anticancer agent ZD1839 in plasma by capillary LC-tandem mass spectrometry, and the limit of quantification was 0.1 ng/mL. Molander et al. [14] reported the determination of retinoids by packed capillary chromatography with large-volume on-column focusing and temperature optimization. Injection volumes up to 100 μL were successfully introduced onto the columns, and a mass limit of detection of 0.5 ng of retinoic acids was found using on-column UV detection at 360 nm. Ling and Baeyens [10] compared the effects of on-column focusing on sensitivity when applied to micro-LC and conventional LC. They observed that the on-column focusing technique allowed large volume injections onto both conventional LC and micro-LC columns for improved sensitivity without severe band broadening. This technique could be applied when using both types of LC systems for late eluting compounds, while for early eluting species, better results were obtained using micro-LC systems. The increase in sensitivity resulting from large volume injection on-column focusing helps to overcome the main disadvantage of low detectability in capillary LC. Mills et al. [8] studied the injection volume limits when using on-column

focusing in microbore LC. It was found that on-column focusing could be considered as a two-step process: focusing of the sample band due to a non- or poor-eluting solvent, and subsequent focusing of the sample band by a sample solvent to mobile phase step gradient. Therefore, the maximum allowable injection volume when using on-column focusing can be described as

$$V_{pc(\max)} = V_{i(\max)} \frac{(k_o + 1)^2}{(k + 1)^2} \qquad \text{(II.2)}$$

where $V_{pc(max)}$ is the maximum injection volume when using on-column focusing, $V_{i(max)}$ is the maximum injection volume that can be tolerabled without on-column focusing, k_o is the retention factor of the solute when eluted by the sample solvent and k is the retention factor of the solute eluted by the mobile phase.

Obviously, on-column focusing would allow the generation of a concentrated sample plug at the very beginning of the column when introducing a continuous sample stream under strongly retained solute conditions for a period of time. This formed sample plug can then be analyzed by applying isocratic or gradient elution. In this part of the dissertation, the possibility of analyzing a continuous sample stream by means of solvent programming and on-column focusing was evaluated. Factors influencing the pseudo-injection and separation processes were investigated.

II.2. Experimental

II.2.1. Chemicals and Instrumentation

All chemicals were obtained from Sigma-Aldrich (St. Louis, MO). Liquid chromatography experiments were conducted using an ExpressLC 100 (Eksigent Technologies, Dublin, CA). The ExpressLC-100 can deliver mobile phase at a flow rate

as low as 0.2 μL/min without a splitter, and can generate a step gradient. This LC system was equipped with a UV diode array detector and a low dispersion, microfabricated 45 nL flow cell to ensure high sensitivity. The column used was an Eksigent 3C-18-EP-120 from Eksigent Technologies. It was 15 cm long with an inner diameter (i.d.) of 300 μm, packed with 3 μm Embedded Polar C18 particles with 120A pore size.

II.2.2. Chromatography of a Continuous Sample Stream

Several model compounds were added to an aqueous mobile phase (HPLC grade water) to simulate a continuous sample flow. In most cases, the model compounds were phenol and benzyl alcohol, which are soluble in water and are well-retained on reversed phase columns when eluted with an aqueous mobile phase. The concentrations of the solutes were 1.6 μg/mL for phenol and 4.2 μg/mL for benzyl alcohol, if not specified otherwise.

A typical solvent program for analysis of a continuous sample stream is shown in Figure II.1 and consists of three steps: pseudo-injection, elution and rinse. The program began with a specific wash time period with a non- or poor-eluting solvent (100% aqueous phase A in this study). This on-column focusing period served as a pseudo-injection step because the solutes stayed at the inlet end of the column due to strong adsorption onto the stationary phase. In the following elution step, an organic phase B was introduced into the mobile phase according to a selected solvent programming profile. The starting point of elution, point S, did not necessarily occur at 0% phase B. Actually, elution could begin from any concentration of phase B if it benefited the

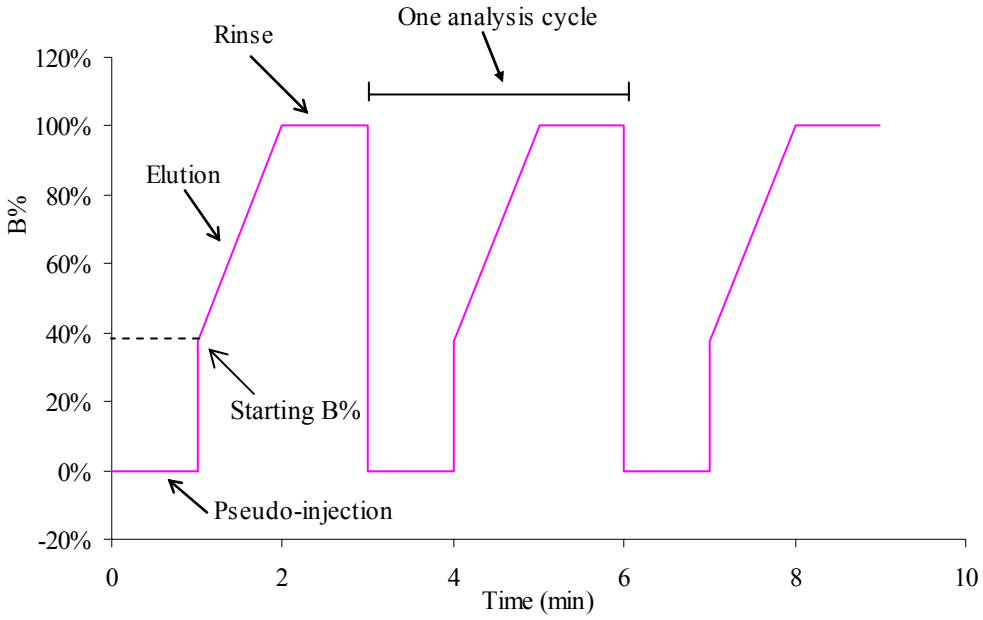

Figure II.1. Typical solvent program for analysis of a continuous sample stream.

separation. The rinse step was a wash period with a high organic content mobile phase (usually acetonitrile). Then the program returned to the pseudo-injection step for the next analysis cycle.

II.3. Results and Discussion

II.3.1. On-column Focusing

As mentioned above, in the pseudo-injection step, 100% aqueous mobile phase containing model compounds entered the column and the compounds were concentrated for a specific period of time. As the solutes were strongly retained, they were focused on the front of the column, forming a sample plug similar to one formed during conventional injection. Figure II.2A shows a series of chromatograms obtained using a series of pseudo-injection steps, while Figure II.2B illustrates that a similar experiment with an eluting solvent (i.e., water/acetonitrile, 50:50) did not produce enough focusing to produce a good injection.

From Figure II.2A, it can be seen that the peaks tailed to some degree. In addition to the typical reasons for tailing, three other reasons related to continuous sampling were possible. In the elution step, especially at the beginning of the gradient where there was a high aqueous composition mobile phase, (1) there was a large sample amount that continued to enter the column after pseudo injection, which I call “the sample lag amount” in this work; (2) the solutes used had high retention on the stationary phase (k was high) and continued to be focused to some extent, and (3) the following gradient elution also had a ‘focusing’ effect. Thus, the greater the mass of solutes that entered the column after the pseudo-injection step, the worse the tailing problem became. In comparison, without the focusing effects from (2) and (3), solutes introduced with the

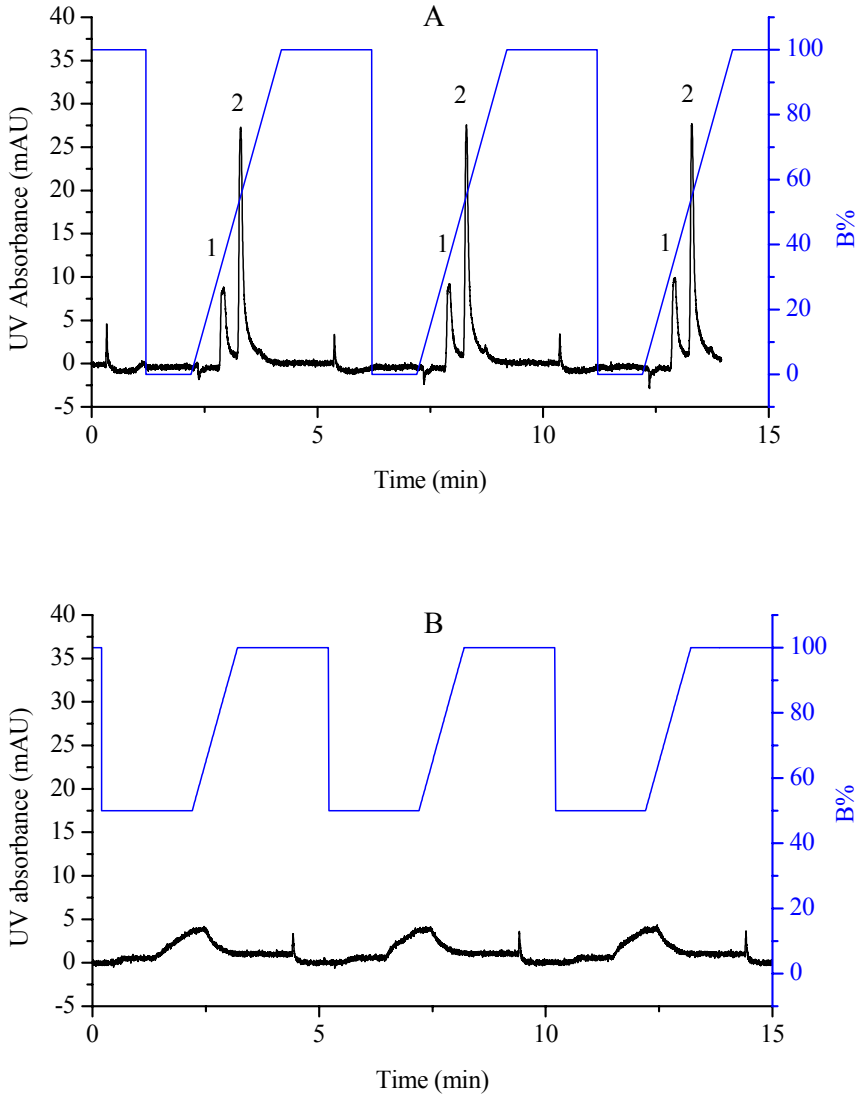

Figure II.2. On-column focusing during pseudo injection. Conditions: 4 µL/min flow rate. Peak identifications: (1) benzyl alcohol and (2) phenol.

mobile phase in (1) would not be a problem because the original concentrations of solutes in the mobile phase would be too low to produce a detector response. Tailing from sample lag is an important concern for continuous sample stream analysis. This tailing can be reduced to a minimum by optimizing the operating conditions (see following context). Actually the elution processes in both isocratic and gradient modes have been intensively studied and well understood [15, 16]. Therefore, in this study, more emphasis was placed on investigating the special phenomena in the analysis of a continuous sample stream.

II.3.2. Factors Influencing the Analysis of a Continuous Sample Stream

Several chromatographic features such as resolution, peak height, peak width, and analysis time should be carefully checked for the analysis of a continuous sample stream, just as in a conventional LC separation. Peak asymmetry is an indicator of tailing from excess solute. Tailing is a major concern in quantitative measurements.

Isocratic elution. Figure II.3 shows chromatograms obtained when eluting isocratically with mobile phases of different solvent compositions. The solutes were strongly retained on the column, even when eluting with mobile phases containing up to 15% phase B. Peak widths were quite broad when eluting with mobile phases with low volume fraction of phase B because the peak width is proportional to $(1+k)$ [17]. Peaks with good shapes could be obtained when phase B concentration in the mobile phase increased to 77%. When an increasing amount of organic solvent was added to the mobile phase, the time to finish one analysis cycle decreased, however, the resolution also became worse.

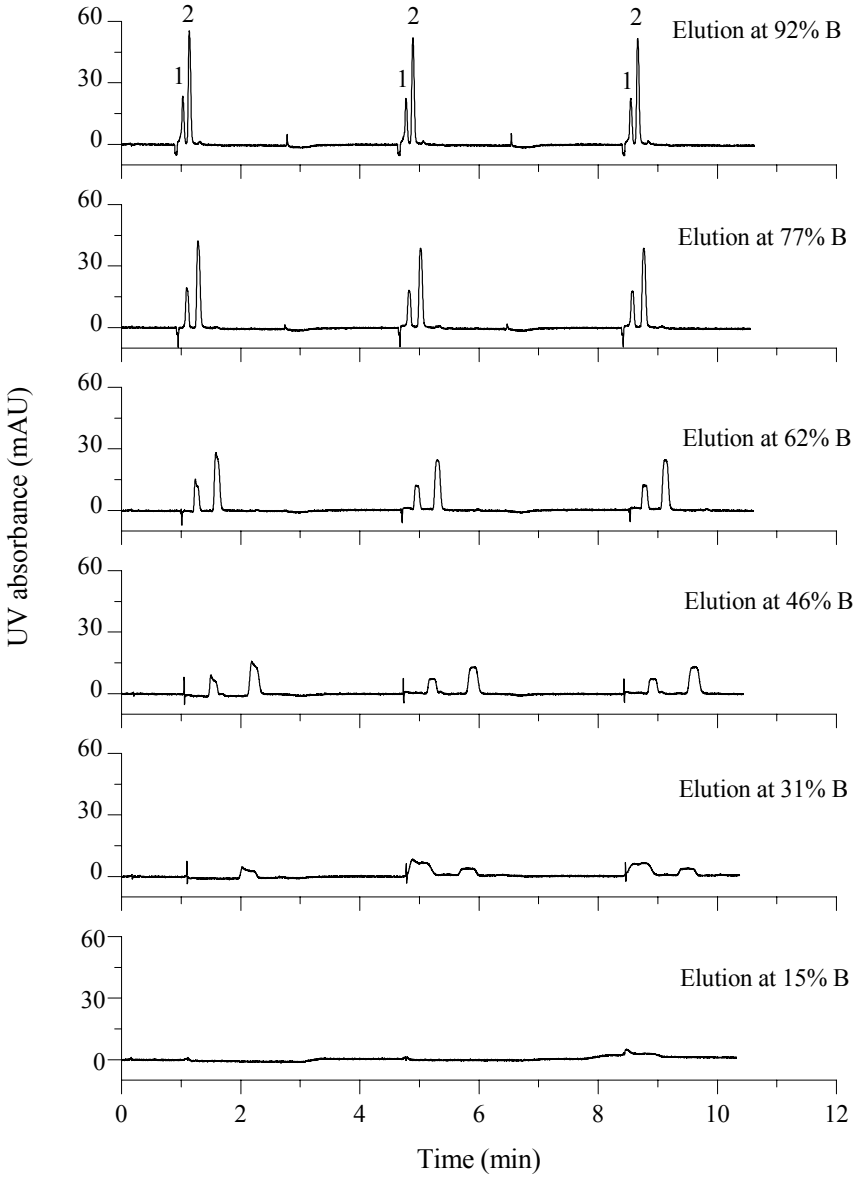

Figure II.3. Chromatograms obtained using isocratic elution. Solvent program: 100-s pseudo-injection followed by 120-s isocratic elution with no special rinse step. Volume fractions of phase B for isocratic elution are given in the figure; 10 μL/min flow rate. Peak identifications: (1) benzyl alcohol and (2) phenol.

Isocratic elution is not attractive because in order to obtain good peak shapes, high solvent strength is required. Although the analysis time might be shortened, poor resolution may prevent some compounds from being separated; furthermore, isocratic elution suffers from the general elution problem.

Gradient elution. Gradient elution is the most commonly used elution mode for LC in method development as well as for routine analysis, especially for separation of solutes that have a wide range of retention factors, *k*. Solvent gradient elution in reversed phase liquid chromatography can be described by the linear solvent strength (LSS) gradient model [17-20]. The retention factor for a given solute in reversed phase LC is usually approximated by

$$\text{Log } k = \log k_w - S\varphi \qquad \text{(II.3)}$$

where k_w is the value of the retention factor when using water as the mobile phase, φ is the volume fraction of organic solvent B, and S is a constant. If the volume fraction of B in the mobile phase entering the column changes linearly

$$\varphi = \varphi_0 + (\frac{\Delta\varphi}{t_G})t \qquad \text{(II.4)}$$

where φ_0 is the value of φ for $t = 0$, $\Delta\varphi$ is the change in φ during the gradient, and t_G is the gradient time (total gradient duration in min). By combining (II.3) and (II.4), we obtain a linear solvent gradient

$$\log k = \log k_0 - b(\frac{t}{t_0}) \qquad \text{(II.5)}$$

where, k_0 is the value of k at the start of the gradient, given by

$$\text{Log } k = \log k_w - S\varphi_0 \qquad \text{(II.6)}$$

and b is called the steepness of the gradient and is defined as

$$b = \frac{t_0 \, \Delta\varphi \, S}{t_G} = \frac{V_m \, \Delta\varphi \, S}{t_G F} \qquad \text{(II.7)}$$

where V_m is the hold-up volume of the column and F is the flow rate of the mobile phase. From the above relationships, if the volume fraction of a strong solvent B increases in a gradient, then the retention factor decreases with elution time, which means that the solute migrates faster and faster, and the whole analysis time is shortened. The mobile phase at the rear of the peak usually has a little higher phase B concentration than at the front of the peak, which means a lower *k* at the rear of the peak. Solute molecules at the rear of a peak always migrate a little faster than those at the front of the peak, and the peak becomes compressed. This is why the gradient elution mode can help to reduce the general elution problem in isocratic elution. Figure II.4 shows an example of the benefits of gradient mode versus isocratic mode. With a linear gradient, the analysis time for alkyl benzenes was shortened, and narrow peaks were obtained for all analytes. Different gradient shapes can be used to optimize the separation. A convex gradient (Figure II.4D) makes early eluting peaks elute even faster, and produces broader late eluting peaks. A concave gradient profile (similar to Figure II.4C) produces an opposite effect.

According to a linear solvent strength model, the resolution, R_s, in gradient elution can be estimated as [21]

$$R_s = \frac{1}{4}(\alpha - 1) N^{1/2} Q \approx \frac{1}{4}(\alpha - 1) N^{1/2} \left(\frac{1}{1 + 1.15b}\right) \qquad \text{(II.8)}$$

considering that $Q \approx \frac{1}{1 + 1.15b}$ for a large k_0. Therefore, the more shallow the gradient, *b*, the greater the resolution. In the analysis of a continuous sample stream, the steepness of the gradient, *b*, also influences the peak shape.

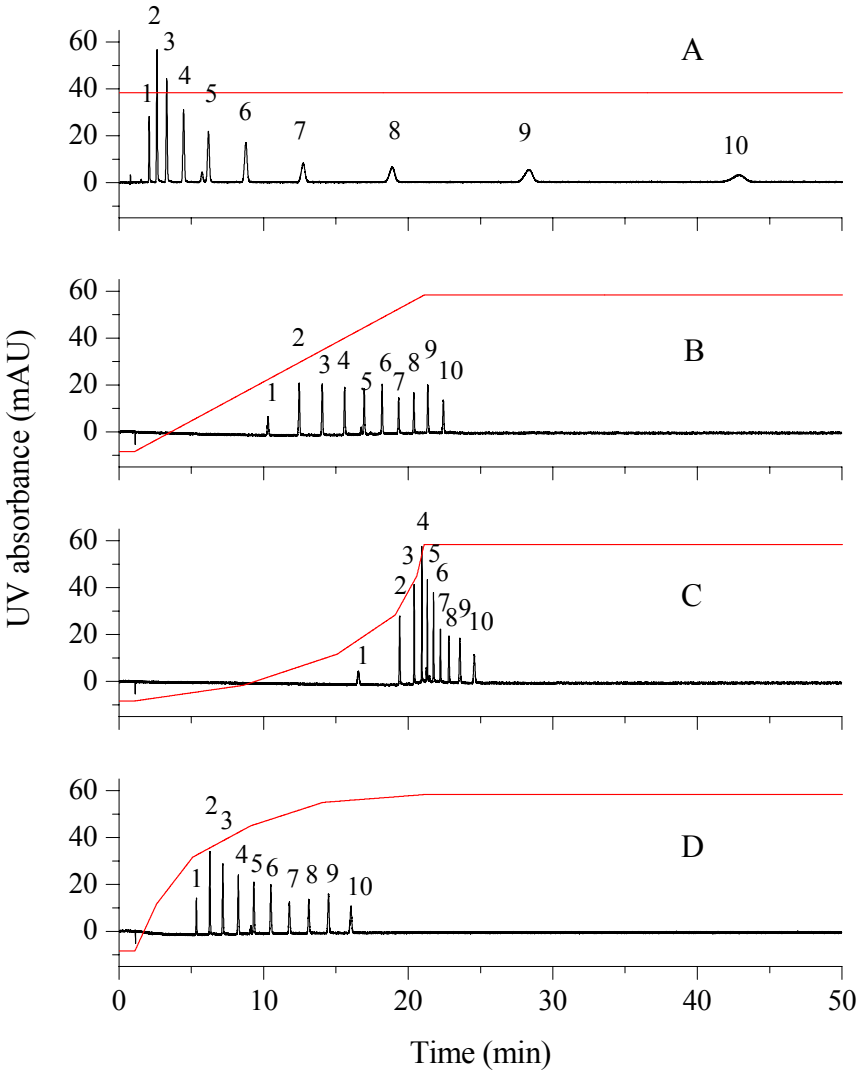

Figure II.4. Benefits of gradient elution of alkyl benzenes. Conditions: 8 µL/min, 255 nm UV detection, water/acetonitrile. Peak identifications: (1) benzene; (2) toluene; (3) ethylbenzene; (4) propylbenzene; (5) butylbenzene; (6) amylbenzene; (7) 1-phenylhexane; (8) 1-phenylheptane; (9) 1-phenyloctane; (10) 1-phenylnonane.

Gradient steepness and gradient shape are important factors that should be considered when developing gradient separation methods. Gradient steepness can be adjusted mainly by changing the flow rate, F, gradient time, t_G, and $\Delta\varphi$, the change in the volume fraction of phase B during the whole gradient. I first considered a linear gradient, and a factorial experiment was designed to conduct a preliminary investigation of the effects of parameters that determine the gradient steepness.

Factorial experiments are very helpful in studying the effects of several factors on a system. A factorial experiment was designed to conduct a preliminary evaluation of the influences of the gradient steepness on the analysis of a continuous sample stream. Table II.1 shows the design of the factorial experiment with three factors: flow rate, F, gradient time, t_G, and the starting volume fraction of phase B, φ_0, which is an indicator of the change in the volume fraction of phase B during the whole gradient. Three responses (performance features) were analyzed: the symmetry factors for the two model solutes, AsF-1 for benzyl alcohol and AsF-2 for phenol, and the resolution of these peaks. The ending volume fraction of phase B in the gradient was 100%. A randomized run order was specified by the statistics software Minitab, which was also used to conduct a statistical analysis of the results.

Each small figure in the main effect plots in Figure II.5 shows the mean of one response at each level of one of the factors. From such plots, one can see the effect of a certain factor on that response. For example, the upper left figure in Figure II.5A demonstrates that the mean of the symmetry factor for benzyl alcohol, AsF-1, increased and became much greater than 1 when the flow rate increased from 4 to 8 μL/min.

Table II.1. Factorial experimental design and results.

Standard order	Run order	flow rate (μL/min)	Starting B%	Gradient time (min)	Asymmetry factor (benzyl alcohol), AsF-1	Asymmetry factor (phenol), AsF-2	Resolution (Rs)
1	8	4	0	0.5	1.00	1.12	1.98
2	1	8	0	0.5	1.31	1.24	2.13
3	7	4	75	0.5	0.96	0.95	2.26
4	2	8	75	0.5	1.00	1.03	2.30
5	5	4	0	2.0	1.75	1.76	2.29
6	4	8	0	2.0	1.66	2.55	2.59
7	3	4	75	2.0	0.75	0.86	2.56
8	6	8	75	2.0	0.96	1.09	2.72

Conditions: model compounds: UV detection at 255 nm; 1 min pseudo-injection time. Other conditions are listed in the table.

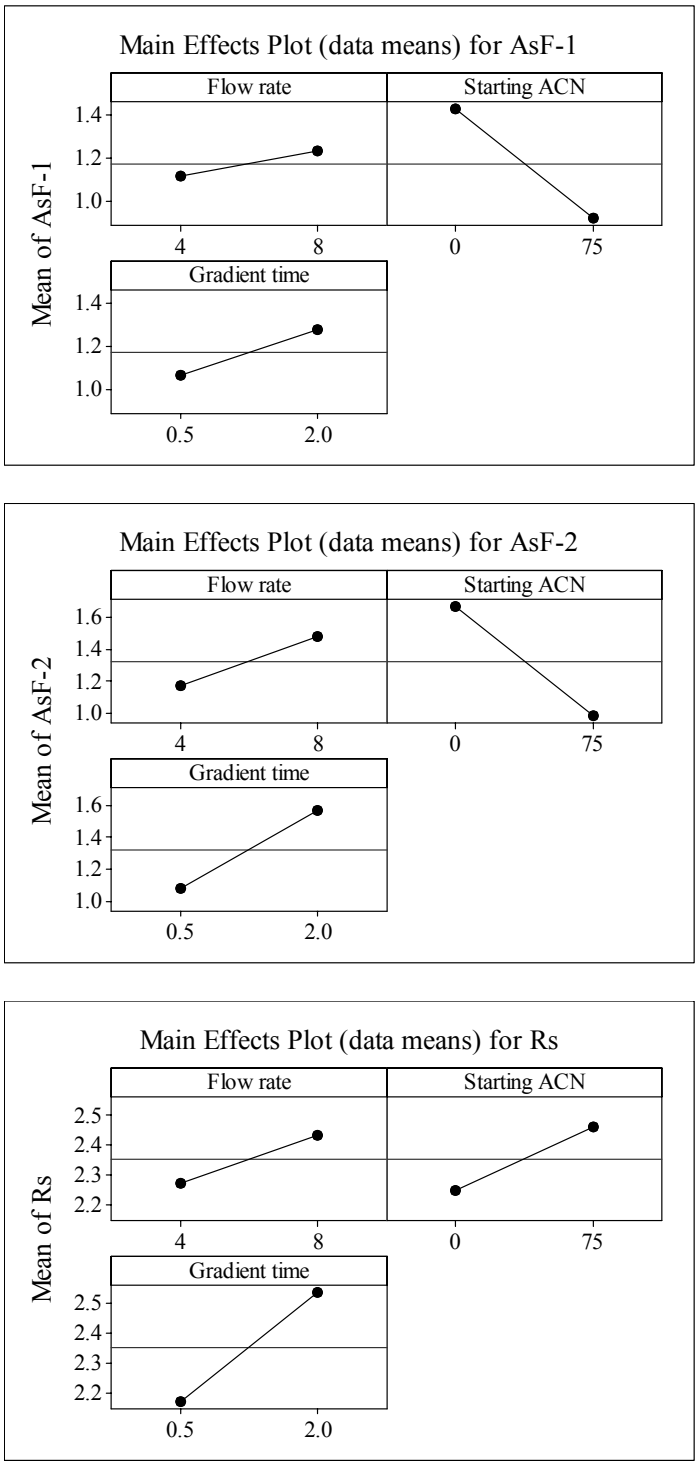

Figure II.5. Main effect plots for the factorial experiments. Conditions: see Table II.1.

From the main effects plots, it can be seen that higher flow rates gave larger asymmetry factors (larger than 1) for both model compounds. This is mainly due to the fact that at higher flow rates there is a large volume of mobile phase entering the column in the gradient profile, which does not allow time for mass transfer from the stationary phase. However, higher flow rates gave better resolution because the gradient was less steep, leading to lower *b* values in equation (6). The starting B% which changes from 0% to 75% greatly reduced the tailing factors for both model compounds. When starting from 75%, compared to situations starting from 0%, the solutes entering the column after the pseudo-injection step experience much less focusing due to the high eluting nature of the mobile phase and flatter gradient profile. Higher starting B% also gave higher resolution because the smaller $\Delta\varphi$ led to smaller *b* values according to equation (5), hence, higher R_s from equation (6) [17, 21]. Shorter gradient times made the asymmetry factors smaller and closer to 1 because shorter gradient times inherently shortened the duration of the low-eluting mobile phase portion in the gradient profile, and consequently reduced tailing from both focusing effects. On the other hand, shorter gradient times also led to steeper gradients and reduced resolution.

Although there are no ideal conditions that yield both no tailing and high resolution, the factorial experimental study still provided important information concerning how to improve the analysis of a continuous sample stream. Usually the requirement for resolution is not to achieve the maximum, but to achieve a resolution that leads to adequate separation of the compounds of interest. This provides more flexibility in optimizing experimental conditions.

Analysis time is also important for many applications, including real-time process chemistry monitoring. For the solvent programming approach to analysis of a continuous sample stream, fast separation means short analysis cycle. The rinse step should be long enough to remove any possible residual solutes, and the pseudo-injection step should be long enough to accumulate enough solutes in the focused sample plug for detection. The length of elution step depends on the retention time of the last eluting analyte. As shown above, isocratic elution with a mobile phase of high B% may give fast separation, but also low resolution of early eluting compounds and broad bands for late eluting compounds (i.e., general elution problem). Use of the gradient mode is a better choice. The retention times in gradient elution for solutes with large k_0 and gradients with low *log(2.3b)* can be estimated from [21]

$$t_R \approx (t_0/b)\ \log k_0 \qquad \text{(II.9)}$$

A steep gradient leads to short elution time. Since a steep gradient, or large *b*, causes low resolution, some compromise must be made between resolution and elution time.

As far as maintaining sufficient resolution, one can use a short gradient time to eliminate possible tailing from nonfocused solute as well as shorten the analysis cycle time; the analysis cycle time can be further reduced by increasing the flow rate if the tailing is in an acceptable range.

Figure II.6 shows a situation in which the gradient was from 0 to 100% B, and the flow rate was kept constant; only the gradient time changed. It can be readily seen that the decrease in gradient time improved the peak shapes. A long gradient process, as in Figure II.6 F and E, creates a large sample lag amount, leading to tailing peaks. Also, the longer migration time broadened the peaks. When the gradient time was decreased to

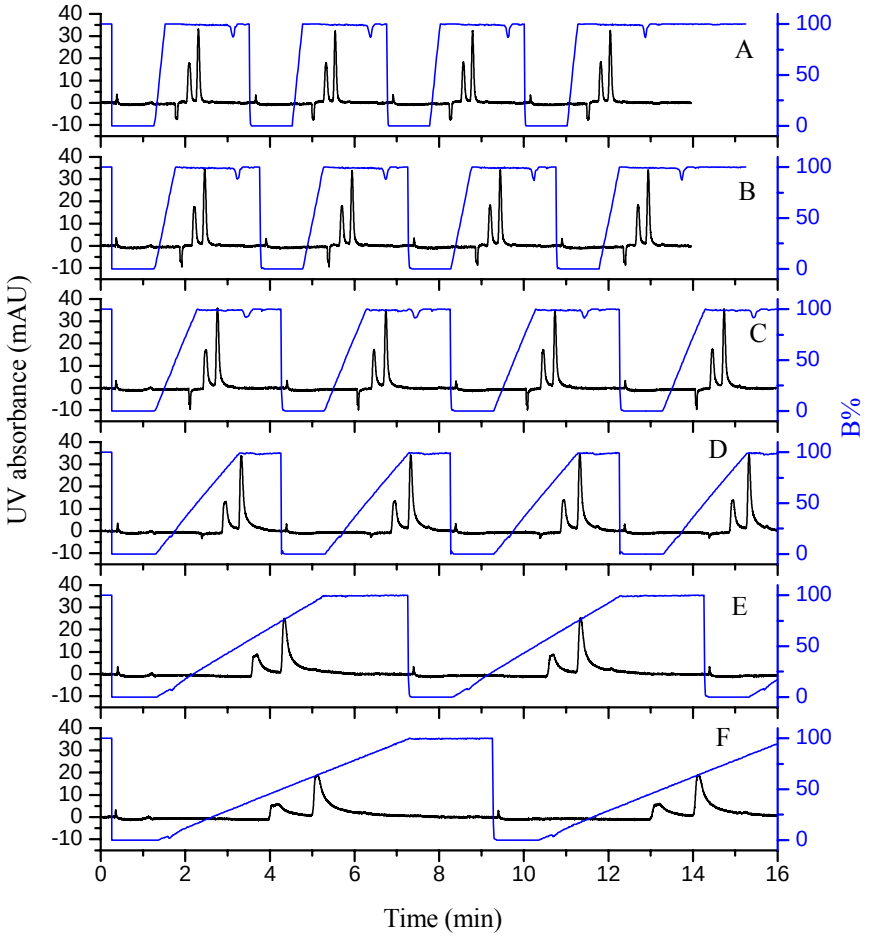

Figure II.6. Effects of gradient time. Conditions: 4 µL/min flow rate, 1 min pseudo-injection time, 0 to 100% of B gradient range, UV detection at 255 nm. Gradient time: (A) 0.25 min, (B) 0.50 min, (C) 1.00 min, (D) 2.00 min, (E) 4.00 min, (F) 6.00 min. Model compounds: benzyl alcohol and phenol.

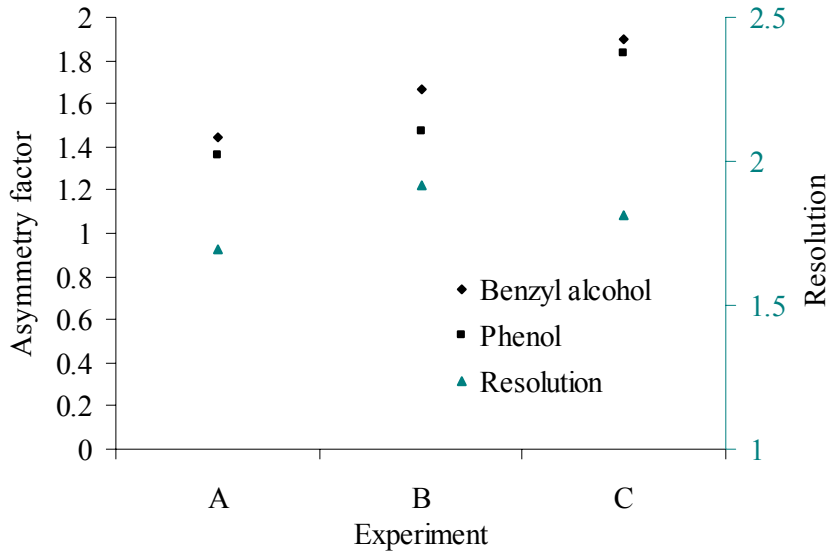

Figure II.7. Average asymmetry factors and resolution values for experiments in Figure II.6 (A, B, and C) with short gradient time.

approximately 1 min, the peak shapes and resolution became acceptable. As shown in Figure II.7, a decrease in gradient time gave more symmetrical peaks; the resolution in each chromatogram was greater than 1.5, meaning baseline separation. The resolution decreased slightly when the gradient time became extremely small in Figure II.6A, probably due to the fact that the gradient duration was too short and the peaks eluted partially isocratically in high organic mobile phase (pure acetonitrile here) after the gradient elution. In this situation, longer gradient times helped to achieve better separation. It is obvious that the analysis cycles became shortened with a decrease in gradient time.

Any change in flow rate may cause changes in the pseudo-injection volume and the sample lag volume that enters the column during gradient elution, and the ratio between them. A flow rate change may also affect the gradient steepness, and the specific mobile phase composition at which the solute elutes from the column. Figure II.8 shows a case in which exactly the same gradient profiles were used but the flow rates were different. The pseudo-injection volume and sample lag volume increased with flow rate, although the ratio remained constant. The results shown in Figure II.9 demonstrate an increase in asymmetry factors and resolution with an increase in flow rate, just as expected.

The gradient range influences the steepness of the gradient profile, and affects conventional LC separations. However, in the analysis of a continuous sample stream in this study, if the gradient range covers a lower organic phase B concentration range, peaks usually tail more due to the sample lag volume. Besides a linear gradient, the gradient shape can also be concave as shown in Figure II.4C or convex as in Figure II.4D. A convex gradient begins with steeper gradient, or larger *b* value, and then changes

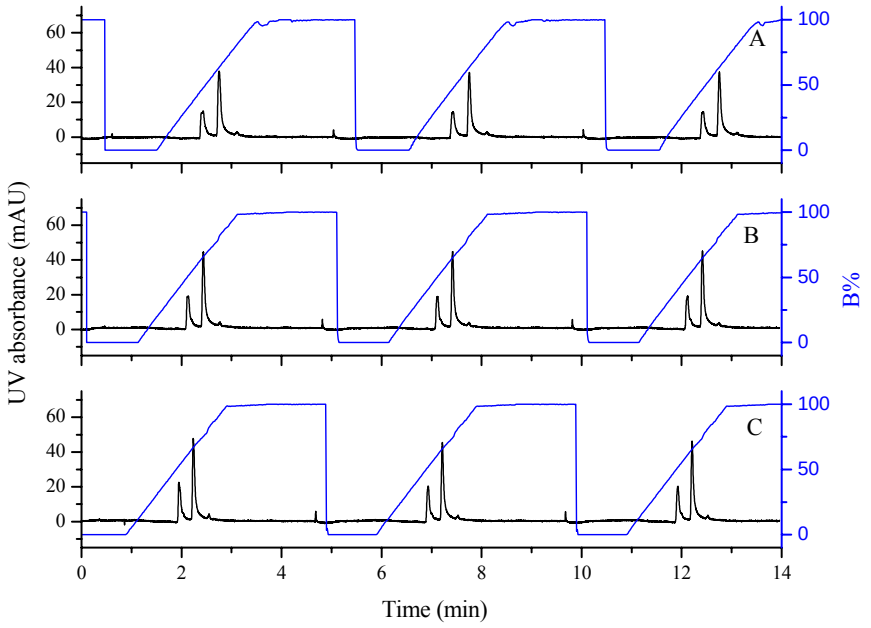

Figure II.8. Chromatograms obtained at different flow rates. (A) 6 µL/min, (B) 8 µL/min, (C) 10 µL/min. 2 min gradient time, 1 min pseudo-injection time, 0 to 100% of B gradient range, UV detection at 255 nm. Model compounds: benzyl alcohol and phenol.

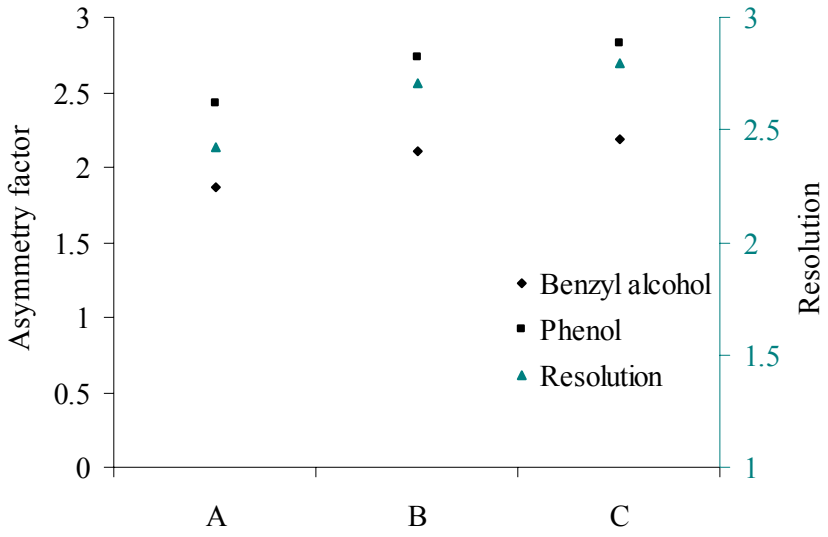

Figure II.9. Asymmetry factors and resolution values from Figure II.8.

gradually to a flatter gradient (*b* decreases gradually), while a concave gradient changes in the opposite way. Therefore, a convex gradient usually results in narrow early-eluting peaks and broader late-eluting peaks, while a concave gradient results in broader early-eluting peaks and narrower late-eluting peaks.

Figures II.10 and Figure II.11 show chromatograms obtained using different gradient shapes. Figure II.12 summarizes the peak asymmetry factors and resolution values calculated for each chromatogram. From Figures II.12A and II.10, it can be seen that when the gradient curves started from 0% phase B, a convex shaped gradient gave the best results: less tailing with asymmetry factors close to 1 and high resolution. A concave shaped gradient led to tailing and low resolution. The reasons are that the convex gradient had less aqueous content in phase A which resulted in less tailing, and the solutes eluted in the flat, or shallow, part of the gradient curve, i.e., low *b* value in equation (6), so higher resolution was achieved. The concave gradient was more like a prolonged pseudo-injection step followed by a steep gradient. In the flat part of the gradient the solutes eluted very slowly, but more sample was introduced which led to greater tailing. The steeper part of the gradient flushed the solutes out quickly, but with lower resolution.

When the gradient started from a high volume fraction of phase B (75%), as shown in Figures II.12B and II.11, the situation was almost the opposite. The concave gradient gave the best performance; i.e. more symmetrical peaks and higher resolution. This is due to the high organic content in the mobile phase for all runs, which led to less focusing and lower solute concentration in the mobile phase, so that tailing was greatly reduced. Solutes eluted in the flat part of the convex gradient with higher φ, the volume fraction of

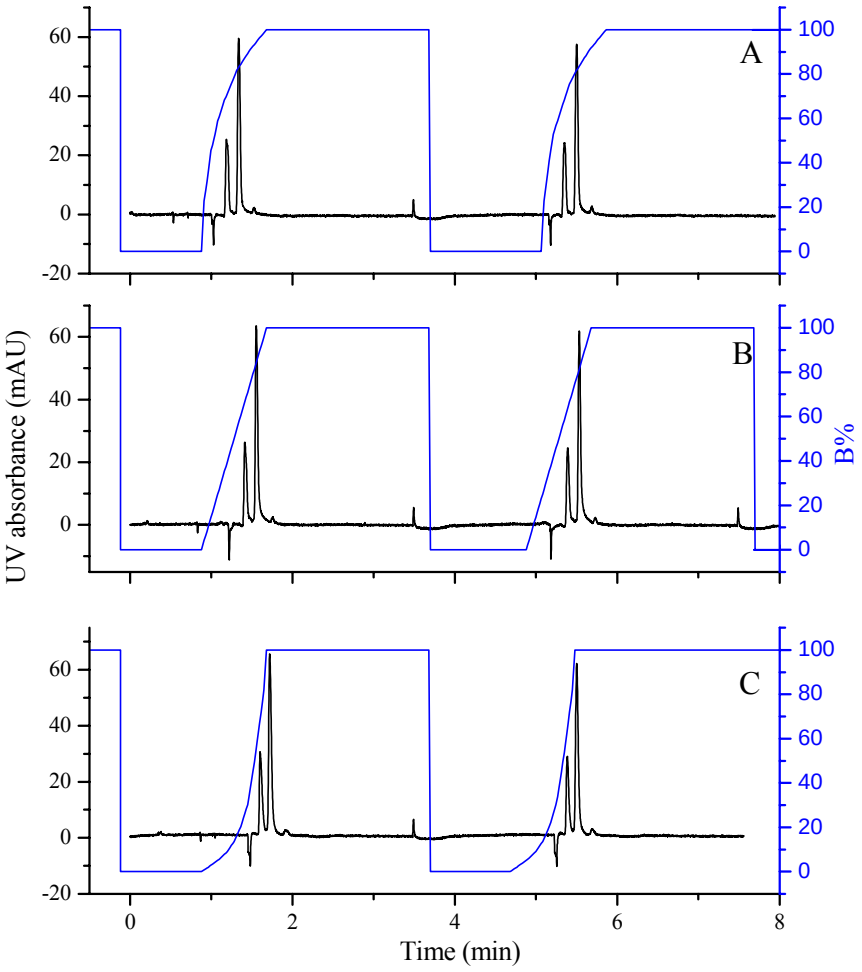

Figure II.10. Effects of gradient shape when elution was started from 0% phase B. Conditions: 10 µL/min flow rate, UV detection at 255 nm. Peak identifications: (1) benzyl alcohol, (2) phenol.

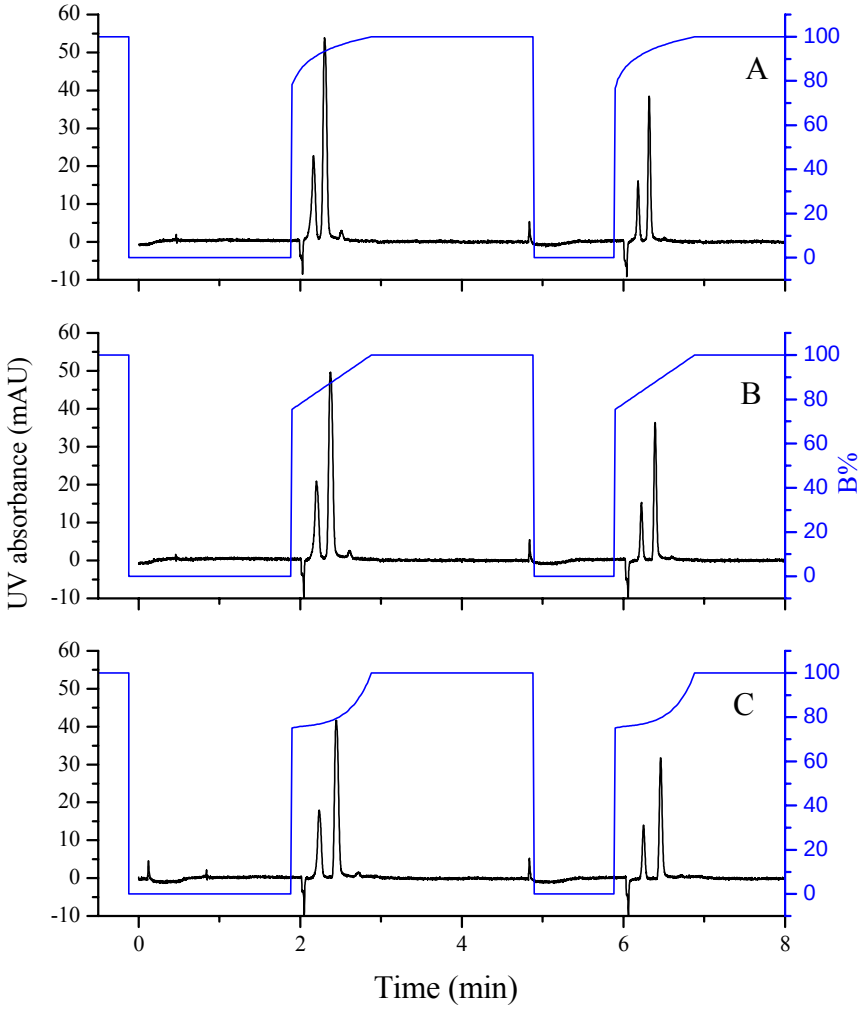

Figure II.11. Effects of gradient shape when elution was started from 75% phase B. Conditions: 10 µL/min flow rate, UV detection at 255 nm. Peak identifications: (1) benzyl alcohol, (2) phenol.

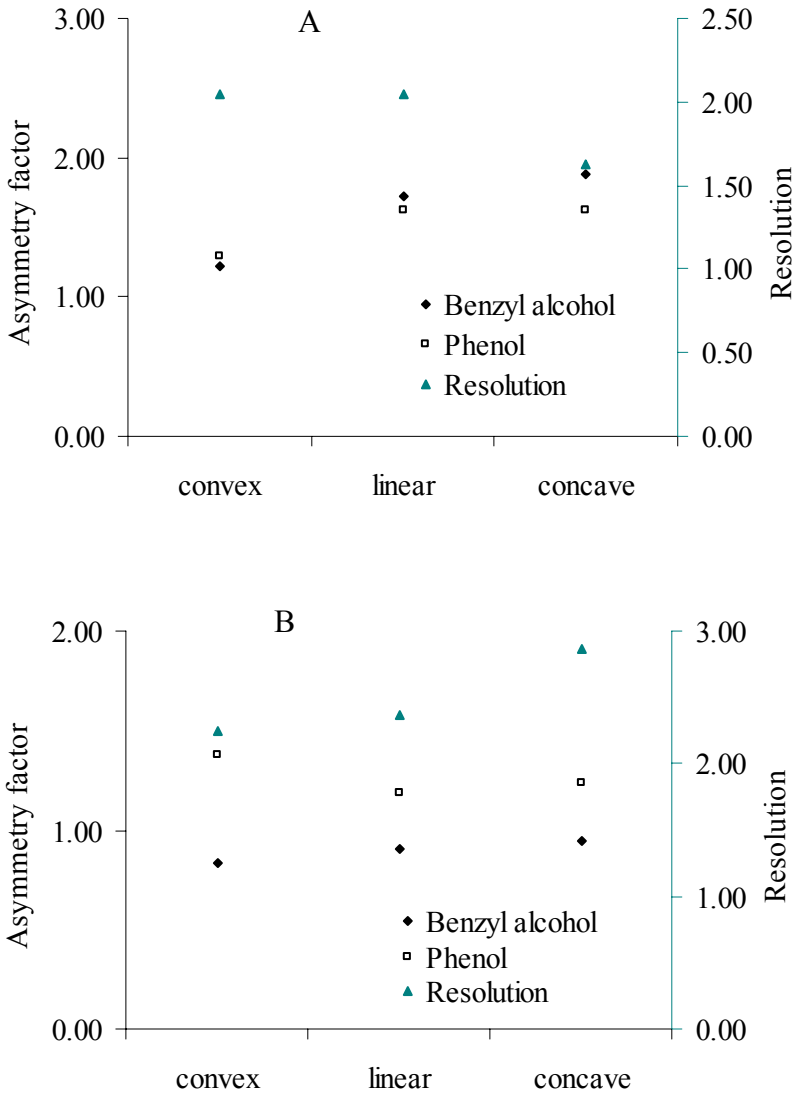

Figure II.12. Influence of gradient shape on peak shape and resolution. (A) averages from Figure II.10, (B) asymmetry factors and resolution from second pair of peaks in Figure II.11 (chosen since they had the same pseudo-injection time as in Figure II.10).

phase B, and produced lower resolution. In concave gradient elution, solutes eluted in the flat part of the gradient with a lower volume fraction of phase B, resulting in higher resolution.

Comparing Figures II.10B and II.11B, it is obvious that the choice of gradient range has a dramatic effect on the separation. After pseudo-injection, if the gradient elution starts from a point with high organic phase B concentration, as in Figure II.11, the influence from sample lag can be reduced greatly, and symmetrical peaks with high resolution would result. Also, the analysis cycle would be shortened due to the shorter retention time.

II.3.3. Quantitative Considerations

If tailing of the peaks is minimized, peak areas can be used for quantitative measurement of the analytes. Figure II.13 shows a chromatogram from an analysis of a continuous sample stream with different pseudo-injection times. The relationship between peak area and pseudo-injection time is shown in Figure II.14. The results show that the peak area changes linearly with the pseudo-injection time.

II.4. Summary and Future Research

A repetitive solvent programming approach was successfully applied to the analysis of a continuous sample stream. Each analysis cycle consisted of three steps: pseudo-injection, elution and rinse. In the pseudo-injection step, elution with a non- or poor-eluting solvent produced a concentrated sample plug due to on-column focusing, however, lagging solute gave peak tailing in the elution step. Preliminary results showed that gradient elution was superior to isocratic elution; factors influencing peak symmetry,

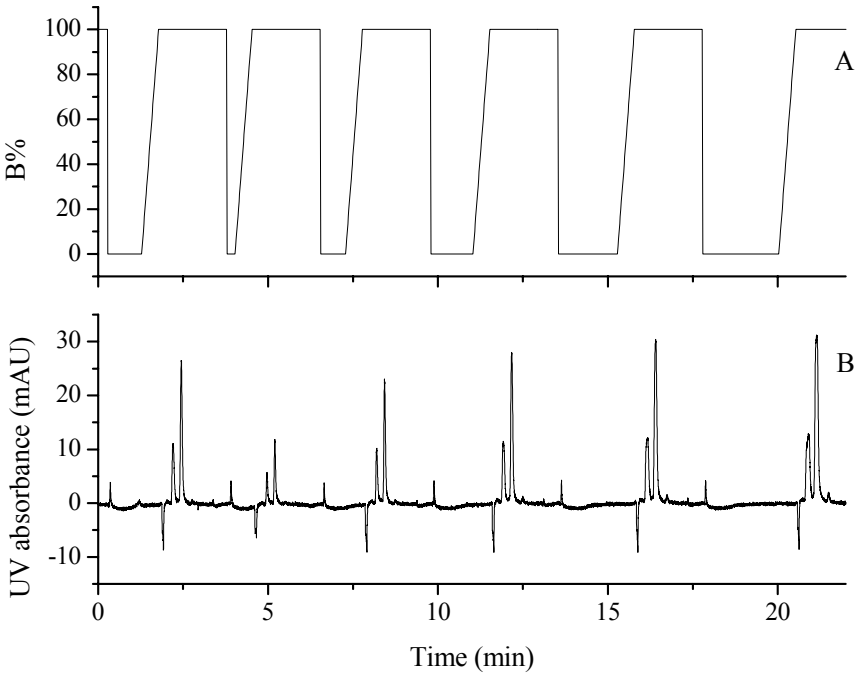

Figure II.13. Solvent program profile and chromatogram for evaluation of the quantitative nature of the pseudo-injection approach. Conditions: 4 µL/min flow rate, 255 nm UV detection.

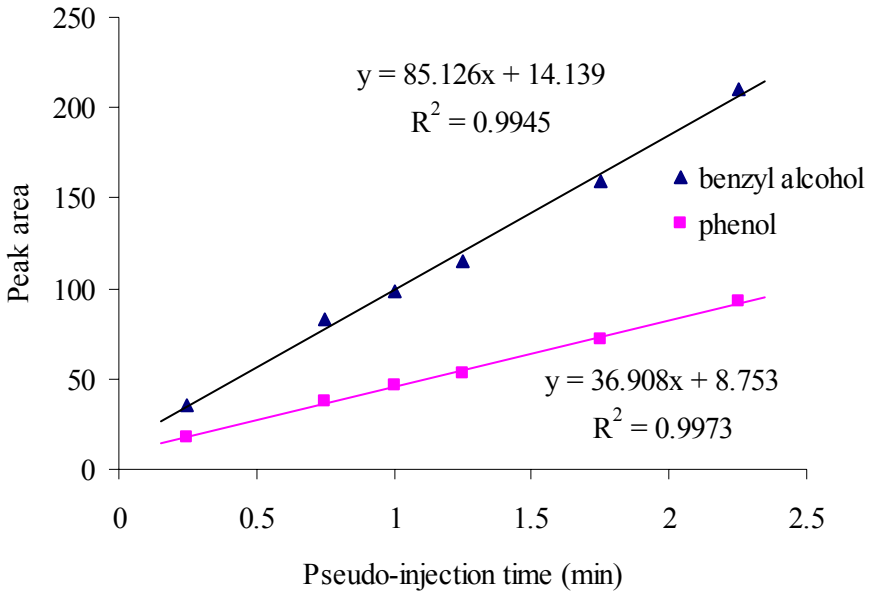

Figure II.14. Relationship between the pseudo-injection time and peak area.

Conditions: same as in Figure II.13.

resolution and analysis cycle length were investigated. Conducting elution with high phase B concentration should greatly reduce the influence from excess solutes that enter the column after pseudo-injection. Utilizing low flow rate and short gradient time should also improve peak shape and resolution. If short analysis time is desired, high flow rates and short gradient times are preferred. Quantitative analysis of a continuous sample stream is possible under certain operating conditions.

Further work is required to clarify the following:

1. Knowing what retention factor, k_0, gives effective on-column focusing would be helpful in selecting the mobile phase composition for the pseudo-injection step. If mobile phases containing some organic solvent can be used to perform on-column focusing, then the range of compounds that can be analyzed in a continuous sample stream will expand to include many compounds not soluble in water.

2. Gradient elution with high starting B% would be beneficial for reducing tailing and increasing resolution, and should be investigated in more detail. It would be useful to know what B% is high enough to limit tailing to an acceptable amount. More details of method development using the gradient mode with high starting B% also should be sought in future research.

3. In this study the model analytes were added into phase A to simulate a continuous sample stream; therefore, the actual sample stream here is not really continuous because no analytes enter the column during the rinse step. A real continuous sample stream can be introduced into the LC system after the gradient mixer. This does not greatly influence the main conclusions obtained in this study because the analyte concentrations in the original solution would typically be at trace level. However, the

method of introducing the continuous sample stream into the liquid chromatograph is a major challenge. If the sample stream is introduced into the mobile phase through a mixing tee, a flow control system should be developed to control the mixing ratio.

References

1. Swadesh, J. *HPLC: Practice and Industrial Applications*; CRC Press: New York, 1997.

2. Rehorek, A.; Urbig, K.; Meurer, R.; Schafer, C.; Plum, A.; Braun, G. *J. Chromatogr. A* **2002**, *949*, 263-268.

3. Pol, J.; Wenclawiak, B.W. *Anal. Chem.* **2003**, *75*, 1430-1435.

4. Bond, A.M.; Garrard, W.N.C.; Heritage, I.D.; Majewski, T.P.; Wallace, G.G.; McBurneyE; Crosher, M.J.P.T.; McLachlan, L.S. *Anal. Chem.* **1988**, *60*, 1357-1360.

5. Oosterkamp, A.J.; Irth, H.; Heintz, L.; Marko-Varga, G.; Tjaden, U.R.; van der Greef, J. *Anal. Chem.* **1996**, *68*, 4101-4106.

6. Fujii, K.; Nakano, T.; Hike, H.; Usui, F.; Bando, Y.; Tojo, H.; Nishimura, T. *J. Chromatogr. A* **2004**, *1057*, 107-113.

7. Scott, R.P.W.; Kucera, P. *J. Chromatogr.* **1976**, *119*, 467-482.

8. Mills, M.J.; Maltas, J.; Lough, W.J. *J. Chromatogr. A* **1997**, *759*, 1-11.

9. Karger, B.L.; Martin, M.; Guiochon, G. *Anal. Chem.* **1974**, *46*, 1640-1647.

10. Ling, B.L.; Baeyens, W.; Dewaele, C. *J. Microcol. Sep.* **1992**, *4*, 17-22.

11. Molander, P.; Thomassen, A.; Kristoffersen, L.; Greibrokk, T.; Lundanes, E. *J. Chromatogr. B* **2001**, *766*, 77-87.

12. Kimball, B.A.; DeLiberto, T.J.; Johnston, J.J. *Anal. Chem.* **2001**, *73*, 4972-4976.

13. Guetens, G.; Prenen, H.; De Boeck, G.; Van Dongen, W.; Esmans, E.; Lemiere, F.; van Oosterom, A.T.; Schoeffski, P.; de Bruijn, E.A. *J. Chromatogr. A* **2005**, *1082*, 2-5.

14. Molander, P.; Gundersen, T.E.; Haas, C.; Greibrokk, T.; Blomhoff, R.; Lundanes, E. *J. Chromatogr. A* **1999**, *847*, 59-68.

15. Snyder, L.R.; Kirkland, J.J. *Introduction to Modern Liquid Chromatography*, *2nd ed.*; John Wiley & Sons: New York, 1979.

16. Snyder, L.R.; Kirkland, J.J.; Glajch, J.L. *Practical HPLC Method Development*, *2nd ed.*; Willey-Interscience: New York, 1997.

17. Snyder, L.R.; Dolan, J.W. *Adv. Chromatogr.* **1989**, *38*, 115-185.

18. Snyder, L.R.; Dolan, J.W.; Gant, J.R. *J. Chromatogr.* **1979**, *165*, 3-30.

19. Dolan, J.W.; Lommen, D.C.; Snyder, L.R. *J. Chromatogr.* **1989**, *485*, 91-112.

20. Poole, C.F. *The Essence of Chromatography*; Elsevier Science: Amsterdam, 2003.

21. Horvath, C. *High-Performance Liquid Chromatography: Advances and Perspectives*; Academic Press: New York, 1980.

PART III. ELECTRIC FIELD GRADIENT FOCUSING OF PROTEINS

III.1. Introduction

III.1.1. Background

Electric field gradient focusing (EFGF) belongs to a family of equilibrium gradient methods of separation [1]. In an equilibrium-gradient method of separation, a set (one or more) of counteracting forces is applied to the analyte particles; along the separation path there is at least one gradient established, which causes the net force on each of the analyte particles to change in its intensity along the separation path, reach zero at one point and then change to the opposite direction after this point, as shown in Figure III.1. Obviously, analyte particles not at that special point will have a non-zero net force applied to them, causing them to move towards that special point, the equilibrium point; analyte particles at that equilibrium point have a net force of zero, and any deviation from that point will cause a net force of non-zero on that particle that can pull it back to the equilibrium point. A common example of a gradient-equilibrium method is isoelectric focusing (IEF) of amphoteric compounds like proteins or peptides [2]. In IEF, a pH gradient is established along the separation channel, and a voltage is applied to the anode at the low pH end. An amphoteric molecule, located where the pH is greater than its isoelectric point, will be negatively charged and will be pushed by the electric field away from the cathode towards the low pH area. Molecules located where the pH is lower than their isoelectric points will be positively charged and will be pushed towards the high pH area. Only at the very point where the pH is equal to the pI of an amphoteric compound, will that compound bear a net charge of zero and will not be moved by the electric field. If any molecules migrate away from the equilibrium point, a non-zero force will push them back

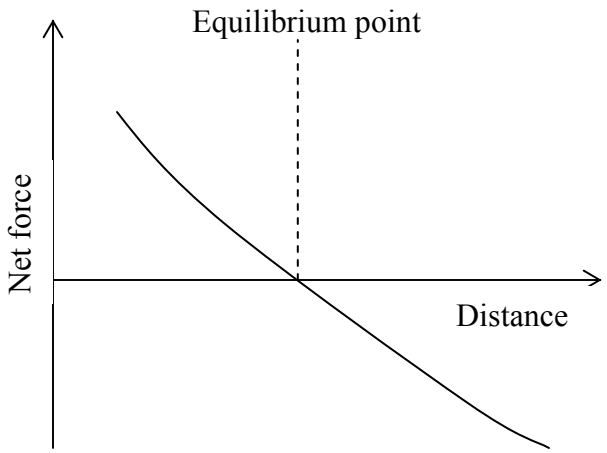

Figure III.1. Gradient-equilibrium method of separation.

to the equilibrium point. Finally, all neutral compound molecules will focus and concentrate at their respective equilibrium points.

O'Farrell [3] described the focusing of proteins at the interface between two different chromatographic packings by means of a gradient equilibrium method, called "counteracting chromatographic electrophoresis" or CACE. CACE made use of the balance between a constant electrophoretic velocity of the protein and its convective velocity that had a jump at the boundary between two different packing areas. Ivory et al. [4-7] improved this method by balancing a constant convective velocity with a gradient electrophoretic velocity, and called it electric field gradient focusing (EFGF) because the gradient electrophoretic velocity was caused by the electric field gradient established along the separation path. The basic principle of EFGF is shown in Figure III.2, and is described as follows.

The charged analyte particles obtain a constant hydrodynamic velocity, u, from the pump and an electrophoretic velocity, $u_{em}=\mu E$, from the electric field. Here, E represents the electric field intensity and μ is the electrophoretic mobility of the analyte particles. If a suitable gradient in E is established along the channel and allows a position to exist where $u = u_{em}$, then analyte particles at this position will have a net velocity equal to zero. This position is the so-called equilibrium position. Analyte particles at any other positions in the channel should have nonzero velocities toward the equilibrium position. Eventually, all charged particles of that analyte will reach this equilibrium position. Since the equilibrium position of an analyte depends on its respective electrophoretic mobility, thus, different analytes have different equilibrium positions and they focus at different positions and are separated.

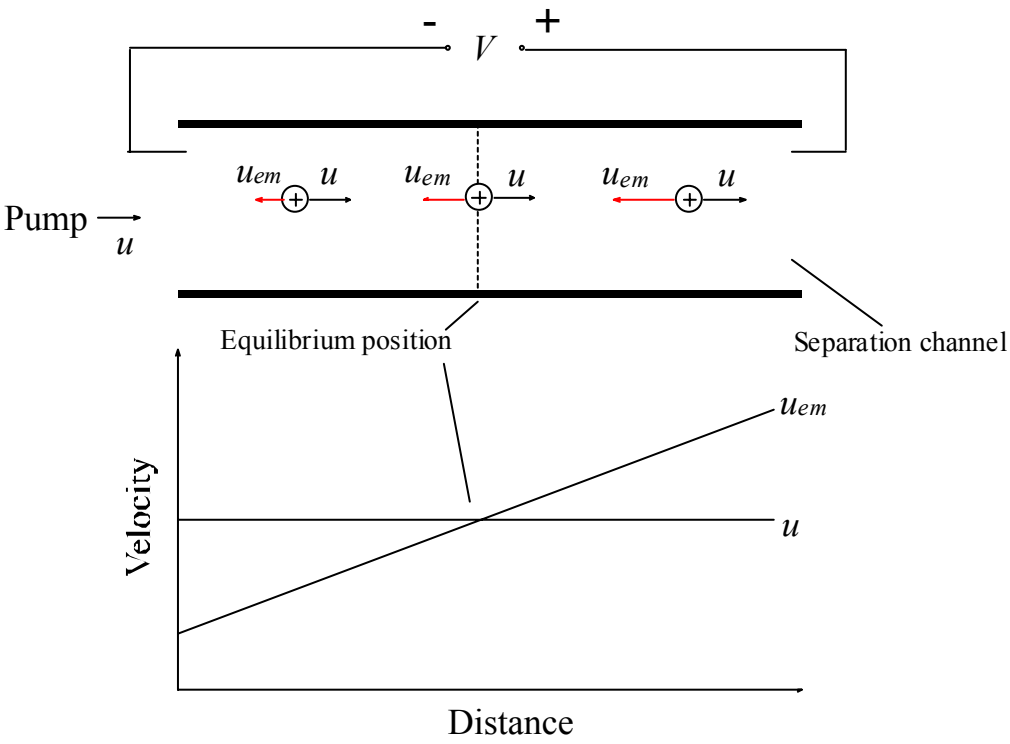

Figure III.2. Principle of electric field gradient focusing.

III.1.2. Theory

The basic theory of EFGF was discussed by Ivory et al. [4, 7] and Tolley et al. [8] in detail, and can be derived starting from the general flux equation. Assuming that the linear flux equations are adequate to represent the transport of analytes, at very low analyte concentration, the one dimensional flux of a charged analyte at position *x* can be described by the following equation

$$J(x) = -D_T \frac{\partial c(x)}{\partial x} + [u + \mu E(x)]c(x) \qquad \text{(III.1)}$$

where *J(x)* is the flux of analyte, which consists of both effective diffusion of the analyte and translational velocity, D_T is the total dispersion, *c(x)* is the concentration, *u* represents the bulk flow, μ is the electrophoretic mobility of the charged analyte, and *E(x)* is the electric field intensity at position *x*.

At the equilibrium position ($x = x_0$) where the analyte is focused, a steady-state band is formed, so the flux should be zero ($J(x) = 0$), or

$$D_T \frac{\partial c(x)}{\partial x} = [u + \mu E(x)]c(x) \qquad \text{(III.2)}$$

and the total velocity

$$u+\mu E(x_0) = 0 \qquad \text{(III.3)}$$

The electric field intensity can be described by a Taylor expansion about the point $x=x_0$

$$E(x) = E(x_0) + (\frac{\partial E(x)}{\partial x})_{x=x_0}(x - x_0) + \frac{1}{2}(\frac{\partial^2 E(x)}{\partial x^2})_{x=x_0}(x - x_0)^2 + ... \qquad \text{(III.4)}$$

For a narrow band, the terms of the second and higher orders are negligible and may be ignored. If we define

$$b = (\frac{\partial E(x)}{\partial x})_{x=x_0} \qquad \text{(III.5)}$$

which is the slope of the electric field intensity at position $x = x_0$, then we obtain

$$E(x) = E(x_0) + b(x - x_0) \tag{III.6}$$

Substituting III.6 into III.2, integrating, and considering III.3, we obtain

$$c(x) = c_0 \exp[\frac{b\mu}{2D_T}(x - x_0)^2] \tag{III.7}$$

Comparing this equation with a Gaussian distribution, we know that the focused band can be represented as a Gaussian distribution with a standard deviation of

$$\sigma = \sqrt{-\frac{D_T}{b\,\mu}} \tag{III.8}$$

Because D_T is always positive, the EFGF experiment must maintain $b\mu < 0$. This means that the electric field should be set in a way that always gives the analyte an electrophoretic velocity in the direction from high to low electric field intensity. If the electric field is set wrong, no focusing will occur.

The band width can be estimated to be $W = 4\sigma$. For two closely focused bands, $\mu_1 \approx \mu_2 \approx \overline{\mu}$. Considering III.6 and III.3, we obtain

$$\Delta x = \frac{\Delta E(x)}{b} = -\frac{1}{b}(\frac{u}{\mu_2} - \frac{u}{\mu_1}) \approx \frac{-u\,\Delta\mu}{b\,\overline{\mu}^2} \tag{III.9}$$

Then the resolution can be expressed as

$$R_s \approx \frac{|\Delta x|}{4\overline{\sigma}} = \frac{|u\,\Delta\mu|}{4\overline{\mu}\sqrt{b\,D_T\,\overline{\mu}}} \tag{III.10}$$

Although this theory cannot explain all aspects of EFGF (for example, in equation III.8 we cannot account for the effect of the bulk flow on the peak width), it can still give much guidance in designing and conducting EFGF experiments. From III.8 and III.10, we know that a high fluid linear velocity, u, gives broad bands but high resolution, while a

steep gradient or large *b* gives narrow peaks but low resolution. There is a trade off between peak width and resolution. Obviously, the key step in EFGF is to establish an electric field gradient in the separation path.

III.1.3. Previous Work

Generally speaking, the intensity of an electric field at position *x* in a channel can be expressed as

$$E(x) = \frac{dU(x)}{dx} = \frac{i(x)\,\rho(x)\frac{dx}{A(x)}}{dx} = \frac{i(x)\,\rho(x)}{A(x)} = \frac{i(x)}{\sigma(x)\,A(x)} \qquad \text{(III.11)}$$

where *i(x), ρ(x), A(x)* and *σ(x)* are the current, resistance, cross-sectional area and conductivity at position x. Therefore, an electric field gradient can be built by changing any of these factors in equation III.11.

The first approach to EFGF reported by Ivory et al. [4, 7] was to change the cross-sectional area of the channel, as shown in Figure III.3. The working buffer solution flowed downward inside the separation channel. The buffer solution in the outside channel, circulated and cooled by a heat exchanger, flowed in the opposite direction to that in the separation channel. Voltage was applied across the top and bottom of the channels. The intensity of the electric field changed along the channel because the total cross-sectional area changed along the channel. The cross-sectional area of the separation channel (i.e., the dialysis tubing) was constant so as to keep the flow rate inside the separation channel constant. It was observed that hemoglobin was focused in a 5 mM Tris-13.3 mM glycine buffer at pH 8.7 with a flow rate of 2.54×10^{-4} mL/s and a voltage of 1,000 V. With the same conditions, myoglobins with different oxidation states were focused and separated.

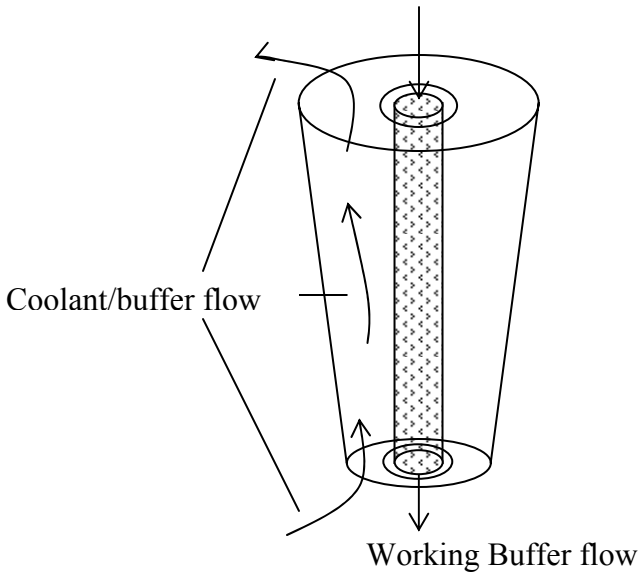

Figure III.3. EFGF device with changing cross-sectional area channel.

One disadvantage of the above mentioned changing cross-sectional area approach is that the separation channel was located inside the purge channel, which gave rise to some difficulties in observing or detecting the focused bands. An EFGF device using a changing cross-sectional area channel in a planar format was investigated in our laboratory. A scanning laser-induced fluorescence detection system was readily mounted to this focusing device. Two miniaturized versions of EFGF units with planar structures were also developed in our laboratory [9, 10]. Humble and co-workers [9] reported a small EFGF device with a changing cross-sectional area channel consisting of an in-situ polymerized ionically conductive polymer sheet. The space left by pulling out a thin metal wire inside that polymer sheet formed the separation channel with a diameter of 120 μm. A 10,000-fold concentration of green fluorescent protein was accomplished with this EFGF device. Separation of a protein mixture was also demonstrated. Liu et al. [10] reported the fabrication of a tiny separation channel and a changing cross-sectional area channel using a microfabrication technique. A polymer membrane with a porous structure, in-situ generated between the two channels, allowed electrical connection between these two channels, and also prevented proteins from escaping from the separation channel. Green fluorescence protein could be focused using this micro EFGF device with a concentration factor of 4,000. A protein mixture was also separated.

Another approach to generating an electric field gradient in EFGF was to change the conductivity and, hence, the resistance of the separation channel. Greenlee et al. [5] placed a semi-permeable dialysis membrane between the separation channel and a purge channel. The working buffer solution contained a high concentration of salt, which permeated through the dialysis membrane gradually. Large molecules like proteins, not

capable of going through the membrane, stayed in the separation channel. The diffusion of salt ions from the separation channel to the purge channel through the membrane allowed a gradient in the salt concentration to be generated along the separation channel. Therefore, an electric field gradient was formed along the channel according to equation III.1. The results showed that bovine serum albumin (BSA) and bovine hemoglobin (Hb) could be focused and separated in the separation channel. This changing conductivity approach was further developed in our group using a hollow fiber. Wang et al. [11] reported that a hollow dialysis fiber, serving as the separation channel, was mounted in the center of a silica capillary; the working buffer solution containing a high concentration salt was introduced into one end of the dialysis fiber, while the space outside the fiber but inside the capillary served as a purge channel. The diffusion of salt from inside the hollow fiber to the purge channel through the fiber wall generated a salt concentration gradient inside the dialysis fiber. Thus, an electric field gradient was established inside the separation channel. Due to the smaller dimensions of the fiber-based device compared to earlier work, better resolution and shorter running time were achieved.

Huang and co-workers [6] demonstrated a digitally controlled electrophoretic focusing device. The strategy was to dynamically establish and maintain the electric field gradient by mounting an array of 50 electrodes along the channel. The potentials on the electrodes were controlled and adjusted individually by a computer. The electrodes were located in a purge channel which was parallel to and electrically connected to the separation channel through a dialysis membrane. The separation channel was packed with size exclusion stationary phase with particle diameter of 45 μm to reduce the dispersion

of the focused band. Single proteins and protein mixtures were focused and separated with this device.

The conductivity of the buffer solution in the separation channel can also be changed by changing the temperature of a buffer inside the channel for which the conductivity is temperature dependent. Ross and co-workers [12] reported a method to establish an electric field gradient by generating a temperature gradient along the channel. The focusing and separation of different compounds including fluorescence dyes, amino acids, DNA, proteins and particles were demonstrated. A concentration factor of 10,000 could be achieved.

III.1.4. Approaches in This Research

To simplify the experimental design, a linear electric field gradient is usually used in EFGF, where $E(x)=E(0)+bx$. The cross-sectional area of the separation channel is usually constant so as to maintain a constant bulk flow. Considering equation III.11 in a separation channel, if using a uniform buffer solution, then the resistance of the solution is also constant. The current inside the separation channel is the only factor we can change to obtain a gradient in E. As shown in Figure III.4, a partner resistor is needed to compensate for this current change. The total current, which should be constant along the channel, will distribute between the separation channel and the partner resistor according to their relative resistance ratio. In this work, a so-called "distributed resistor" was used as the partner resistor. The distributed resistor was so designed that its resistance changed along the channel in a way that allowed the current inside the separation channel to change linearly, i.e., the electric field intensity inside the separation channel changed linearly.

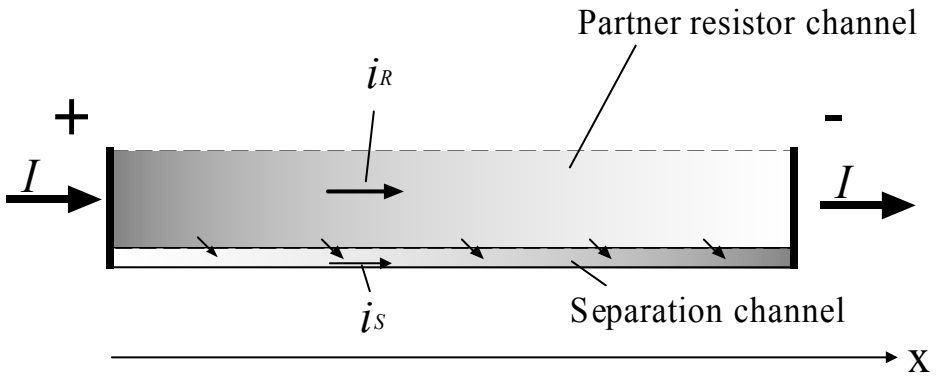

Figure III.4. EFGF device with partner resistor channel.

The changing cross-sectional area EFGF approach is a simple method to generate a gradient in *E*. Different EFGF devices with planar structures were built and evaluated in this research. The planar structure made this type of device easier to make, convenient to couple with detectors, and suitable for microfabrication.

Using a low concentration of analyte is important for EFGF, or the focused band may cause distortion in the electric field profile along the channel. Therefore, highly sensitive detection is needed for EFGF. Laser-induced fluorescence detection is a very sensitive detection method due to its low background and high signal to noise ratio, and should be a good choice for EFGF. For elution separation methods, results can be obtained by monitoring only one point with the detector. However, EFGF produces focused bands along the whole channel. In this research a scanning laser-induced fluorescence detection system was constructed and used to monitor the focusing process and the analyte bands along the separation channel.

III.2. Experimental

III.2.1. Chemicals

Tris-HCl, Tris base, BSA, hemoglobin and conalbumin were purchased from Sigma (St. Louis, MO). Other chemicals were obtained from Aldrich. Spectra/Por 4 dialysis membrane with molecule weight cut off (MWCO) of 10,000-12,000 was purchased from Spectrum Laboratories (Rancho Dominguez, CA). The dialysis hollow fiber, a modified cellulose fiber with internal diameter of 200 μm and dry wall thickness of 8 μm, was purchased from Membrana (Wuppertal, Germany). This dialysis fiber had a molecular

weight cut-off (MWCO) of approximately 10,000. Untreated fused-silica capillaries (250 μm i.d. , 360 μm o.d.) were purchased from Polymicro Technologies (Phoenix, AZ).

Proteins were labeled with FITC using a FluoroTag^{TM} FITC conjugation kit (Sigma, St. Louis, MO). After labeling, the products were separated with size exclusion chromatography to remove unlabeled proteins, free FTIC and possible impurities. The concentrations of labeled proteins were determined by means of a UV spectrophotometer.

III.2.2. Device Using Distributed Resistor Substrate

A distributed resistor substrate was constructed from a ceramic substrate with distributed resistors incorporated on its surface (Figure III.5A). The middle strip between the distributed resistors was left for the separation channel. The distributed resistor substrates used in this research were designed and manufactured by David A. Lefebre, Camino, CA, who first conceived the idea of using distributed resistors. Two types of EFGF devices were built with distributed resistor substrates. Type I (Figure III.5B) was a one-layer EFGF device without purge channel. The middle separation channel was filled with working buffer solution, and maintained ohmic contact with the edges of the distributed resistors. Type II (Figure III.5C) was a 2-layer EFGF device with the lower channel serving as a purge channel to wash out bubbles and products generated during the electrochemical process. Between the lower purge channel and the upper separation channel was a layer of dialysis membrane, which allowed the transport of small buffer ions, but prevented protein molecules from escaping the separation channel.

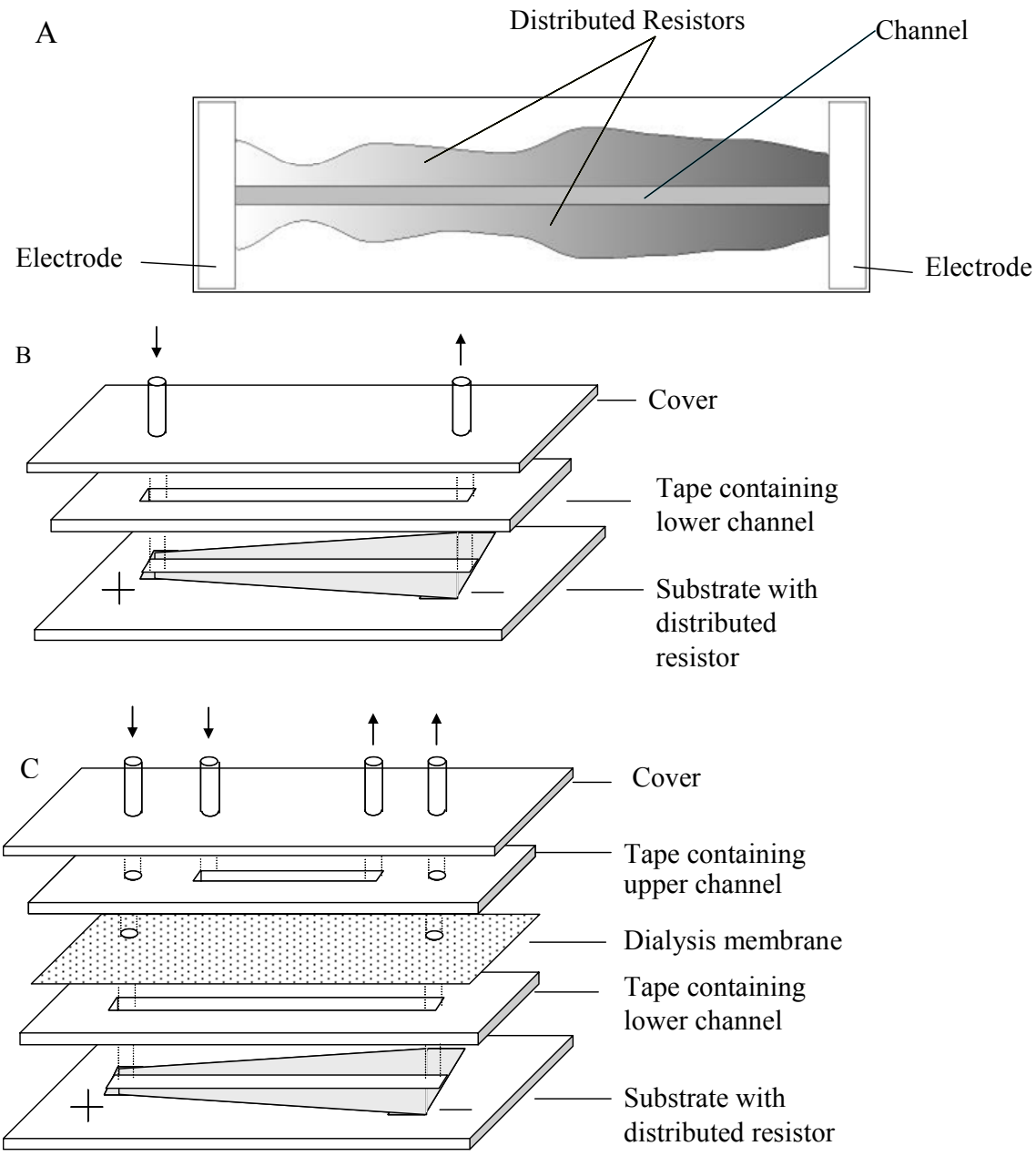

Figure III.5. Distributed resistor substrate and related EFGF devices.

III.2.3. Manufacture of Porous Glass Capillary

A glass capillary with porous wall was chosen as a possible separation channel for changing cross sectional area EFGF devices. The porous wall provided electrical connection with the partner resistors, while at the same time retained large analyte molecules inside the separation channel. Also, the rigid wall maintained the shape of the separation channel and gave stable electric field profile and constant bulk flow inside the channel. The small i.d. helped to reduce band dispersion.

The porous glass capillaries used in this research were made by modifying commercially available borosilicate glass tubing. The procedure to manufacture the required porous glass capillaries included a number of steps. First, a glass capillary was drawn from borosilicate glass tubing and heated at 580 °C for 24 h to allow partial phase separation into two different phases: a boron-rich phase and a silicon-rich phase. The capillary was then treated with ~11% HCl(aq) at 80~90 °C for 24~28 h, allowing dissolution of the boron-rich phase. Finally, the capillary was washed with deionized water.

Figure III.6 shows an SEM sectional view of a typical porous glass capillary at different magnifications. The porous capillaries used in the EFGF tests usually had an i.d. of approximately 80 μm, and an o.d. of 260 μm. The structure was uniform and no obvious defects were observed even at large magnification. Figure III.7 shows the change in elemental composition of the glass capillary phase after separation and acid treatment. Clearly, a capillary with silicon-rich composition was obtained after the above described processing.

A

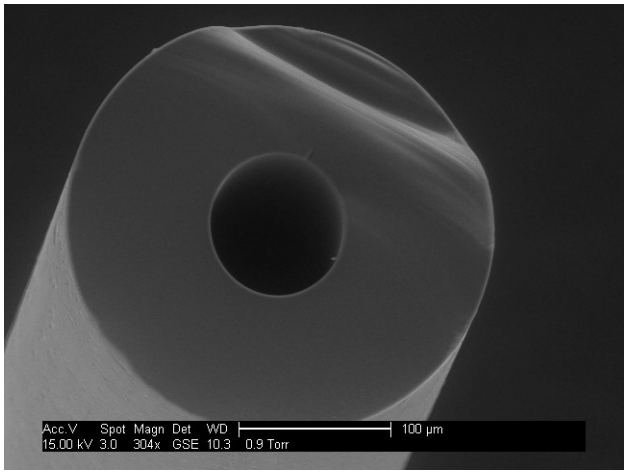

B

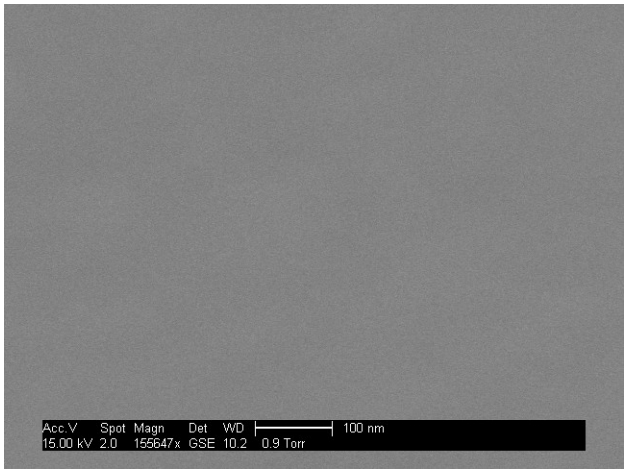

Figure III.6. SEM view of a porous glass capillary. (A) 304× and (B) 155,647× magnification.

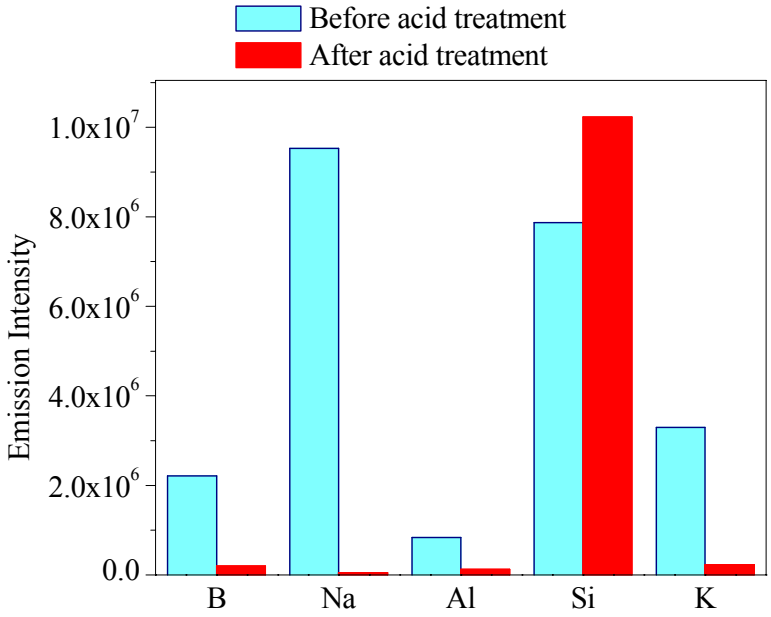

Figure III.7. Results of ICP-AES analysis of the glass capillary before and after acid treatment.

III.2.4. Changing Cross-sectional Area Devices with Planar Structures

Planar CCSA EFGF devices were prepared with narrow, shallow separation channels engraved on a PMMA sheet, as shown in Figure III.8. The partner resistor was a channel cut out of the Mylar tape with a specially designed shape. This shape was designed to provide a linear electric field gradient along the top edge of the channel. The separation channel was cut out of a sheet of tape, or engraved as a narrow shallow groove on the top cover. The separation channel was located on the top of the partner channel and connected to it through a layer of dialysis membrane. Typical dimensions of the separation channel were 0.8 mm wide and 0.15 mm deep.

The planar CCSA EFGF channel was further improved by using a segment of hollow dialysis fiber which was then incorporated inside the partner channel, as shown in Figure III.9. The partner channel was cut out of a sheet of Mylar double stick tape. These channels were then sandwiched between two flat PMMA sheets.

The curve defining the shape of the CCSA channel was determined by the required electric field gradient profile. Linear electric field gradient profiles were used in this research as represented by

$$E(x)=E(x_0)+bx \qquad \text{(III.12)}$$

where x is the distance along the separation channel. From this equation

$$E(x)=\frac{dU}{dx}=\frac{I\rho}{A}=\frac{I\rho}{t\,y(x)} \qquad \text{(III.13)}$$

where t is the thickness of the CCSA channel. Finally, we can obtain

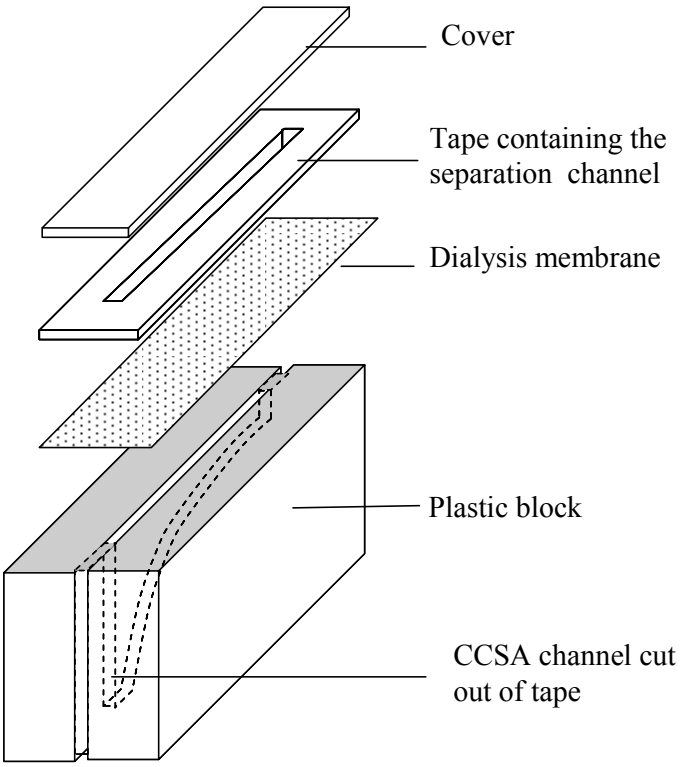

Figure III.8. EFGF device with a vertical CCSA channel.

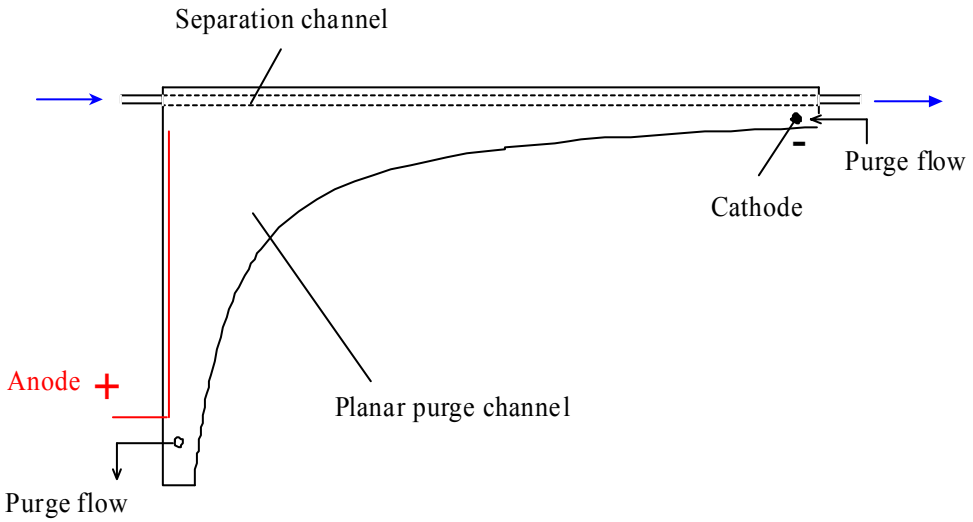

Figure III.9. Planar CCSA EFGF device with a hollow dialysis fiber or porous glass capillary as the separation channel.

$$y(x) = \frac{I\rho}{t[E(x_0) + bx]} \qquad \text{(III.14)}$$

The channel curve can be calculated using this equation, and the voltage needed can also be calculated. Once the curve was cut and the channel was constructed, changing the actual applied voltage changed the total current and, hence, the field gradient profile, especially the slope of the gradient.

III.2.5. Scanning Laser-induced Fluorescence Detection System

Figure III.10 is a schematic diagram of the scanning laser-induced fluorescence detection system. This home-made detection system used the 488 nm line of an argon ion laser (Model 95 Ion Laser, Lexel, Palo Alto, CA) as the excitation wavelength. The fluorescence signal was collected using a photomultiplier tube (PMT) through a narrow slit with a width of 50 μm, and then amplified and transferred to a PCI-6034E data acquisition board (DAQ) (National Instruments, Austin, TX). The EFGF device was mounted on a moving stage that was controlled by a PC. A Labview program was designed to control the moving stage as well as the collection of data from the PMT. Data were usually collected after every 50 μm movement of the channel.

With this detection system, fluorescence signals from the whole channel could be collected and monitored during the focusing process. It not only provided information on the focused bands, but also provided information about changes of analyte concentrations along the channel during focusing, which helped in understanding the principles of EFGF.

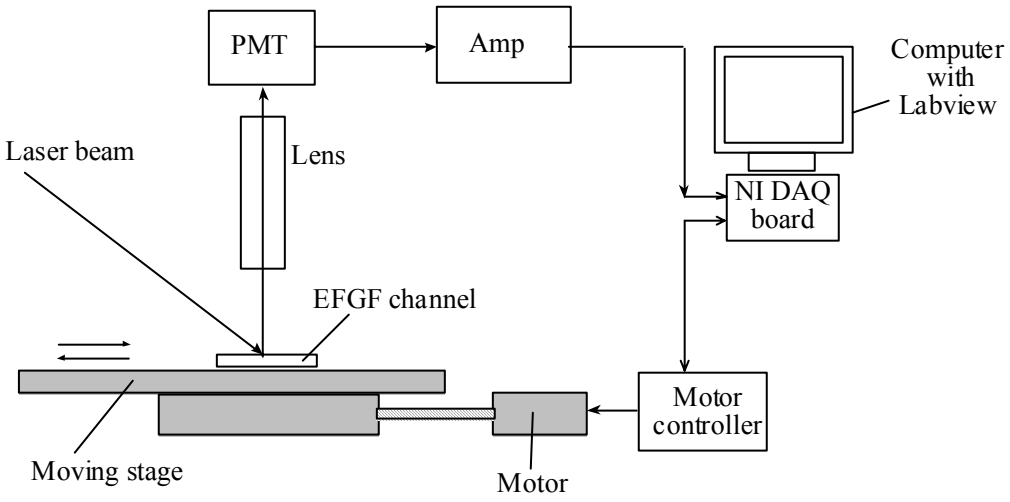

Figure III.10. Scanning laser-induced fluorescence detection system.

III.3. Results and Discussion

III.3.1. Distributed Resistor Devices

All protein focusing experiments were performed in buffer solutions with pH values greater than the pI values of the protein analytes. Therefore, the protein molecules were kept negatively charged, and the anode was set at the low electric field end of the channel. Using Type-I EFGF devices containing distributed resistors, proteins could be focused quite well in Tris buffer solution with pH 8.7. Figure III.11 shows two focused protein bands. However, the bands continued to move after being focused, and the band widths changed with time. Furthermore, the repeatability was poor from test to test.

One reason for the unstable bands was the formation of bubbles inside the separation channel. It was observed that there were tiny bubbles formed along the edges of the separation channel during the focusing process, as shown in Figure III.12. Some of these bubbles grew gradually and became very large with diameters up to a few millimeters.

In the meantime, electric current decay was observed during focusing. The current usually started to decrease rapidly after the voltage was applied. The bubbles formed during focusing changed the resistance of the separation channel and, hence, the current and electric field profile, and was the main cause for the unstable bands. It was noticed that the bubbles were generated along the edges of the distributed resistors and at the two electrodes at the ends of the separation channel; in other words, bubbles formed on the boundaries between the solid surfaces and the liquid phase. It was concluded that bubble

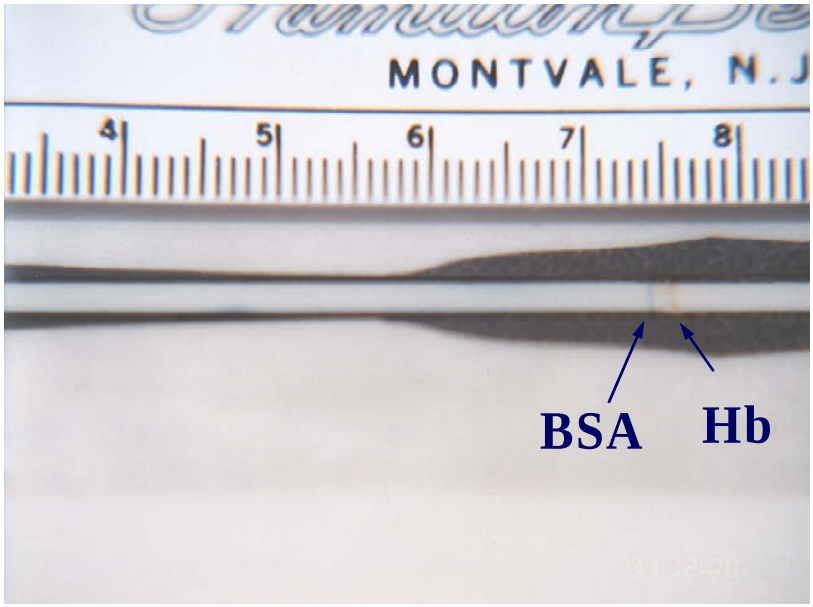

Figure III.11. Separation of two proteins in a Type-I EFGF device. Conditions: 10 mM Tris buffer, pH 8.7; 20 µL 0.02 mg/mL BSA and 0.02 mg/mL Hb sample; 1.0 µL/min buffer flow rate; 1500 V voltage.

A.

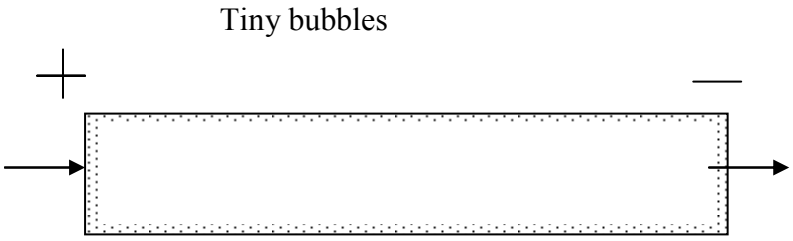

B

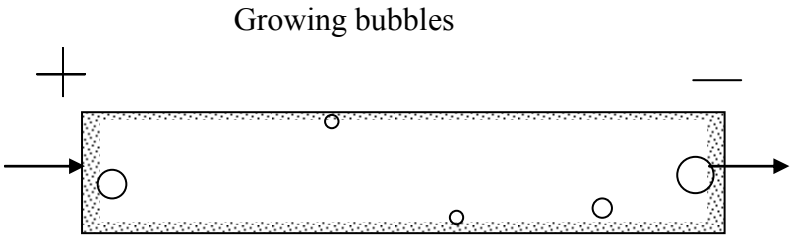

C

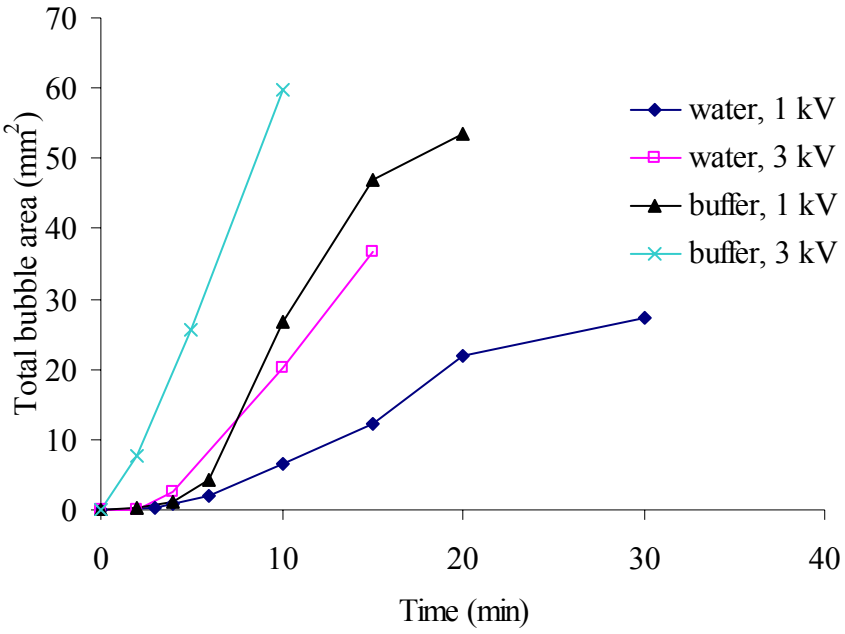

Figure III.12. Bubble formation (A) and growth (B and C) in the separation channel. In (C), buffer is 1 mM Tris buffer.

formation was due to electrochemical processes occurring at the boundaries between the solid and liquid phases. It was necessary to have current flow across the boundaries between the distributed resistors as mentioned above, and the current was conducted between the metal electrodes (anode and cathode) and the buffer solution in the separation channel. When crossing the boundaries between a solid surface and a liquid phase, the current is sustained through the transfer of electron between them, which must be accompanied by reduction/oxidation reactions of the species in the buffer solution. For the focusing conditions used, the anode was located at the low electric field end of the device, so the current direction was from the anode and the distributed resistors into the separation channel. This meant that the electrons moved in the opposite direction. Therefore, in aqueous solution, the following reactions most probably occurred

Anode & sides: $4\ OH^- \rightarrow 2\ H_2O + O_2(g) + 4e^-$ (III.15)

Cathode : $2\ H_2O + 2e^- \rightarrow H_2(g) + 2OH^-$ (III.16)

Thus, gases were generated and accumulated at the boundaries between the solid surfaces and the liquid phase.

Different approaches have been evaluated for suppression of bubble formation during the focusing process. First, the addition of various redox pairs in the separation channel was tested in hopes that the reduction/oxidation of these redox pairs could replace the redox reactions containing oxygen and hydrogen. Ascorbic acid/dehydroascorbic acid (1 mM), and quinine/hydroquinone were evaluated. The current remained constant with time for a few minutes at the beginning of the focusing step, but then the current dropped rapidly just as before with the emergence of bubbles. This indicates that the addition of certain redox pairs were effective in reducing the

formation of bubbles at the boundaries between the solid phases and liquid phase. However, after the oxidation/reduction agents in the vicinity of the boundaries were used up, soluble redox species could only reach the boundaries gradually by diffusion, which was not significant to support the needed current. Therefore, bubble formation reactions shown in equations (III.15) and (III.16) started again.

Further experiments showed that using different buffer solutions (Tris, tricine and phosphate) did not help in bubble suppression. The addition of surfactants was also tested. The addition 0.5% Brij 35 did not reduce bubble formation, but it lowered the surface tension of the liquid phase so that the maximum bubble size was reduced.

Another effect caused by the electrochemical processes at the boundaries between the solid surface and liquid phase was the generation of a pH gradient. As indicated by equations (III.15) and (III.16), the electrochemical processes produced OH^- anions at the cathode and consumed OH^- cations at the anode and distributed resistor edges. Consequently, this changed the pH in these areas. This pH change expanded along the separation channel with time and generated a pH gradient. Figure III.13 shows an experimental set-up to illustrate the formation of a pH gradient during separation. In this experiment, 1 mM phosphate buffer solution with pH of 7.4 was used. Phenol red was added to the buffer solution as a pH indicator. The color of phenol red is yellow for pH below 6.6, exhibits a gradual transition from yellow to red over the pH range of 6.6 to 8.0, and turns bright pink above pH 8.1. The bulk flow in the separation channel was set to 1 μL/min. After applying a voltage of 1000 V for 20 s over the channel, a red color zone appeared at the cathode end while the anode end turned yellow (Figure III.13A). Three minutes later,

A

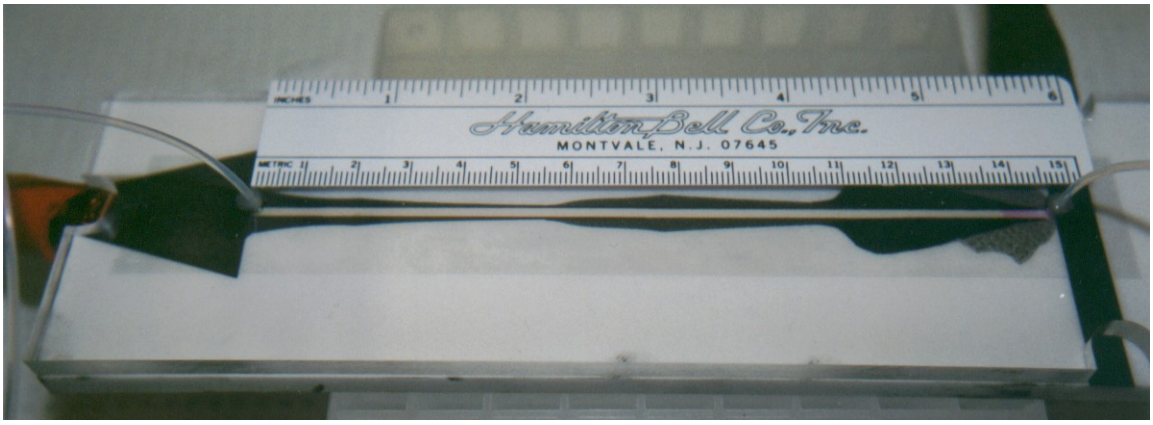

B

Figure III.13. Formation of a pH gradient in the separation channel. For conditions, see text.

the red and yellow color zones extended to the middle of the channel (Figure III.13B).

In summary, electrochemical processes must occur in the separation channel to conduct electrical current between the solid surfaces and liquid phase. However, formation of bubbles and pH gradient had deleterious effects on EFGF. Addition of certain redox pairs helped to reduce bubble formation, but the effects could only be sustained for a short period of time compared to the time needed for protein focusing. New methods need to be found to overcome the difficulties imposed by the electrochemical processes at the boundaries between the solid phases and the buffer solution. One choice was to use a purge channel to flush away bubbles and any other electrochemical reaction products so as to keep the composition in the channel uniform. To achieve this, a new 2-layer channel EFGF device was designed and tested.

The structure of the Type-II device with 2-layer channels is illustrated in Figure III.5. The idea was to use high bulk flow rate in the lower purge channel to flush out bubbles and any possible electrochemical reaction products so as to keep the composition of that channel uniform. Thus, the electric field gradient profile formed in the channel could be stabilized. The upper channel was electrically connected with the lower channel through a dialysis semi-permeable membrane. The membrane also prevented proteins from passing from the separation channel to the lower channel and ensured a constant flow rate in the separation channel. Experimental results showed that there was no observable pH gradient formed in the channels. Single proteins could be focused in the upper channel. Figure III.14 shows a typical focused band.

With high buffer flow rate in the lower channel, the 2-layer channel device basically solved the pH gradient problem, and also removed most of the bubbles formed

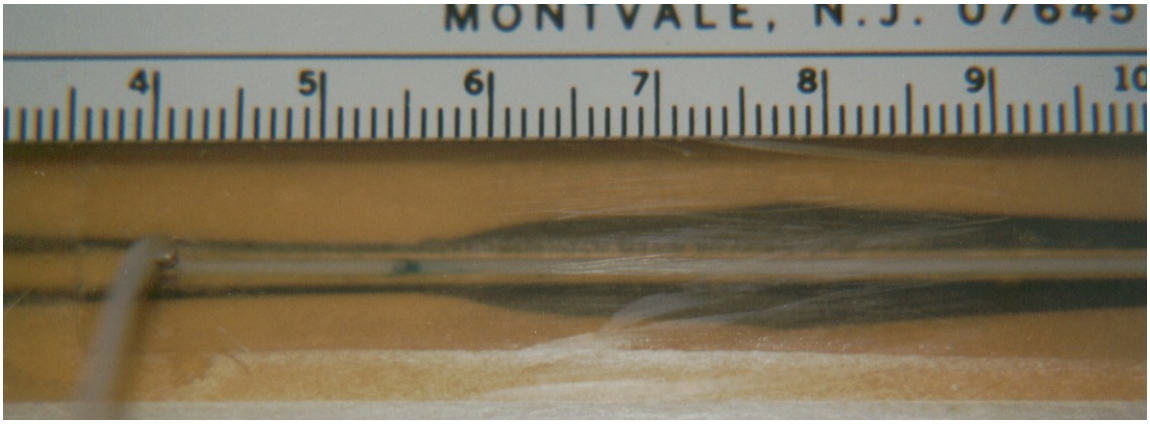

Figure III.14. Focused band of BSA in the upper channel of a two-layer channel EFGF device.

during focusing. However, the focused bands were still unstable, and sometimes moved to one end and disappeared. One possible reason for the unstable bands was due to the dialysis membrane used to separate the upper and lower channels. The membrane became soft and swelled somewhat when it was surrounded by the buffer solution. The solution also penetrated into the membrane layer, including the area of the membrane outside the channel. This generated variation in the electric field in the channel, and also made it difficult to attach the membrane securely to the double-stick tape.

Because the pressure in the lower channel was usually higher than that in the upper channel, the membrane was most likely pushed upward in the center. This changed the shape of the upper channel and disturbed the focusing.

III.3.2. Planar Changing Cross-sectional Area Devices

As stated above, EFGF devices with distributed resistors forming the partner channel had one inherent weakness: electrochemical processes at the boundaries between the distributed resistors and the buffer solution in the separation channel. A way to completely overcome this weakness was to use a liquid phase partner resistor channel. For this type of EFGF device, the partner resistor could be a channel with cross-sectional area that changed along the channel that was filled and purged with buffer solution. This partner resistor channel could be connected to the separation channel through a semi-permeable wall. Therefore, both the separation channel and the partner resistor channel would contain buffer solutions, and the current would be transported between them by means of ion migration, so no electrochemical processes result. There would still be electrochemical reactions occurring at the electrodes, but the electrodes could be placed away from the channels to reduce the influence of the electrodes on the focusing process.

Planar CCSA EFGF devices with planar membrane. A EFGF device with CCSA channel was first built and tested due to its ease of construction. The typical structure is illustrated in Figure III.8. The electric field in the CCSA channel was estimated by using an array of electrodes that were inserted along the separation channel. The plan was to measure the potential of each electrode inserted into the CCSA channel relative to the cathode, and then from a curve of voltage vs distance, the distribution of the electric field along the channel could be estimated. This would only be an estimate because the electrodes modify the electric field inside the channel. The experimental results showed that the electric field ($E = dU/Dx$) changed linearly with distance, however the slope measured was much lower than desired.

Experimental results showed that no pH gradient formed in the upper separation channel, and no bubbles formed in the channel. Single proteins were focused, and a mixture of two proteins were focused and separated. Figure III.15 shows typical focused protein bands. This type of EFGF device overcame the inherent weakness of the devices with distributed resistors. Ivory's original version of CCSA EFGF devices had a separation channel mounted in the center of a cylindrical CCSA channel [4], which was very inconvenient for observing the focused bands. The separation channel for the EFGF devices presented here was placed on one side of the device, which allowed easy observation by eye or with a detector.

The anode and cathode were placed far from the working channels (and connected to them through buffer solution) to minimize the influence from the electrochemical

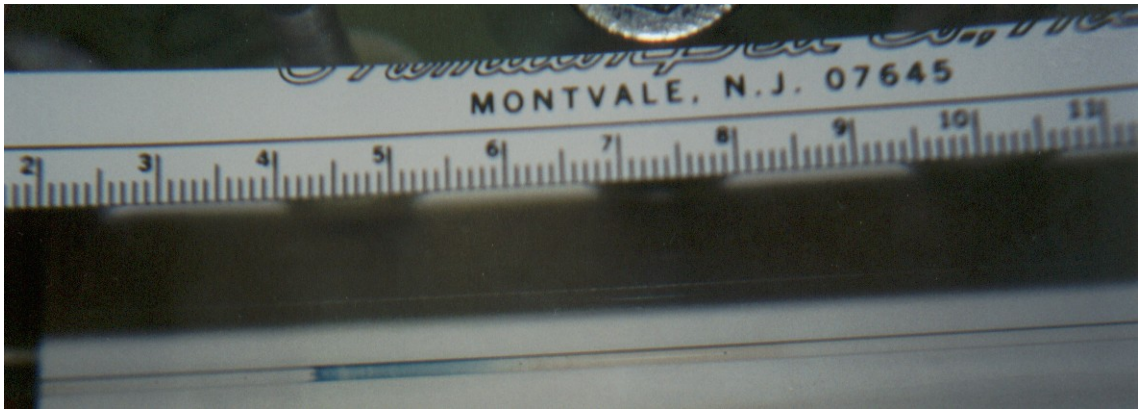

Figure III.15. Focused protein bands in the separation channel of a planar CCSA device. Conditions: u_{upper} = 7 μL/min, u_{purge} = 500 μL/min, V = 1 kV; 50 mM Tris buffer solution, pH 8.7. Band identifications: the left blue band is BSA, and the right brown band is hemoglobin.

processes occurring at the electrodes. However, there were still problems associated with the dialysis tape. The wetted membrane became soft and was hard to fix in place by the double stick tape. This wet conductive membrane most likely caused variation in the electric field in the separation channel. The focused protein bands were also rather wide. Efforts were needed to improve the EFGF devices to obtain narrower focused bands so as to increase the peak capacity of the EFGF technique.

Planar CCSA EFGF device with dialysis fiber. The hollow dialysis fiber had an inner diameter of 200 μm, and a dry wall thickness of 8 μm, and it was suspended in the CCSA channel. The dialysis fiber overcame most of the problems in the previous EFGF devices, except that it also became soft. The small diameter of the hollow fiber helped to reduce dispersion of the focused bands so that narrower bands could be formed.

The electric field in the CCSA channel was estimated by the method mentioned above, and proved to be a linear gradient profile. The slope measured was much lower than what was desired probably due to the use of a large total current when designing the channel.

The small diameter of the separation channel increased the difficulty in observing protein bands inside the channel by eye. Also, the concentrations of the analytes were sufficiently low so that their focused bands did not interfere with the electric field inside the separation channel. Therefore, a scanning laser-induced fluorescence detection system was constructed due to its high sensitivity.

Figure III.16 shows the influence of flow rate on the focused BSA band. It can be seen that increasing the flow rate broadened the peak, just as predicted by equation (III.7), and the peak position moved toward the high electric field direction.

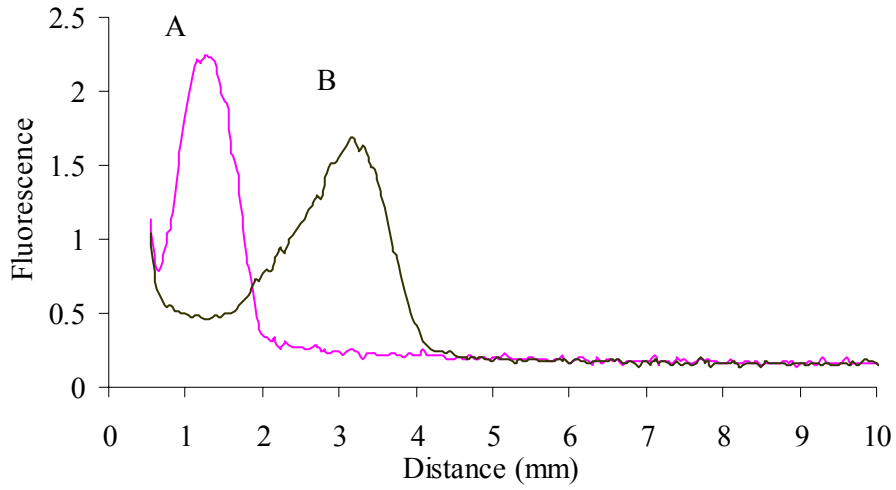

Figure III.16. Effect of flow rate on focusing of BSA. Conditions: (A) u = 0.02 µL/min, V = 400 V; (B) u = 0.05 µL/min, V = 400 V.

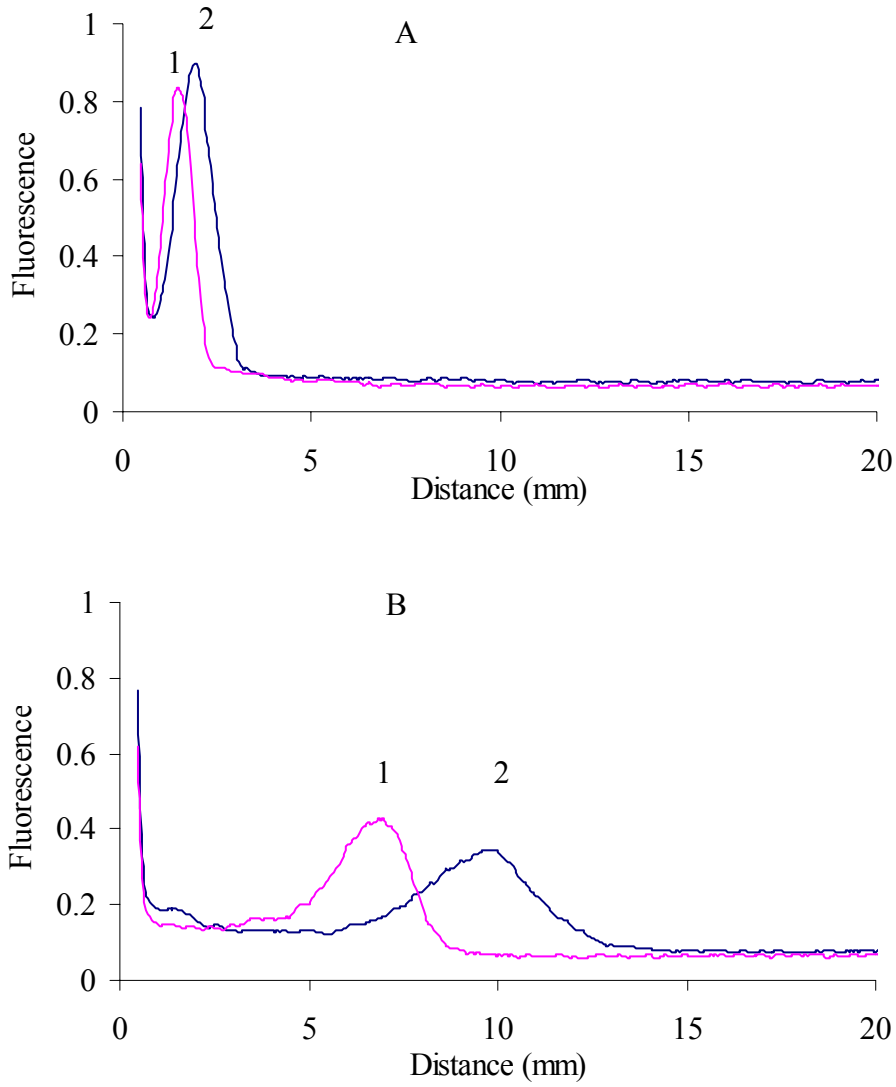

Figure III.17. Effect of voltage on focusing of single proteins. Conditions: (A) u = 0.02 µL/min, V = 400 V; (B) u = 0.02 µL/min, V = 100 V. Band identifications: (1) BSA and (2) conalbumin.

As shown in Figure III.17, when decreasing the applied voltage from 400 V to 200 V, the BSA peak moved from the low field end of the channel toward the high field end, and the peak width increased. Similar phenomena were also seen for conalbumin. However, the distance between these two peaks increased, although they still could not be totally separated.

Effort was made to reduce dispersion by packing the separation channel or growing a monolith inside the dialysis fiber. Experimental results showed that packing the dialysis fiber was very difficult. There were differences between growing a monolith inside the hollow dialysis fiber and inside a commonly used fused silica capillary. The greatest difficulty was that the wall of the dialysis fiber was semi-permeable, so some volatile components in the monomer solution most likely escaped through the porous wall of the dialysis fiber. Therefore, carefully controlling the original monomer solution composition during the procedure of filling the fiber with monomer solution and during polymerization was difficult. Figure III.18 shows results of a focused band of BSA using an EFGF device containing a dialysis fiber filled with EDMA-MMA monolith. It can be seen that BSA could be focused inside the monolith and detected using the scanning LIF detection system. The peak width was comparable to that obtained using an open tubular fiber. Obviously, better methods are needed to synthesize a monolith inside the dialysis fiber.

Planar CCSA EFGF device with porous glass capillary. Porous glass capillaries were made according to the procedure described above. The conductivity of the wall of the porous glass capillary was confirmed using a simple setup shown in Figure III.19. The typical current measured with a porous glass capillary was 28 μA when a 3 kV

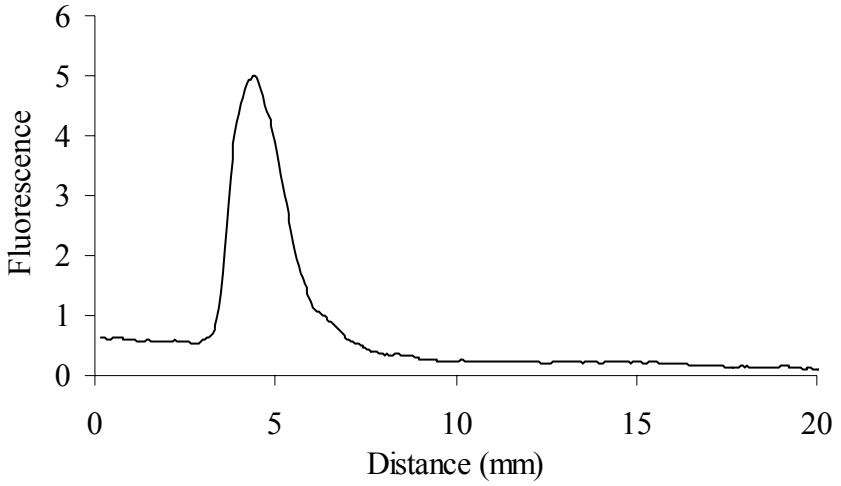

Figure III.18. Focusing of BSA in a hollow dialysis fiber filled with EDMA-MMA monolith.

voltage was applied. With an untreated glass capillary, the current reading was basically zero.

Using EFGF devices with porous glass capillary as separation channel, single proteins could be readily focused, as shown in Figure III.20. The positions of focused protein bands were not stable, probably due to electroosmotic flow (EOF) in the silica-rich porous glass capillary. After adding 1% polyvinylpyrolidone (PVP) in the buffer solution to reduce EOF, the bands became more stable [13].

Figure III.21 shows an example of the focusing and separation of a mixture of 3 proteins. It was observed that the peak positions were often different from those when focusing single proteins. This indicates that the interactions between protein peaks may have an influence on the local electric field.

Ucon was used as a surface treatment for the porous glass capillary, hoping that it would reduce protein adsorption and EOF. The channel was flushed with 0.2 M NaOH, water, 0.2 M HCl and then water again, and finally with 20% (by weight) Ucon aqueous solution at 2 μL/min for 2 h. For a channel with 0.5 mL (~20 times channel volume) of operating buffer, a peak for BSA was formed at ~7.5 mm from the anode end after 30 min with a width less than 1 mm, as shown in Figure III.22, and stayed there for about 20 min. A channel treated with Ucon, was able to focus a rather narrow peak of for BSA.

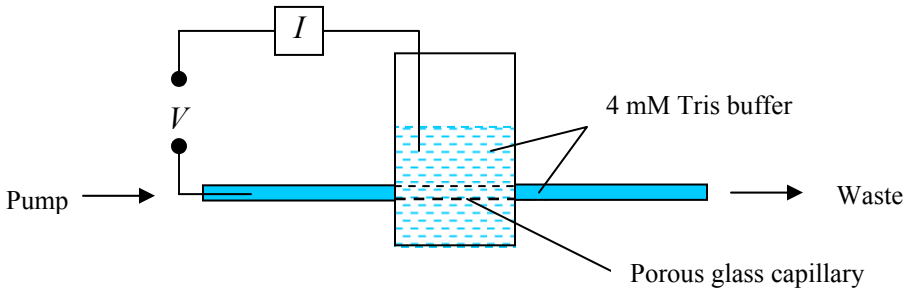

Figure III.19. Setup to test the conductivity of the wall of the porous glass capillary.

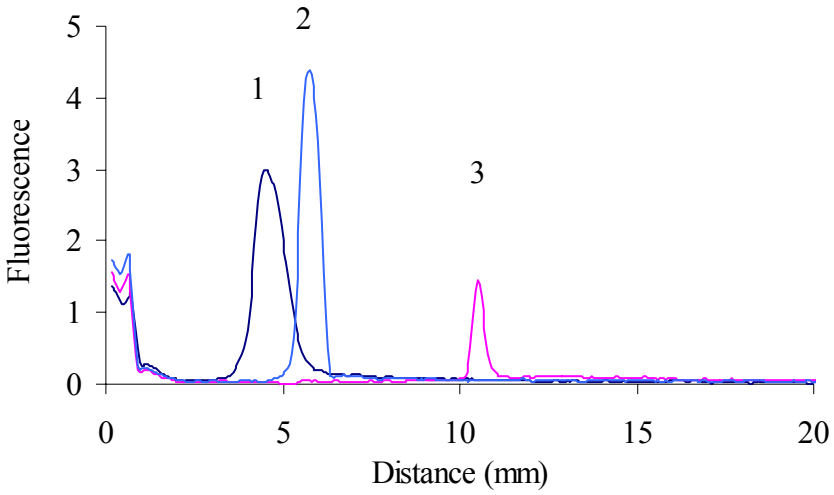

Figure III.20. Focusing of single proteins using an EFGF device with porous glass capillary as a separation channel. Conditions: u = 0.005 μL/min, V = 400 V. Peak identifications: (1) BSA, (2) conalbumin, (3) hemoglobin.

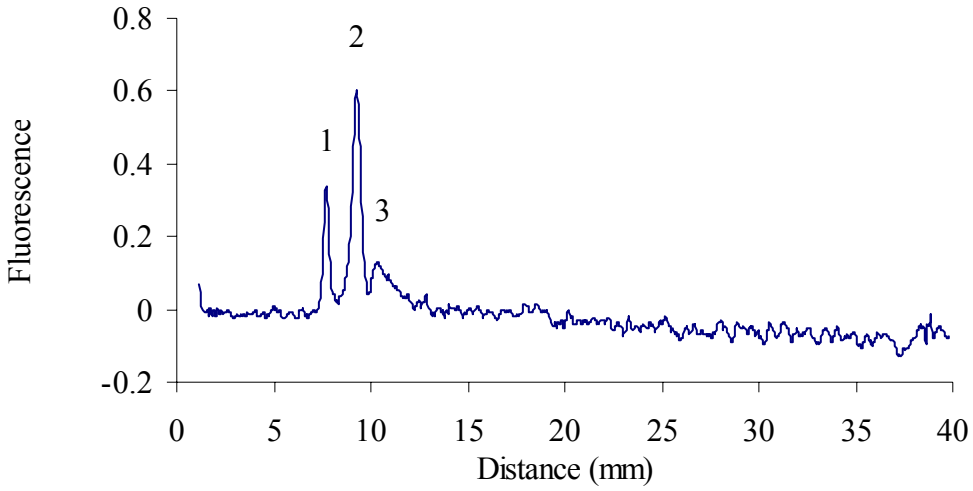

Figure III.21. Focusing of proteins using an EFGF device with porous glass capillary as a separation channel. Conditions: u = 0.005 μL/min, V = 800 V. Peak identifications: (1) BSA, (2) β-lactoglobulin A, (3) hemoglobin.

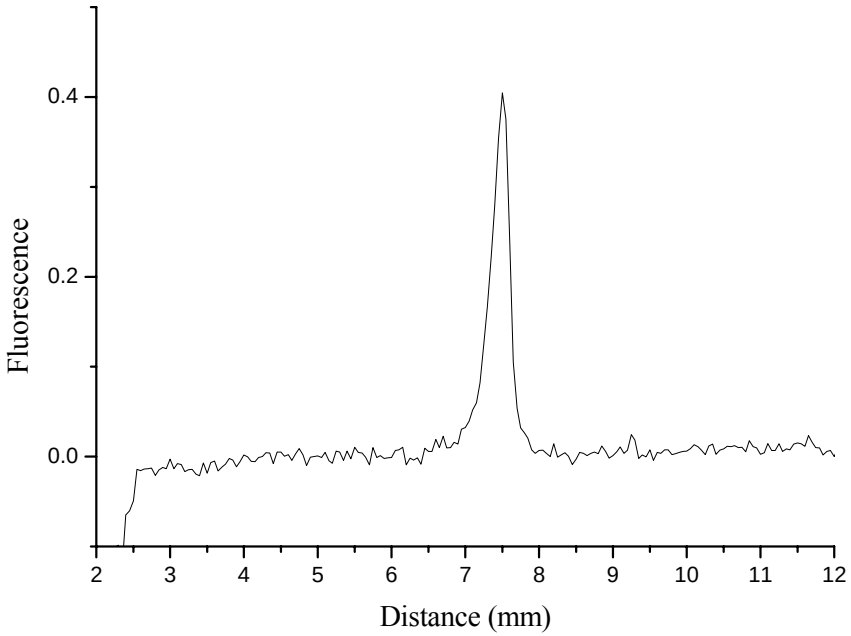

Figure III.22. Focused BSA band using an EFGF device with Ucon treated separation channel. Conditions: u = 0.2 μL/min, V = 200 V.

III.4. Summary and Future Research

EFGF devices with distributed resistor substrates could focus proteins in the separation channel, however, the focused bands were not stable, and the repeatability was poor. The main reason is that electrochemical processes occurred at the boundaries between the solid surfaces and the buffer solution, and bubbles and pH gradient were produced during this process. Using a 2-layer type EFGF device with a purge channel helped reduce the influence of the electrochemical processes. However, further improvement of the 2-layer type EFGF device is necessary for obtaining more stable results, mainly by using suitable materials as the separation/connection media between the upper channel and the lower channel.

Both fiber-based and porous glass capillary-based planar EFGF with CCSA channels performed protein focusing. The fiber-based CCSA EFGF devices gave low performance compared with glass capillary based devices. A fiber-based device with monolith inside the separation channel was constructed and tested. EFGF devices with porous glass capillaries could focus single proteins and separate mixtures of two to three proteins. The positions and shapes of the focused bands were not stable with time, probably due to surface properties of the glass capillary and EOF. Addition of PVP in the buffer partially reduced the influence from EOF and protein adsorption. Ucon treatment significantly improved the performance of capillary-based EFGF devices, however, the effects were not stable.

Suggestions for further work include: (1) miniaturizing the structures of EFGF devices, which should provide narrower peaks and better resolution (however, the ion depletion phenomenon in the miniaturized devices will be a challenge, and providing a

suitable purging scheme as demonstrated in this work might help reduce the ion depletion phenomenon); (2) exploring better porous materials that are suitable for separating/connecting the separation channel and the CCSA channel; and (3) adjusting the surface properties of the separation channel to reduce protein adsorption and EOF.

References

1. Giddings, J.C.; Dahlgren, K. *Sep. Sci.* **1971**, *6*, 345-356.

2. Righetti, P.G. *Isoelectric Focusing: Theory, Methdology and Applications*; Elsevier Biomedical Press: Amsterdam, 1983.

3. O'Farrell, P.H. *Science* **1985**, *227*, 1586-1589.

4. Koegler, W.S.; Ivory, C.F. *J. Chromatogr. A* **1996**, *726*, 229-236.

5. Greenlee, R.L.; Ivory, C.F. *Biotechnol. Prog.* **1998**, *14*, 300-309.

6. Huang, Z.; Ivory, C.F. *Anal. Chem.* **1999**, *71*, 1628-1632.

7. Koegler, W.S.; Ivory, C.F. *Biotechnol. Prog.* **1996**, *12*, 822-836.

8. Tolley, H.D.; Wang, Q.; LeFebre, D.A.; Lee, M.L. *Anal. Chem.* **2002**, *74*, 4456-4463.

9. Humble, P.H.; Kelly, R.T.; Woolley, A.T.; Tolley, H.D.; Lee, M.L. *Anal. Chem.* **2004**, *76*, 5641-5648.

10. Liu, J.; Sun, X.; Farnsworth, P.B.; Lee, M.L. *Anal. Chem.* **2006**, *78*, 4654-4662.

11. Wang, Q.; Lin, S.-L.; Warnick, K.F.; Tolley, H.D.; Lee, M.L. *J. Chromatogr. A* **2003**, *985*, 455-462.

12. Ross, D.; Locascio, L.E. *Anal. Chem.* **2002**, *74*.

13. Gao, Q.; Yeung, E.S. *Anal. Chem.* **1998**, *70*, 1382-1388.